National Library of Canada
Acquisitions and Bibliographic Services Branch
395 Wellington Street
Ottawa, Ontario
K1A 0N4

Bibliothèque nationale du Canada
Direction des acquisitions et des services bibliographiques
395, rue Wellington
Ottawa (Ontario)
K1A 0N4

Your file Votre référence

Our file Notre référence

NOTICE

The quality of this microform is heavily dependent upon the quality of the original thesis submitted for microfilming. Every effort has been made to ensure the highest quality of reproduction possible.

If pages are missing, contact the university which granted the degree.

Some pages may have indistinct print especially if the original pages were typed with a poor typewriter ribbon or if the university sent us an inferior photocopy.

AVIS

La qualité de cette microforme dépend grandement de la qualité de la thèse soumise au microfilmage. Nous avons tout fait pour assurer une qualité supérieure de reproduction.

S'il manque des pages, veuillez communiquer avec l'université qui a conféré le grade.

La qualité d'impression de certaines pages peut laisser à désirer, surtout si les pages originales ont été dactylographiées à l'aide d'un ruban usé ou si l'université nous a fait parvenir une photocopie de qualité inférieure.

Canada

A POTENTIAL MODEL IN N_2-FIXATION: SYNTHESIS, REDOX PROPERTIES OF [MoCl(dttd)(L)] (L=NMe, NPh, $NNMe_2$, $NNPh_2$; dttd=2,3,8,9-Dibenzo-1,4,6,10-Tetrathiadecane) AND CRYSTAL STRUCTURES OF [$MoCl(NNPh_2)$(dttd)] AND [(dttd)Mo(μ-NMe)(μ-S-dttd)MoCl]

Xuan Li

A Thesis

in

The Department

of

Chemistry and Biochemistry

Presented in Partial Fulfilment of the Requirements

for the Degree of Doctor of Philosophy at

Concordia University

Montreal, Quebec, Canada

August 1992

ISBN 0-315-81024-6

Canada

ABSTRACT

A Potential Model in N_2-Fixation:
Synthesis, Redox Properties of Molybdenum Complexes [MoCl(dttd)(L)]
(L = NMe, NPh, $NNMe_2$, $NNPh_2$; dttd = *2,3,8,9*-dibenzo-*1,4,7,10*-tetrathiadecane)
and Crystal Structures of
[$MoCl(NNPh_2)$(dttd)] and [(dttd)Mo(μ-NMe)(μ-S-dttd)MoCl]

Xuan Li, Ph. D.
Concordia University, 1992

Two hydrazido(2-) and two imido (2-) molybdenum(V) complexes [MoCl(dttd)(L)] (L= NMe (**1**), NPh (**2**), $NNMe_2$ (**3**) and $NNPh_2$ (**4**); dttd = *2,3,8,9*-dibenzo-*1,4,7,10*-tetrathiadecane) have been synthesized and characterized. The precursor complex [$Mo(dttd)Cl_2$] reacted with bis(trimethylsilyl)amine and bis(trimethylsilyl)hydrazine leading to the formation of the model molybdenum complexes. They exhibited similar electrochemical behaviour and underwent an irreversible two-electron redox process between -0.1 and -1.8 V.

Complex (**4**) crystallized in an orthorhombic space group *Pbca* with lattice constants of a = 21.298(15) Å, b = 14.056(10) Å, c = 17.732(11) Å and Z = 8. The Mo is approximately octahedral with a linear Mo-N-N and planar $MoNNC_2$ fragment unit in which the Mo-N-N angle is 172(2)°, and the distances of Mo-N and N-N are 1.749(15) Å and 1.342(25) Å respectively.

The chemical reduction of complexes (**1**)~(**4**) by zinc or sodium amalgam was carried out in the absence or presence of H^+. In the presence of H^+ the imido and hydrazido ligands were eliminated. However in the absence of H^+ a green product was obtained from the reduction of (**1**) by zinc amalgam. It crystallized in a monoclinic space

group $P2_1/c$ with lattice constants of a = 16.888(6) Å, b = 11.258(4) Å, c = 24.011(20) Å, β = 106.60(4)° and Z = 4. It is dimer possessing an imido and a sulfur bridge, and a Mo(III)-Mo(IV) distance of 2.609(5) Å. The structural data suggests the existence of π interaction between the lone pair of the nitrogen atom on the imido ligand and the $d\pi$ orbitals of the two molybdenum centres.

ACKNOWLEDGEMENT

I wish to express my sincere appreciation to my supervisor Dr. P.H. Bird for his guidance and help throughout this research and preparation of this thesis.

I am grateful to the members of my research committee, Dr. L.D. Colebrook and Dr. J.A. Capobianco for their helpful suggestions.

I would also like to thank Dr. R.T. Rye for his help in mass spectrometry and to numerous other individuals who have contributed to my knowledge of chemistry.

Thanks are also given to the Department of Chemistry and Biochemistry for financial support.

To

My Parents, My Wife and My Daughter.

CONTENTS

LIST OF FIGURES

LIST OF SCHEMES

LIST OF TABLES

LIST OF ABBREVIATIONS

ATP	2-aminothiophenyl
AU	arbitrary unit
Bu	*n*-butyl
Cp	cyclopentadiene
Cp^*	*1,2,3,4,5*-pentamethylcyclopentadiene
CV	cyclic voltammetry
DAPTE	*1,2*-di(*o*-aminophenylthio)ethane
depe	*1,2*-bis(diethylphosphino)ethane
DME	*1,2*-dimethoxyethane
DMF	*N,N*-dimethylformamide
dmpe	*1,2*-bis(dimethylphosphino)ethane
dttd·H_2	*2,3,8,9*-dibenzo-*1,4,7,10*-tetrathiadecane
dpepp	bis(2-diphenylphosphinoethyl)phenylphosphine
dppe	bis(diphenylphosphino)ethane
dtc	dialkyldithiocarbamate
dtp	dialkyldithiophosphate
EPR	electron paramagnetic resonance
Et	ethyl
EXAFS	extended X-ray absorption fine structure
FTIR	fourier transform infrared spectroscopy
IR	infrared spectroscopy

L	ligand
m	medium
Me	methyl
$Me_8[16]aneS_4$	*3,3,7,7,11,11,15,15*-octamethyl-*1,5,9,13* tetrathiacyclohexadecane
MS	mass spectroscopy
NMF	*N*-methylformamide
NMP	*N*-methylpyrolidone
NMR	nuclear magnetic resonance spectroscopy
Ph	phenyl
Py	pyrrole
quin	*8*-hydroxyquinolate
R	organic substituent
s	strong
sh	shoulder
THF	tetrahydrofuran
TLC	thin layer chromatography
TMS	tetramethylsilane
TsO	toluene *p*-sulphonate or tosylate
UV-VIS	ultra violet-visible spectroscopy
w	weak
XPE	X-ray photoelectron spectroscopy

CHAPTER 1

INTRODUCTION TO NITROGEN FIXATION

In order to supply millions of tons of N-fertilizer at low cost to increase the yield of crops which are needed by the rapidly expanding population of human beings, chemists, especially inorganic chemists, have put great efforts in the elucidation of the course of nitrogen fixation in nitrogenase. The coordination of N_2 followed by its reduction protonation to produce ammonia at a transition metal centre is the central problem. Although thousands of model complexes and clusters have been synthesized and characterized, and many significant breakthroughs have been made, we are still far from completely understanding the function of the active site, the FeMo-cofactor, in nitrogenase. This study focuses on the hydrazido and imido molybdenum complexes which may relate to the intermediates in the course of N_2-fixation. In the first chapter, a brief review is given of the general ideas about nitrogen-fixation in inorganic chemistry and the significance of my work.

Dinitrogen reduction in industry is achieved under ~200 atm. pressure and at ~500^0, even in the presence of the best heterogeneous iron catalyst, and although the conversion of N_2 to ammonia is thermodynamically favoured, the very large triple bond energy (945KJ/mol) makes N_2 "almost as inert as a noble gas" [1]. Conversely biological nitrogen fixation proceeds under mild conditions, and the stoichiometric reduction [2] appears to be:

$$N_2 + 8H^+ + 8e^- \text{------>} 2NH_3 + H_2 \qquad (1.1)$$

1.1 Nitrogenase and the Iron-Molybdenum Co-Factor (FeMo-co)

Bacterial nitrogenase was first isolated in an active form by Carnahan and co-workers at Dupont in 1960 [3]. It consists of two distinct proteins with molecular weight of ~60,000 and ~220,000, respectively. The smaller iron containing protein has two identical subunits sharing one Fe_4S_4 cubane-like cluster. The large FeMo protein, which has four subunits, two α and two β, contains 2Mo, ~30Fe, and ~30 inorganic S atoms. These Mo, Fe and S atoms form four Fe_4S_4 clusters and two Fe-Mo-S clusters.

The iron-molybdenum co-factor, in which the molybdenum is believed to provide the active site where the N_2 molecule is attached, was first obtained from FeMo protein by acid treatment and NMF extraction in 1977 [4]. It is an extremely insoluble and highly air-sensitive species with a molecular weight of 1,000 to 1,500 [5]. It has 2Mo, 6-8Fe, and ≥6S atoms. Epr studies suggest three oxidation states for the cofactor metal centre, and EXAFS studies [6] indicate that it contains some sort of Fe-Mo-S cluster with 4.5S at 2.37Å and 3.5Fe at 2.67Å from the Mo atom. No evidence showing the existence

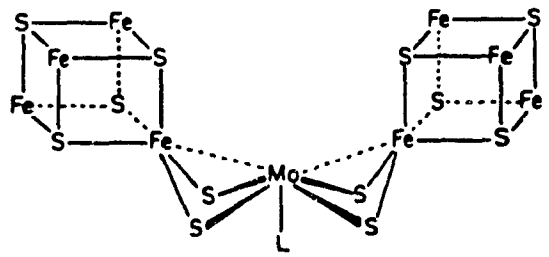

Fig. 1.1 A proposed active site in nitrogenase.

of a short Mo-Mo distance has been found. The structure of the cluster will only be firmly characterized after the completion of the ongoing X-ray crystallography. One of

the proposed structures [1, 4] of the Fe-Mo-S cluster is shown in fig.1.1.

1.2. Dinitrogen Transition Metal Complexes

Since the discovery of the first dinitrogen transition metal complex in $[Ru(NH_3)_5(N_2)]X_2$ (X=Br, I, BF_4, PF_6) by Allen and Senoff in 1965, extensive studies have been carrie i out by inorganic chemists on preparation, characterization and reduction of dinitrogen complexes.

1.2.1. Synthesis

The methods of preparation of dinitrogen complexes can be divided into two categories, depending on the source of the dinitrogen ligand. The most common method is to treat high valence complexes with reducing agents in the presence of ligands such as phosphines under a nitrogen atmosphere [7-10] (Eq. 1.2-1.4).

$$[Mo(acac)_3 \xrightarrow[N_2]{AlR_3,\ dppe} \textit{trans}\text{-}[Mo(N_2)_2(dppe)] \qquad (1.2)$$

$$[WCl_4(PMe_2Ph)_3] \xrightarrow[N_2]{PMe_2Ph,\ Mg} \textit{cis}\text{-}[W(N_2)_2(PMe_2Ph)_4] \qquad (1.3)$$

$$[Cp^*_2ZrCl_2] \xrightarrow[N_2]{Na/Hg} [\{Cp^*_2Zr(N_2)\}_2(\mu\text{-}N_2)] \qquad (1.4)$$

Several improved methods were developed to increase the yield. A suitable choice of reducible precursors and reducing agents is very inportant. A typical one involves the reaction of $MoCl_3(THF)_3$ with Mg in the presence of dppe and N_2 [11] (Eq. 1.5).

$$MoCl_5 \xrightarrow{EtCN} [MoCl_4(EtCN)_2] \xrightarrow[CH_2Cl_2/THF]{Zn} [MoCl_3(THF)_3] \xrightarrow[N_2]{Mg,\ dppe} trans\text{-}[Mo(N_2)_2(dppe)_2] \qquad (1.5)$$

Indirect methods for preparation of dinitrogen complexes are known, these methods, however, are often specific for one metal [12-16]. Some dinitrogen complexes are listed in Table 1.1. and 1.2.

1.2.2. The Bonding Mode

Although N_2 is analogous to CO, RNC and RCN, the very low energy level (-15.5 eV) of the $3\sigma_g$ HOMO and the high energy level (-7 eV) of the $1\pi_g^*$ LUMO lead to poor σ-donating and relatively poor π-accepting character in dinitrogen [33]. A synergistic overlap of dinitrogen with metal orbitals is required to ligate N_2 to a metal. An electron-rich site (i.e. metal with low oxidation state) is favoured for back donation. The greater the contribution to bonding from π back donation compared to σ donation, the more basic and polarized is the ligating dinitrogen.

Two types of bonding mode are known, end-on and side-on. They are further

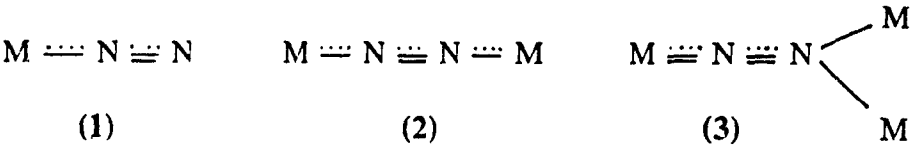

(1) (2) (3)

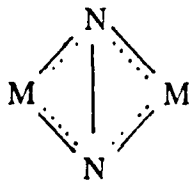

(4)

(5)

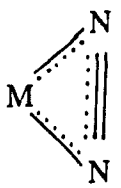

(6)

divided into terminal and bridging to give the six modes as shown above. All the structures except type **6** have been unambiguously detected by X-ray crystallographic analysis. The corresponding complexes, their bond lengths and IR data are shown In Table 1.1.

The most common structure of dinitrogen complexes is the end-on type **1**. Sigma donation may be largely responsible for the stability of dinitrogen complexes, whereas π back donation is responsible in activating (lengthening) the N-N triple bond. This is reflected in IR and crystallographic data. This lengthening not only depends on the electron density in the dπ orbital, but also on the degree of the overlap between dπ and the $1\pi_g^*$ orbitals (LUMO) of N_2. In general, the $\nu(N_2)$ of ligating dinitrogen is lower and the N-N distance is slightly longer than that of free N_2 (2331 cm^{-1} (Raman); N-N 1.09768(5) Å [30]). The relative importance of the σ and π contributions to the bonding dinitrogen depends on the co-ligands, the nature and the oxidation state of the metals. For example, the N-N distance in *trans*-$[Cr(N_2)_2(dmpe)]$ is only 0.985(4) Å, even shorter than in free N_2 (Table 1.1). The origin of this shortening is unknown.

Type **2** is also commonly observed in dinitrogen complexes [34-35]. In a four-centre linear unit, M-N-N-M, the interactions between N_2 π orbitals and metal dπ orbitals form 1e, 2e, 3e and 4e molecular orbitals [36-37] as shown in Fig. 1.2. Theoretical calculation indicates that the important orbital is 2e, which is contributed by $1\pi_g^*$ and dπ, and represents a strong interaction between them [39].

Usually the N-N distance in type **2** is longer than that in type **1**, especially in the cases of tantalum μ-N_2 complexes (Table 1.1, [19-21]). They are considered as μ-N_2^4 or hydrazido(4-) complexes with a Ta═N–N═Ta bonding mode. They afford hydrazine

Table 1.1 Some dinitrogen compounds, their bonding modes and structure data.

Complex	Bonding Mode	M—N (Å)	N—N (Å)	∠M-N-N (deg)	$\nu(N_2)$ (cm^{-1})	Ref
trans-$[Mo(N_2)_2(dppe)_2]$	1	2.014(5)	1.118(8)	176.6	2020	
					1970	17
trans-$[Mo(CO)(N_2)(dppe)_2]\cdot 1/2C_6H_6$	1	2.068(12)	1.087(18)	177	2128	14
$[CoH(N_2)(Pph_3)_3]$	1	1.806(16)	1.123(12)	178	2088	18
$[Os(NH_3)_5(N_2)]Cl_2$	1	1.842(13)	1.12(2)	178.3	2010	19
trans-$[Cr(N_2)_2(dmpe)_2]$	1	1.957(4)	0.985(4)	177.3	1932	20
trans-$[Mo(N_2)_2Me_8[16]aneS_4]$	1	2.008(5)	1.108(7)	176.7	1955	
		1.991(5)	1.105(7)	176.2	1890	21
$[\{Cp^*_2Zr(N_2)\}_2(\mu N_2)$	1	2.188(4)	1.116(8)	177.9(5)	2040	
		2.188(4)	1.114(7)	177.8(5)	2003	
	2	2.087(3)		176.7(3)	1578	
		2.075(3)	1.182(5)	177.4(3)		22
$[\{Mo(\eta^6\text{-}C_6H_3Me_3)(dmpe)\}_2(\mu\text{-}N_2)]$	2	2.042(4)	1.145(7)	175.6	1989	23
$[MoCl_4\{(\mu\text{-}N_2)ReCl(PMe_2Ph)_4\}_2]$	2	1.99	1.28(5)		1800	24
$[\{Ta(CHCMe_3)(CH_2CMe_3)(PMe_3)_2\}_2(\mu\text{-}N_2)]$	2	1.837(8)	1.298(12)	171.43(65)	847	
		1.842(8)		172.42(65)		25
$[\{(PhMe_2P)_3(Py)ClW(\mu\text{-}N_2)AlCl_2\}_2]\cdot C_6H_6$	3	1.85(3)*	1.46(4)	175	1400	
			1.25(3)	178	1350	26
$[\{Me_2P)_3Co(\mu\text{-}N_2)AlMe_2\}_2]$	3	1.642(4)	1.252(6)	171.5(4)	1530	
		1.931(4)*				
		1.915(5)*				27
$[\{PhLi)_6Ni_2(\mu\text{-}N_2)(Et_2O)_2\}_2]$	4		1.35			28
$[(\mu_3\text{-}N_2)\{(\eta^5,\eta^5\text{-}C_{10}H_8)Cp_2Ti_2\}$ $\{\eta^1,\eta^5\text{-}C_5H_4)Cp_3Ti_2\}]$	5		1.301(12)		1282	29

* Al—N distance.

** N—N distance(Å): N≡N 1.09768(5) [30], N_2^+ 1.118 [31], MeN=NMe 1.23 [32], H_2N—NH_2 1.46 [32].

in high yield upon hydrolysis. Powell proposed that the key to nitrogen fixation may lie in d^2 type **2** systems [38]. However the bridging end-on bonding mode of dinitrogen seems unlikely between the two Mo centres in nitrogenase [3]. Orme concluded based on his ESR data that the two Mo atoms, in nitrogenase, should be 11-15 Å apart.

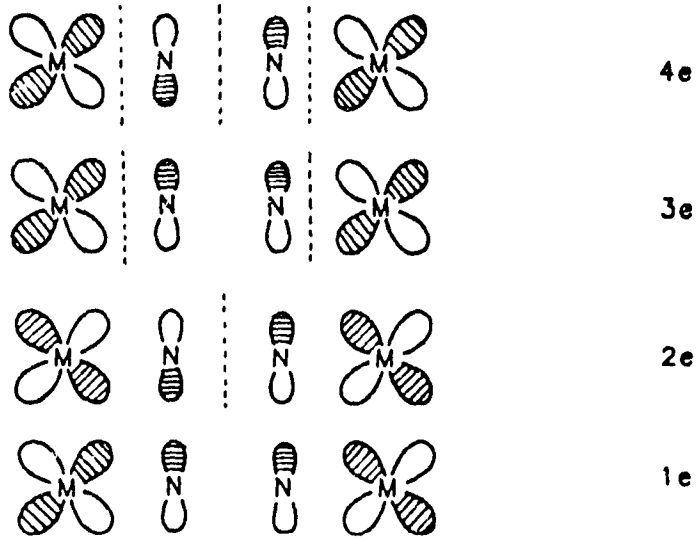

Fig. 1.2 The simple qualitative four-centre molecular orbital scheme.

Two examples confirm the existence of the bonding mode type **3** in Table 1.1. The MNN linkage is essentially linear, and two M, four N, two Al atoms almost lie in the same plane. They may be regarded as dimers of metallo diazenido complexes, and described as a combination of two resonance structure:

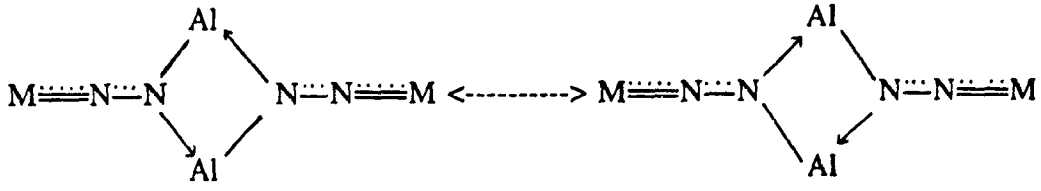

Although the two M-N and two N-N distances are different, the data show multiple bonding between M and N, and a bond order 1~2 for N-N.

In a bridging side-on structure of type **4**, the N-N distance is extremely long

compared to free N_2 (Table 1.1), This may be due to the synergistic effect of the strong back donation from side-on electron-rich Ni atoms and the electrons withdraw by the end-on atoms. In this structure, two nitrogen atoms and two Ni atoms form a distorted tetrahedron. This synergistic effect and structure were also found in some other compounds [39].

Type **5** was recently discovered (Table 1.1, [40-41]). The dinitrogen ligand is σ bonded to one titanium atom and $\sigma + \pi$ bonded to two others. This bonding mode leads to remarkable lengthening of the N-N distance and the very low $\nu(N_2)$.

Although there is no crystallographic evidence to show the existence of type **6**, the side-on structure has been proposed based on the ESR data [42] for $[Cp_2Zr(N_2)CH(SiMe_3)_2]$. In this bonding mode, only one of the $1\pi_g^*$ orbitals is used to accept the back donation. Compared to type **1**, in which both $1\pi_g^*$ orbitals can take part in the π bond formation, type **6** may be found in d^1 or d^2 systems whereas type **1** prefers the d^4 system [43]. Theoretical studies [44-45] also suggested that type **1** is more favourable than type **6** thermodynamically.

1.2.3 Electronic Properties and Reactivity of Ligating Dinitrogen

In comparison with carbon monoxide, organic cyanides and isocyanides, N_2 is the weakest σ-donor ligand whereas its π acceptor capacity lies between them. It is believed that N_2 coordinated in an end-on fashion has an overall negative charge to an extent about equal to CO, although N_2 is weaker than CO in both its σ-donor and π-acceptor functions. The extent of charge distribution on ligating N_2 can be directly measured by XPS of the N(1s) core energy. In general the N(1s) binding energy appears in the 398.3 - 400.4 eV

region which corresponds to a slight negative charge [46]. The N(1s) spectrum is resolved as a doublet, the higher energy peak is assigned to the αN, while the lower energy peak is assigned to the βN. However, in the bridging dinitrogen complex, $[MoCl_4(OMe)(\mu\text{-}N_2)ReCl(PMe_2Ph)_4]$, the nitrogen atoms could not be distinguished in the XPS spectrum, even though the oxidation states of Mo and Re are quite different [47]. Strangely, only the manganese complex $[CpMn(CO)_2(N_2)]$ shows electron-poor character of the ligating N_2: the N(1s) binding energy appear at 403.0 and 401.8 eV [48].

Theoretical calculations give the charge distributions Mo(+0.15)-N(-0.11)-N(- 0.88) and Mo(-0.59)-N(+0.05)-N(-0.67) for model compounds *cis-* and *trans-* $[Mo(N_2)_2(PH_3)_4]$, respectively [49]. However, the relative polarization of ligating N_2 seems to change from one type of complex to another. An *ab initio* molecular orbital calculation on the complex, $[Ru(NH_3)_5(N_2]^{2+}$, shows the ligating N_2 is positively charged and the polarization is described as Ru(δ+)-N(δ-)-N(δ+) [50]. Normally, the greater the π back bonding from the metal, the more basic is the terminal nitrogen atom. Like coordinated CO and R-NC, the N_2 coordinated in an end-on fashion shows chemical reactivity in the sense that the αN is susceptible to nucleophilic attack, whereas the βN is attacked by electrophiles.

^{15}N NMR studies are expected to give useful information about the electronic state of the ligating N_2, but they are still at an early stage and only a few kinds of complexes have been examined [50-53].

1.2.4 Protonation of Ligating Dinitrogen

Dinitrogen complexes can react with protic acid or metal hydrides to give ammonia and/or hydrazine. Published reports of electrophilic attack of protons on ligating dinitrogen

Table 1.2 Yields of ammonia and hydrazine from dinitrogen complexes of molybde·um and tungsten

Complex	Reagent	Solvent	Yield*			Ref
			NH_3	N_2H_4	N_2	
cis-$[Mo(N_2)_2(PMe_2Ph)_4]$	H_2SO_4	MeOH	0.64	Trace	1.23	55
cis-$[Mo(N_2)_2(PMe_2Ph)_4]$	HCl	DME	0.31	0.32		41
trans-$[Mo(N_2)_2(PMePh_2)_4]$	H_2SO_4	MeOH	0.66	0	1.64	55
trans-$[Mo(N_2)_2(PMePh_2)_2(dppe)]$	H_2SO_4	MeOH	0.56	0	1.2	55
$[Mo(N_2)_2(triphos)(PPh_3)]$	HBr	THF	0.7	0	1.3-1.5	58
trans-$[Mo(N_2)_2(PMePh_2)_2(dppe)]$	HBr	THF	0.68	0	1.49	59
trans-$[Mo(N_2)_2(dppe)_2]$	HBr(aq.)	N[illegible]	0.29	0		60
cis-$[Mo(N_2)_2(PMe_2Ph)_4]$	$NaAlH_2(OCH_2CH_2OCH_3)_2$	C_6H_6	0.77	Trace	61	
cis-$[W(N_2)_2(PMe_2Ph)_4]$	H_2SO_4	MeOH	1.83	0.02	0.97	55
cis-$[W(N_2)_2(PMe_2Ph)_4]$	H_2SO_4	THF	0.89	0.18	0.98	55
cis-$[W(N_2)_2(PMe_2Ph)_4]$	HCl	DME	0.22	0.63		41
cis-$[W(N_2)_2(PMe_2Ph)_4]$	HBr	DME	0.34	0.16		41
cis-$[W(N_2)_2(PMe_2Ph)_4]$	HI	DME	0.92	0.26		41
trans-$[W(N_2)_2(PMePh_2)_4]$	H_2SO_4	MeOH	1.80	0.07	0.99	55
cis-$[W(N_2)_2(PMe_2Ph)_4]$	H_2O	THF	1.34	Trace		62
cis-$[W(N_2)_2(PMe_2Ph)_4]$	MeOH		1.64	0.02	1.00	55
cis-$[W(N_2)_2(PMe_2Ph)_4]$	EtOH		0.43	Trace	1.72	55
cis-$[W(N_2)_2(PMe_2Ph)_4]$	EtOH/KOH		1.08	0.06		62
cis-$[W(N_2)_2(PMe_2Ph)_4]$	$FeH_2(CO)_4$	MeOH	0.06	Trace		63
cis-$[W(N_2)_2(PMe_2Ph)_4]$	$HFeCo_3(CO)_{12}$	MeOH	0.32	0.01		64
cis-$[W(N_2)_2(PMe_2Ph)_4]$	$NaAlH_2(OCH_2CH_2OCH_3)_2$	C_6H_6	1.83	0		63

* Mol/M atom.

in mononuclear compounds have been confined to the molybdenum and tungsten species. In the case of other mononuclear dinitrogen complexes, the metals are first attacked by protons resulting in the oxidation of the metals, concurrent with loss of dinitrogen as gas [33]. The yields of ammonia and hydrazine in various acid/solvent systems are listed in Table 1.2 for some molybdenum and tungsten dinitrogen complexes.

Chatt and co-workers [54-55] found that dinitrogen complexes $[M(N_2)_2(L)_4]$ (M=Mo or W; L= PMe_2Ph or $PMePh_2$) gave high yields of ammonia and a little hydrazine on treatment with H_2SO_4 at room temperature in methanol. For M=W, the yield of ammonia was essentially 2 mol/M atom, but only about 0.7 mol/M atom for M=Mo. The remaining nitrogen was mostly evolved as molecular nitrogen. In the course of the reactions, the tungsten atoms were finally oxidized to a six-valent state [56-57]. A stoichiometric reaction might be:

$$\text{cis-}[W(N_2)_2(PMe_2Ph)_4] \xrightarrow[MeOH]{H_2SO_4} 2NH_3 + N_2 + 4PMe_2Ph + W(VI)\ \text{products.} \quad (1.6)$$

The yields of ammonia and hydrazine depend greatly on acids and solvents used, and also depend on the types of dinitrogen complex and co-ligands. Thus if THF is used instead of MeOH as solvent, the yield of hydrazine increases with decrease of the yield of ammonia [56]. When HCl gas and 1,2-dimethoxyethane (DME) are used for the protonation reaction [41], the W(IV) species $[WCl_4(PMe_2Ph)_2$ is isolated. The HCl/DME system favours hydrazine formation [65]:

$$\text{cis-}[W(N_2)_2(PMe_2Ph)_4 \xrightarrow{HCl/DME} N_2H_4 + N_2 + 2PMe_2Ph + [WCl_4(PMe_2Ph)_2 \quad (1.7)$$

Whereas an HI/DME system favours the ammonia formation.

Molybdenum dinitrogen complexes show differences in chemical behaviour when compared with the corresponding tungsten complexes. The yields of ammonia in protonation reactions have not exceeded 1 mole per mole of complex [56], and the final oxidation state of molybdenum is III. A clear stoichiometry of the protonation reaction has been observed in the case of $[Mo(N_2)_2(dpepp)(PPh_3)]$ (dpepp=$PhP(CH_2CH_2PPh_2)_2$).

$$2[Mo(N_2)_2(dpepp)(PPh)_3] + 8HBr \xrightarrow[THF]{} 2NH_4Br + 3N_2 + 2PPh_3 + 2[MoBr_3(dpepp)] \quad (1.8)$$

It is noteworthy that the almost quantitatively recovered Mo(III) species is the precursor for preparation of the starting dinitrogen complex [42, 58].

Dinitrogen complexes can also give moderate or high yields of ammonia when they are treated with metal hydrides, such as $[NaAlH_2(OCH_2CH_2OCH_3)_2]$, $[FeH_2(CO)_4]$, B_2H_6, $LiBH_4$. The reactions of this type may be quite different from the protonation reactions described above, and no evidence shows that the hydrogen atoms of ammonia originally come from the metal hydrides.

In 1985, Pickett and Talarmin reported the controlled-potential electrolysis of a dinitrogen complex to produce ammonia [66]. *Trans*-$[W(N_2)_2(dppe)_2]$ first reacts with tosylic acid, p-$CH_3C_6H_4SO_3H{\cdot}H_2O$ ($TsOH{\cdot}H_2O$), in THF to give the hydrazido(2-) cation *trans*-$[W(NNH_2)TsO(dppe)_2]^+$. This cation undergoes electrolysis under nitrogen to give ammonia, hydrazine and the parent dinitrogen complex. Treatment of the produced dinitrogen complex with $TsOH{\cdot}H_2O$ again, followed by electrolysis, completes a reduction cycle.

The protonation of ligating dinitrogen demonstrates that when N_2 is suitably attached to a metal in a low oxidation state it can be reduced and protonated to give

ammonia. However, there is no reaction cycle competitive with the existing processes such as the Haber process so far, although there are indications of the directions to follow.

1.2.5 Mechanism of Protonating Coordinated Dinitrogen

It is widely accepted that in biological nitrogen fixation, the protonation and reduction reactions of dinitrogen ligating an enzyme-bound transition metal centre occur successively, in order to minimize the change of the active centre charge [66]. Based on the data and hypothesis, Pickett et al proposed a stepwise reduction of dinitrogen to ammonia and hydrazine, Scheme 1.1 [2]. However little is really known about the biological nitrogen fixation mechanism.

Scheme 1.1 Stepwise reduction of ligating dinitrogen to ammonia and hydrazine.

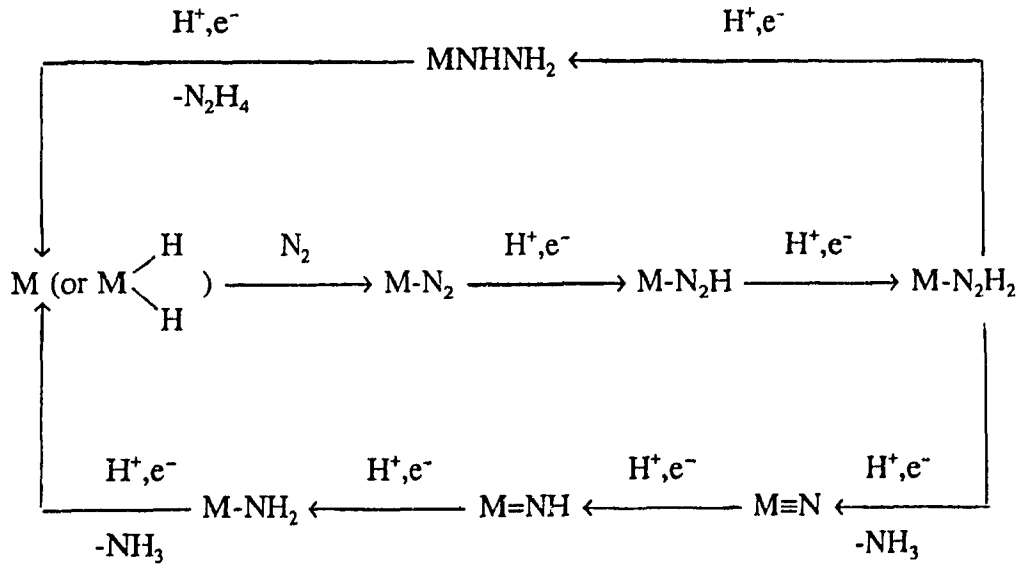

^{15}N NMR studies of the protonation of *cis*-$[M(N_2)_2(PMe_2Ph)_4]$ (M=Mo, W) with

excess H_2SO_4 in THF [67] have been performed. When the reaction proceeds, the resonances characteristic of ligating dinitrogen disappear with appearance of free $^{15}N_2$ and two resonances assigned to a ^{15}N-$^{15}NH_2$ ligand. For M=W, four further distinct stages without any change in the NNH_2 group have been observed. These species are probably hydride-hydrazido and hydrazido(2-) intermediates in which the monophosphine ligands are displaced by the HSO_4^- anions or by solvent. No further intermediates have been detected until the final product $^{15}NH_4^+$ appears [68]. For M=Mo, in addition to the hydrazido(2-) intermediates, no other resonances appear, not even the $^{15}NH_4^+$ resonance, which may be due to the formation of a paramagnetic Mo(III) species as the final metal product. The proposed protonation mechanism is shown in Scheme 1.2 [33].

The first step is probably proton attack on the βN atom. This causes electron withdrawal from the metal to that dinitrogen ligand, resulting in loss of the second ligating dinitrogen and formation of a diazenido complex. Another mechanism involves initial acid anion attack on the central metal to replace one of the dinitrogen ligands forming a complex anion in which the remaining dinitrogen ligand receives more electronic charge and becomes more susceptible to electrophilic attack by protons. This process seems unlikely [69]. The second protonation also occurs at βN atom to give a hydrazido(2-) species, $[M(IV)X_2(NNH_2)L_3]$ (X=anion, L=monophosphine).

The third protonation, when M=W, may occur at βN atom if H_2SO_4 is used, giving one ammonia molecule and probably a nitrido W(VI) species (Scheme 1.1, pathway B). Further hydrolysis by acid produces another ammonia molecule (Eq. 1.6). The six electrons required for the formation of two ammonia molecules come from W(0) ----> W(VI) + 6e$^-$. The high yield of ammonia obtained by using H_2SO_4 is probably

Scheme 1.2 The proposed protonation mechanism of *cis*-$[M(N_2)_2(PMe_2Ph)_4]$ (M=Mo, W) in H_2SO_4/THF [33].

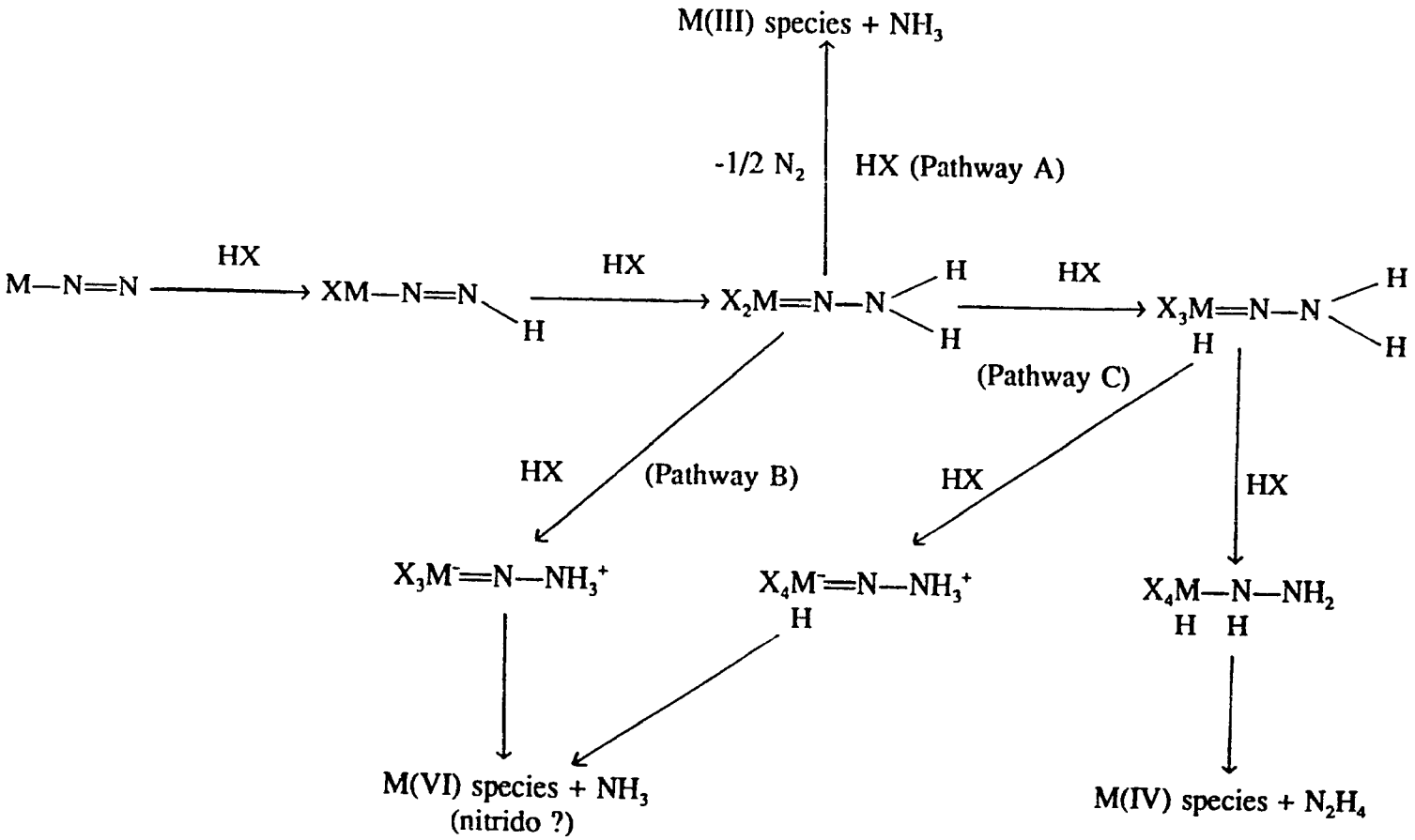

due to the π-electron donation ability of the HSO_4^- anion which makes the terminal nitrogen more negative and susceptible to attack by protons. When treated with HCl in DME, the third protonation may give a hydride-hydrazido(2-) complex (pathway C) which finally leads to the formation of hydrazine [41]. The ratio of ammonia to hydrazine is affected by the sort of solvent and acid HX (X=Cl, Br, I). The mechanism of hydrolysis of the hydride-hydrazido(2-) complex is still under question.

In contrast, when the hydrazido(2-) molybdenum species is formed, it undergoes a net multistep disproportionation reaction [57] as shown in Eq. 1.9.

$$2[MoX(NNH_2)L_4]^+ \xrightarrow{4HX} 2NH_4^+ + N_2 + 2[MoX_3L_3] + 2L \qquad (1.9)$$

Thus one hydrazido complex loses N_2 and affords 3e to another one which is reduced to give two ammonia molecules.

$$Mo(IV)(NNH_2) \dashrightarrow Mo(III) + N_2 + 2H^+ + 3e^- \qquad (1.10)$$

$$Mo(IV)(NNH_2) + 6H^+ + 3e^- \dashrightarrow Mo(III) + 2NH_4^+ \qquad (1.11)$$

Although the total reaction agrees with that of Eq. 1.8, the details remain unresolved.

The key requirement for reduction of ligating dinitrogen is the presence of a labile ligand at the hydrazido(2-) stage [57]. Typically this would be a monodentate organophosphine ligand [70-73]. Protonation of a dinitrogen complex containing chelating diphosphines such as dppe usually stops at the hydrazido(2-) stage without the cleavage of N-N bond [55, 74]. This strongly suggests a requirement of a vacant site *cis* to the hydrazido ligand for N-N cleavage. Nugent and Mayer [75] believe that when further protonation occurs at the hydrazido(2-) stage, the metal is protonated at the vacant site to give a hydride, which is followed by α-elimination to produce NH_3.

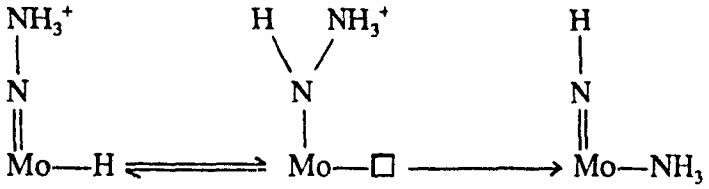

(1.12)

Some monodinitrogen complexes have also been investigated [70, 76-79]. Only hydrazido(2-) complexes and sometimes, a trace of ammonia were obtained. Why they are not easily protonated to give ammonia is not clear.

1.3 Hydrazido(2-) and Imido(2-) Complexes

Hydrazine is the only product obtained from nitrogenase if it is quenched with acid or alkali while it is reducing N_2 [80]. This suggests the existence of a bound N_2H_x species during the fixation process. This bound N_2H_x was confirmed to be a NNH_2 hydrazido(2-) ligand by protonation of dinitrogen molybdenum and tungsten complexes [81-86]. Although imido(2-) complexes have not been isolated from those protonation reactions, the complex $[MoX_2(NH)(dppe)_2]$ has been reported [87] and many imido complexes have been synthesized. Since they are intimately involved in N_2 fixation and other catalytical systems, they have been widely studied, especially those complexes having NNRR' or NR ligands. In this thesis, attention will paid to molybdenum and tungsten complexes which closely relate to the N_2 fixation intermediates. Table 1.3 lists some of these compounds and their structure data.

1.3.1 Synthesis of Hydrazido(2-) and Imido(2-) Complexes

1.3.1.1 Cleavage of α Bond of Precursor

So far the most common method to prepare imido and hydrazido complexes is the

Table 1.3 Some imido and hydrazido complexes and their structure data.

Complexes	M—N (Å)	∠M—N—R (deg)	d^{e^-} (#)	C.N.*	Ref
(Imido)					
$[MoBr(NH)(dppe)_2]Br$	1.73(2)		2	6	88
$[Mo(O)Cl_2(NH)(PEtPh_2)_2]$	1.70(1)	157(10)	0	6	89
$[Mo(N^tBu)Me_2]_2(\mu\text{-}N^tBu)_2]$	1.730(2)	167.4(1)	0	5	90
$[Mo(NPh)_2(S_2CNEt_2)_2]$	1.754(4)	169.4(4)	0	6	128
	1.789(4)	139.4(4)			
$[MoCl_2(NPh)(S_2CNEt_2)_2]$	1.734(4)	166.8(3)	0	7	127
$[Mo(NTol)(S_2P(OEt)_2)_3]$	1.732(4)	168.4(4)	1	6	91
$[MoCl_4(NTol)(THF)]$	1.717(3)	174.6(3)	0	6	121
$[MoCl_3(NTol)(PEtPh_2)_2]$	1.725(6)	176.7(5)	1	6	92
$[MoCl_2(NTol)(PMe_3)_3]$	1.739(2)	175.4(2)	2	6	93
$[W(N^tBu)Me_2]_2(\mu\text{-}N^tBu)_2]$	1.736(5)	168.3(4)	0	5	94
$[WCl_3(N^tBu)]_2(\mu\text{-}Cl)_2]$	1.704(5)	172.9(5)	0	6	95
$[W(NPh)(NMe_2)_4]$	1.758(5)	180	0	5	96
$[WCl_3(NPh)(PMe_3)_2]$	1.731(6)	175.8(6)	1	6	97
$[WCl_3(NPh)(PPh_3)_2]$	1.742(8)	172.3(7)	1	6	133
$[WCl_2(NPh)(PMe_3)_3]$	1.755(3)	179.5(3)	2	6	133
$[Cp^*_2V(NPh)]$	1.730(5)	178.2(6)	1	7	98
$[Cp^*_2V(NC_6H_3Me_2)]$	1.707(6)	179.7(5)	1	7	99
$[Cp_2V(NSiMe_3)]$	1.665(10)	178.0(6)	1	7	100

Table 1.3 Continued

(Hydrazido)		∠M—N—N			
$[Mo(O)(NNMe_2)(SPh)_3]PPh_4$	1.821(9)	152.5(10)	0	5	101
$[MoCl(NNMe_2)_2(PPh_3)_2]BPh_4$	1.752(5)	168.2(7)	0	6	104
	1.763(4)	163.8(4)			
cis-$[Mo(NNMePh)_2(S_2CNMe_2)_2]$	1.709(9)	172.6(8)	0	6	114
cis-$[Mo(NNPh_2)_2(S_2CNMe_2)_2]$	1.709(8)	169.9(8)	0	6	114
cis-$[Mo(O)(NNPh_2)(SCH_2CH_2NMeCH_2)_2]$	1.778(3)	172.9(2)	0	6	102
$[Mo(O)(NNMe_2)(S_2CNMe_2)_2]$	1.799(8)	168.0(7)	0	6	103
$[MoF(NNH_2)(dppe)_2]BF_4$	1.762(12)	176.4(13)	2	6	147
$[MoI(NNHC_8H_{17})(dppe)_2]I$	1.801(11)	174(1)	2	6	104
$[MoCl(NNH_2)(triphos)(PPh_3)]Cl$	1.694(12)	172.2(11)	2	6	73
$[MoCl(NNH_2)(triphos)(PPh_3)]Cl$	1.778(18)	178.1(15)	2	6	73
$[WCl_3(NNH_2)(PMe_2Ph)_2]$	1.752(10)	178.7(9)	1	6	205
$[WCl_3(NNHPh)(PMe_2Ph)_2]$	1.738(5)	172.5(6)	1	6	105
$[W(NNH_2)Cl(dppe)_2]BPh_4$	1.73(1)	171(1)	2	6	84
$[WBr(NNHMe)(dppe)_2]Br$	1.768(14)	174(1)	2	6	106
$[WI_2(NNHSiMe_3)(PME_2Ph)_3]$	1.777(17)	171.4(16)	2	6	107

* Coordination Number

cleavage of α bond of a ligand precursor, that is the α atom of the ligand precursor undergoes deprotonation, desilylation, dealkylation or cleavage of electronegative leaving group.

Removal of the αH from amido or hydrazido(1-) ligand [108-109] leads to the formation of imido(2-) or hydrazido(2-) ligand.

$$[Cp^*WMe_4(NHNH_2)] \xrightarrow{-CH_4} [Cp^*WMe_3(NNH_2)] \quad (1.13)$$

$$[Ta(NMe_2)_4(NHt^tBu)] \xrightarrow{-Me_2NH} [Ta(NMe3)(NtBu)] \quad (1.14)$$

In these cases the precursor complexes possess strong basic leaving groups such as σ alkyl or dialkylamido ligands. Complexes of MX_mL_n type can react with alkylamine to give rise to an imido compound [110].

$$WCl_6 + 10^tBuNH_2 \longrightarrow [W(N^tBu)_2(NH^tBu)_2 + 6^tBuNH_3Cl \quad (1.15)$$

The cleavage of an α-silylsubstituent can also give a M-N multiple bond. This approach is productive in the synthesis of imido [111-113] and hydrazido [113-114] compounds. Two examples are shown.

$$WF_6 + (Me_3Si)_2NMe \xrightarrow{MeCN} [WF_4(NMe)(MeCN)] + 2Me_3SiF \quad (1.16)$$

$$[MoCl_4(PPh_3)_2] + (Me_3Si)NHNMe_2 \longrightarrow [MoCl(NNMe_2)_2(PPh_3)_2]Cl \quad (1.17)$$

This method offers some advantages. The formation of a strong covalent bond, particularly a Si-F or Si-O bond, enhances the driving force for such reactions. The side products such as Me_3SiCl, $(Me_3Si)_2O$ are volatile and can easily be distilled away with the solvent.

The cleavage of other α atoms, such as α-carbon [115-117], α-halogen [118], α-

oxygen [119] and α-nitrogen [120-124], also result in M-N multiple bonds.

1.3.1.2 "Wittig-Like" (2+2) Replacement

This class of reaction, in which an existing multiply bonded ligand is directly replaced by another on treatment with an unsaturated reagent, is useful for the synthesis of organoimido complexes from either oxo or alkylidene complexes. It is believed that all of these reactions involve a four-centre mechanism [125] as shown in Eq. 1.18.

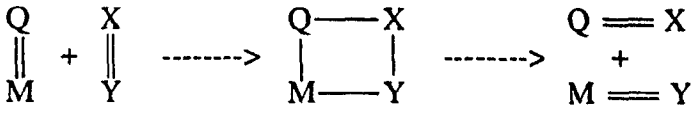

(1.18)

However replacement of an oxo by imido ligand is generally not a thermodynamically favoured reaction. The required driving force comes from the formation of a stable oxide (CO_2, SO_2, R_3PO). Two types of reagent are valuable for replacing an oxo ligand to give rise to a imido ligand. Phosphinimines $R_3P{=}{=}NR$ are used to synthesis rhenium, molybdenum and osmium imides [126-129].

$$[MoOCl_2(S_2CNEt_2)_2] \xrightarrow{PhN{=}{=}PPh_3} [MoCl_2(NPh)(S_2CNEt_2)_2] \qquad (1.19)$$

Isocyanates, $RN{=}{=}C{=}{=}O$, are more commonly used and this route has been developed into an important synthetic method. It was first used to convert oxo rhenium to imido rhenium [130]. A general reaction for synthesis phenylimido tungsten (n=4), rhenium(n=4) and vanadium (n=3) complexes [131-135] is shown in Eq. 1.20.

$$[M(O)Cl_n] + PhNCO \xrightarrow{\Delta} [MCl_n(NPh)] + CO_2 \qquad (1.20)$$

The release of CO_2 as gas shifts the reaction equilibrium to the right. Thus high yield are

normally obtained. Recently isocyanates have also been used to synthesize imido molybdenum complexes.

$$[MoO_2Cl_2(MeCN)_2] \xrightarrow{^tBuNCO} [MoOCl_2(N^tBu)(MeCN)_2] + CO_2 \qquad (1.21)$$

Other reagents that can be used to replace oxo ligands by organoimido ligands include arylsulfynilamines, ArNSO [136] and arylformamidines ArNHCH=NAr [137].

Methods for the conversion of alkylidene and alkylidyne complexes into their imido and hydrazido [138-140] analogs by using PhCH=NR and PhCH=NN=CHPh have also been demonstrated.

1.3.1.3 Formation of a bond to the αN Atom or βN Atom

Although the protonation and alkylation of nitrido complexes are known, these processes are far from common due to the poor nucleophilicity of the tightly bonded nitrogen atom. However, molybdenum and tungsten nitrido complexes [141-142] with chelating phosphine ligands, such as dppe, can be protonated to give cationic imido complexes. The complex $Mo(N)(dtc)_3$ (dtc=dimethyldithiocarbamate) possesses an unusually electron-rich nitrido ligand, thus it can be alkylated with methyl iodide [143].

$$[Mo(N)(dtc)_3] + MeI \longrightarrow [Mo(NMe)(dtc)_3]^+I^- \qquad (1.22)$$

Other alkylation reagents, such as PhCOCl, $(R_3O)BF_4$, $(Ph_2Cl)BF_4$ are also used [144-146].

Proton electrophilic attack on the βN of ligating dinitrogen produces hydrazido(2-) complexes. This has been described in Section 1.2.4 and 1.2.5. The typical ones are $[M(N_2)_2(dppe)_2]$ M=Mo in HBF_4 [147], M=W in TsOH [148], $[M(N_2)_2(PMe_2Ph)_4]$ M=Mo or W in HCl [107] and $[Mo(N_2)_2(triphos)(PPh_3)]$ in HCl [150].

Alkylation and acylation of ligating dinitrogen are processes of importance in industrial N_2 fixation. This type of reaction leads to the formation of N-C bonds and normally organodiazenido(1-) MNNR species are obtained, except those dinitrogen complexes with electron rich coligand such as depe [151] or crown thioether [21]. Further protonation or alkylation gives organohydrazido(2-) MNNHR or MNNRR' complex respectively [152-154]. Acyl, aroyl and alkyl halides are used as the alkyl and acyl sources [155-159]. Four examples are:

a). *trans*-$[M(N_2)_2(dppe)_2]$ $\xrightarrow{RCOCl/HCl}$ $[MCl(NNHCOR)(dppe)_2]Cl$

$\underset{H^+}{\overset{OH^-}{\rightleftharpoons}}$

$[MCl(NNCOR)(dppe)_2]$ (1.23)

(M=Mo, W; R=alkyl, aryl)

b). *trans*-$[M(N_2)_2(dppe)_2]$ $\xrightarrow{RX}$ $[MX(NNR)(dppe)_2]$

$\underset{H^+}{\overset{OH^-}{\rightleftharpoons}}$

$[MX(NNHR)(dppe)_2]$ (1.24)

(M=Mo, W; R=alkyl; X=Br, I)

c). *cis*-$[W(N_2)_2(dppe)_2] + Me_3SiI \xrightarrow{PMe_2Ph} [WI(NNSiMe_3)(PMe_2Ph)_4]$ (1.25)

d). $[M(N_2)_2(dppe)_2] + Br(CH_2)_nBr \longrightarrow [WBr(NN(CH_2)_{n-1}CH_2)(dppe)_2]Br$ (1.26)

(M=Mo, W; n=4,5)

All the examples above involve electrophilic attack on the βN atom of a metal-bound N_2. Nucleophilic attack of hydrido ligands on the βN of diazonium salts also gives

hydrazido(2-) compounds [160-161].

$$[Cp_2W(H)_2] + (Ph\text{-}N{\equiv}N)^+ \text{----------} > [Cp_2WH(NNHPh)] \qquad (1.27)$$

1.3.2 Electronic Structure of the M-N Multiple Bond

Imido and hydrazido complexes have metal-nitrogen multiple bonds which consist of a σ-bond and one or two π-bonds. The π interactions involve the overlap of metal dπ orbitals with pπ orbitals of the nitrogen atom. If the multiple bond is along the z axis, the π overlap will occur between d_{xz} and p_x, and/or between d_{yz} and p_y as illustrated in Fig.1.3. The p orbitals of nitrogen are lower in energy than those of metal d orbitals due to the high electronegativity of nitrogen. Thus in complexes, imido and hydrazido ligands are described as closed-shell anions NR^{2-} and NNR_2^{2-}, respectively [162]. Since these anions have their p orbitals filled, the formation of π bonds requires the metal d orbitals to be empty, i.e. the metal centre is in a high oxidation state with a low d electron count. In fact the majority of complexes with these ligands have d^0, d^1, d^2 electronic configurations [163].

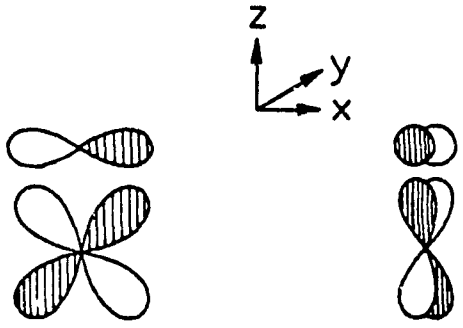

Fig. 1.3 Interaction between dπ and pπ orbitals.

In simple valence bond pictures, imido and hydrazido ligands form double bonds with metal atoms. However, they have the capability to form triple bonds with one filled

orbital of σ-symmetry and two filled p orbitals of π-symmetry perpendicular to the Z axis. In the case of imido, a linear M-N-R unit as (A) shown in the following, suggests

A B

that the ligating N atom is sp hybridized and there is triple bond, one σ-bond and two degenerate π-bonds. Bending of the M-N-R linkage (B) indicates the ligating N atom is sp^2 hybridized and the bond order of M-N is reduced. The bent structure B should be observed when there is only one metal orbital of π-symmetry available for bonding to the N atom. This can happen due to either a competition with another π-bonding ligand such as NR^{2-}, NNR_2^{2-}, O^{2-}, N^{3-} or the presence of two dπ orbitals which are filled, consistent with a stable 18-electron core. Complex $[Mo(NPh)_2(S_2CNEt_2)_2]$ clearly shows both bent and roughly linear imido ligands [128]. The bent imido ligand has a smaller Mo-N-C angle of only $139.4(4)^0$ and a longer Mo-N bond of 1.789(4)Å compared to the linear one whose Mo-N-R angle is $169.4(4)^0$ and M-N distance is 1.754(4)Å. This molecule is described having one M-N double bond and one triple bond, using the three π-symmetry d orbitals on the Mo centre. Monoimido complexes normally contain M-N triple bonds (represented by short M-N distance) and linear bonding modes ($\angle$M-N-R>155^0). In the case of $[MoCl_2(NPh)(S_2CNEt_2)_2]$, the Mo-N distance is only 1.734(4)Å (see Table 1.3).

The substituents (-R) of imido groups are very important to the chemistry of the M-N multiple bond. This is particularly true when R has an accessible π symmetry orbital, since the π orbital can conjugate with the M-N π orbitals. This interaction splits the degeneracy of the π orbitals of the triple bond and reduces the M-N bond order.

Therefore the M-N bond order of alkylimido should be higher than that of phenylimido. This can be seen clearly in the imido vanadinum complexes (Table 1.3). The M-N bond order decreases on going from $[Cp^*_2V(NSiMe_3)]$ to $[Cp^*_2V(NC_6H_3Me_2)]$ to $[Cp^*_2V(NPh)]$ with increasing the M-N-R conjugation.

In the hydrazido ligand, NR_2^{2-} can be treated as the -R group of an imido ligand (NR^{2-}). Since there is a lone pair on the βN atom, a variety of resonance forms are possible for the hydrazido ligand [49, 164-165], as illustrated in the following. However most of the hydrazido(2-) complexes exhibit a linear M-N-N linkage.

$M^-\equiv N^+-NH_2$ $\qquad$ $M^{2-}=N^+=N^+H_2$ $\qquad$ 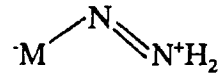

Calculations [162] on the hydrazido tungsten complex $[WCl(NNH_2)(dppe)_2]^+$ indicate that the lone pair on the βN atom is very involved in the bonding and there is multiple bond character in the N-N linkage. Therefore longer M-N bonds are often observed , and hydrazido ligands are probably best considered as vinylidene analogues with M-N double bond.

As in the case of imido, the βR groups on the hydrazido ligand are important when they have accessible π orbitals. The interaction between the βN lone pair and the βR π orbitals diminishes the conjugation between the βN and the multiple bond, thus the overlap of the αN p orbitals with the metal dπ orbitals is enhanced. This can be clearly seen from the data in Table 1.3. For example, the complex $[WCl_3(NNH_2)(PMe_2Ph)_2]$ has an M-N distance of 1.752(10)Å, whereas complex $[WCl_3(NNHPh)(PMe_2Ph)_2]$ has a shorter M-N distance of 1.738(5)Å. On the contrary, the complex $[WBr(NNHMe)(dppe)_2]^+$ has an M-N distance 0.038Å longer than that in the complex $[WCl(NNH_2)(dppe)_2]^+$

perhaps due to the donation of the methyl group promoting the conjugation between the βN and the multiple bond. In fact most hydrazido(2-) complexes derived from Mo and W dinitrogen complexes exhibit M-N bond distance ranging from 1.73 to 1.80Å and M-N-N angle from 171 to 179^0.

The bond strength and the reactivity of the M-N multiple bond depends greatly on the nature and the oxidation state of the metal centre and the other ligands presented. Normally, the higher the oxidation state of the central metal, and the higher its electronegativity, the less repulsion exists between the d electrons and the multiple bond, thus the shorter the M-N distance. For example, W(V) complex $[WCl_3(NPh)(PMe_3)_2]$ has an M-N distance 0.024Å shorter than W(IV) analogue $[WCl_2(NPh)(PMe_3)_3]$ (Table 1.3). The co-ligands exhibit either electronic or steric effects, or both on the multiple bond. Usually those co-ligands with bulky substituents or possessing high donation capability lead to the reduction of the multiplicity of the bond. Theoretical calculations [32] on the model $X_4M{\equiv}N\text{-}N{\equiv}MX_4$ (M=Mo, W; X=F, Cl, Br) indicate that the addition of σ-donor ligands such as phosphines, amines or ethers will expand the metal d orbitals, enhancing the overlap with the nitrogen p orbitals and increasing the M-N π-bond strength. Alternatively, substitution with less electronegative ligands, for example substitution of fluoro, oxo with chloro or bromo will also expand the d orbital, increasing the M-N π-bond strength. Also, substitution of Mo with W will increase the inherent size of the d orbital, thus strengthening the M-N π-bond [166].

Interestingly, there are isomers of $[MoCl(NNH_2)(triphos)(PPh_3)]$ which show quite different M-N distances and M-N-N angles (Table 1.3) and their solutions are different coloured. But they are not *cis/trans* isomers. Recently they were described as a pair of

"distortional isomers" with two equal arrangements of ligands but different in the distortion of the coordination polyhedron of the metal [73].

1.3.3 Ligand Field Description of M-L Multiple bond

The majority of complexes containing a M-L multiple bond are six-coordinate and adopt an octahedral geometry. Complexes having an octahedral geometry are easy to analyze in molecular orbital terms. In the molecule which has Oh symmetry the five metal

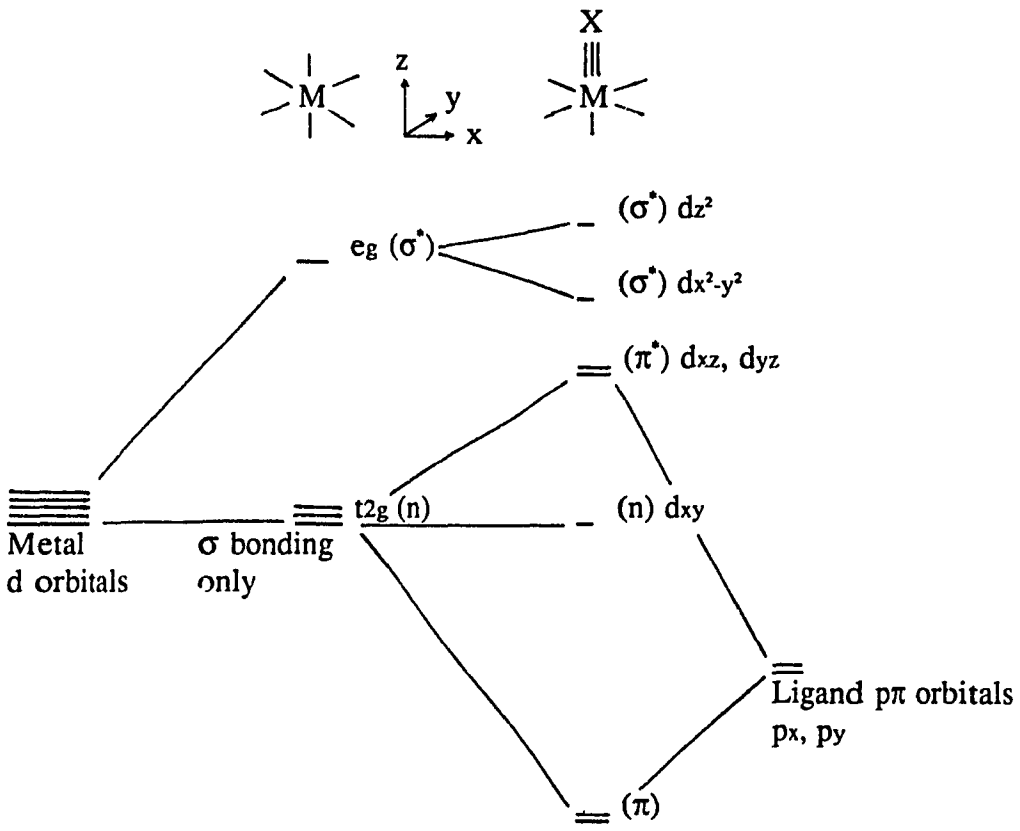

Fig.1.4 Partial molecular orbital diagram for an octahedral complex with one M-L triple bond.

d orbitals split into a degenerate e_g ($d_{x^2-y^2}$, d_{z^2}) set of σ^* character and a nonbonding t_{2g} (d_{xy}, d_{xz}, d_{yz}) set. Introducing of a cylindrically symmetric π-bonding ligand, a ligand

which can form a triple bond such as N^{3-}, NR^{2-}, O^{2-} and CR^{3-}, lowers the symmetry to C_{4v} d splits t_{2g} as well as e_g orbitals (Fig. 1.4) [162].

Qualitatively the t_{2g} orbitals are substantially split because two of them form π bonds. Normally they are d_{xz} and d_{yz} if Z axis is taken as multiple bond axis. The two orbitals of the e_g set are also no longer degenerate. Although both of them remain σ^* character and the split is small, the energy level of d_{z^2} is higher than that $d_{x^2-y^2}$, because the interaction between metal centre and the ligand is stronger in Z direction than in X and Y directions. Thus the ligand field portion of the molecular orbital diagram contains, in the order of increasing energy, a nonbonding d_{xy} orbital, a degenerate π^* set of d_{xy} and d_{yz}, and two σ^* levels $d_{x^2-y^2}$ and d_{z^2}. This is consistent with the fact that M-L triple bonds are found predominantly in d^0, d^1, d^2 electronic configurations. In d^3 and d^4 complexes electrons will occupy π^* orbitals and destabilize the π^* orbitals [167].

The ligand field arguments have been supported by spectroscopic data, structural data and theoretical calculations [168-172]. These data also indicate a large gap between the nonbonding d_{xy} and the π^* d_{xz}, d_{yz} orbitals. It explains why all octahedral d^2 complexes with multiply bonded ligands are diamagnetic. The two electrons are paired in the d_{xy} orbital. Furthermore d^2 complexes with π-acid ligands (such as CO) prefer the ligands lying *cis* to the multiple bond, so that the filled d_{xy} is used for back donation [173-174].

Octahedral d^0 complexes with two multiple bonds prefer that the two ligands adopt *cis* geometry, in order to use all three $d\pi$ orbitals. The net bond order to each ligand is 2.5 [128]. The *cis* arrangement satisfies the formation of the multiple bonds, but introduces great distortion into the geometry. This distortion is mainly due to the

repulsion between the two multiple bonds, consequently a large angle is observed. For example, in bisimido complexes $[Mo(NPh)_2(S_2CNEt_2)_2]$ the N-Mo-N angle is 103.5^0. In the d^2 case the two multiply bonded ligands adopt a *trans* structure, so that the two electrons can occupy a nonbonding d_{xy} orbital, leaving d_{xz} and d_{yz} orbitals to form π bonds. In this case a *trans*-influence should be observed.

The molecular orbital description for octahedral complexes presented above can also be used in the square pyramidal geometry, another common structure adopted by five coordinated complexes with multiple bonds and C_{4v} symmetry. It can be treated as a defective octahedral geometry which exhibits a large *trans* influence and a better M-L overlap of the multiple bond. The optical spectra [175] indicate that the absence of the sixth ligand does not significantly alter the relative d_{xy} and d_{xz}, d_{yz} orbital energies, but it may have the effect of lowering the energy of a σ^* component of the multiple bond.

1.3.4 Reactivity of Multiple Bond

The reactivity of multiple bonded ligands depends on the the metal and its electron affinity, the ligand and ancillary ligands. It has been discussed in terms of both charge control [176-177] and frontier orbital control [178-180]. The nature of the frontier orbitals (HOMO) and the electron density on the ligand vary markedly with the ligand and the metal. In one extreme case (A in Fig. 1.5), the energy of the ligand $p\pi$ orbitals is lower than the metal d orbitals and the ligand is an anion acting as a π donor. The π-bonding molecular orbitals (HOMO) are contributed mainly by the ligand orbitals while the π^* orbitals are principally metal d orbitals. In this case, the ligand is a nucleophile. In another extreme case (C), the energies of the ligand $p\pi$ orbitals, which are empty, are

higher than the metal dπ orbitals. The π bonding molecular orbitals are predominantly

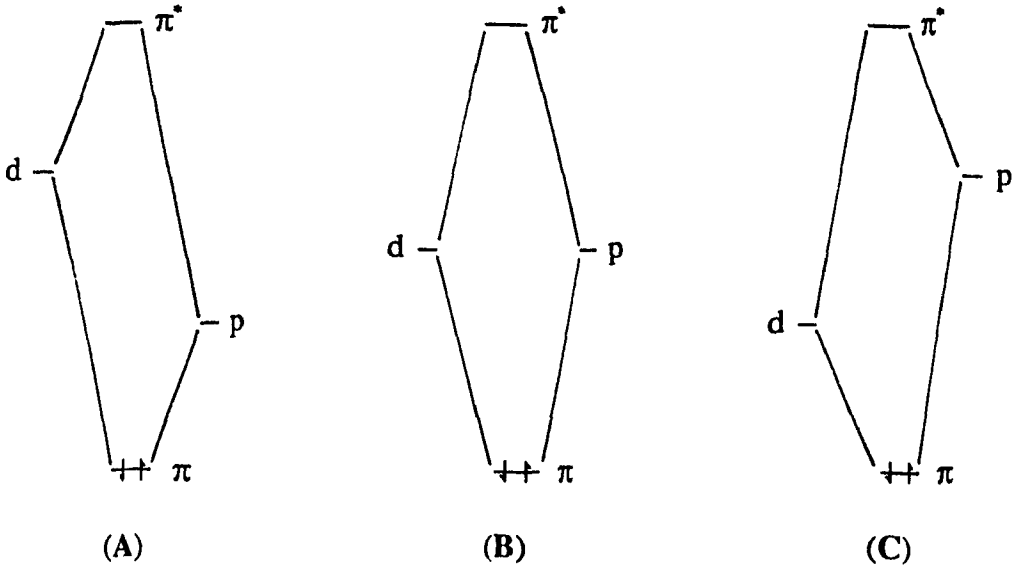

Fig. 1.5 Changes in metal d-ligand pπ interactions as the relative energies of the atomic orbitals are changed.

metal d orbitals in character and the π^* (LUMO) are based principally on the ligand, giving rise to electrophilic reactivity. There is a continuum between the two extreme cases, which is partially traversed on moving from oxygen to nitrogen to carbon ligands and on moving from early to later transition metals. (**B**) is the description of the situation in which the p orbitals of the ligand α atom and the metal d orbitals are involved in covalent bonds. This will diminish markedly the nucleophilicity of the α atom and the electrophilicity of the metal.

As an example of situation (**A**), the complex $[Ta(NEt)(NEt_2)_3]$ cleaves its Ta-N multiple bond by treatment with ethanol. This reaction is assumed to involve protonation of the imido nitrogen. In contrast the alkylimido osmium(VIII) species $OsO_3(NR)$ can be

used as a model to account for the situation (**B**). On treatment even with HCl, it is not the Os-N bond cleavage, instead the C-N bond is broken [181]. This is due to the π donation by the N atom in Os complex being much higher than that in Ta complex. In fact the Os-N bonds are predominantly covalent in character. The effects of increasing π donation are summarized in Fig. 1.6. Increasing the electronegativity of the metal also increases the π donation and decreases the bond strength between N and the β atom. For example, in *trans*-[MX(NH)(dppe)$_2$]X complexes the acidity of the imido proton is increased 1000-fold on changing M from tungsten to molybdenum [182].

In general the complexes possessing M-N multiple bonds fall in the range between A and B, while C is a description of bonding involving π acid ligands. It should be noted

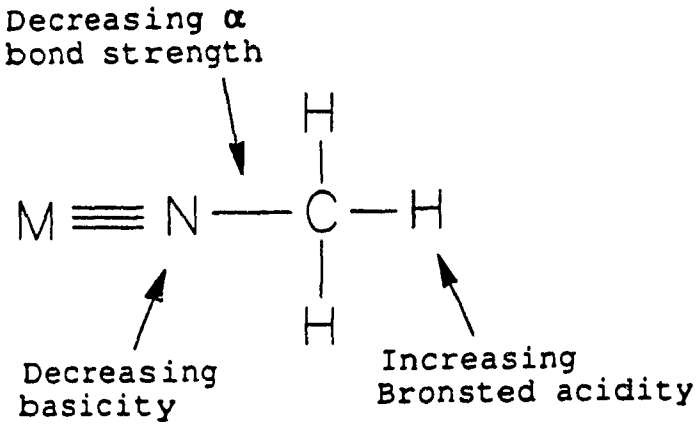

Fig. 1.6 Some effects of increasing the π-acceptor capability of the metal on the reactivity of a methylimido complex.

that in addition to the arguments based on orbital energies, the reactivity of the M-L multiple bond is also significantly influenced by the size of the metal and ligand orbitals and the magnitude of the M-L overlap [176, 183].

1.3.5 Reaction of Imido and Hydrazido Ligands

1.3.5.1 Reactions with Electrophiles

Imido complexes, *trans*-$[MX(NH)(dppe)_2]X$ (M=Mo, W; X=F, Cl, Br, I) undergo ready protonolysis in basic methanol [141, 182]. It is believed that the imido ligand is first deprotonated by the base to form a nitrido ligand. Its strong trans effect labilizes the halide ligand to form an ion pair $[M(N)(dppe)_2]^+X^-$. Addition of methanol produces a new imido complex with a trans methoxo ligand, $[M(NH)(OCH_3)(dppe)_2]^+$. The π donation capability of the methoxo activates the imido ligand toward protonation and finally ammonia is obtained. Organoimido complexes can also be N-protonated. An example is shown in Eq. 1.28 [184].

$$[Re(NPh)(Me)_3(PMe_3)_2] + HBF_4 \dashrightarrow [ReF(NHPh)(Me)_2(PMe_3)_2]BF_4 \qquad (1.28)$$

The protonation of hydrazido(2-) complexes is more complicated. Several possible products may be obtained: hydride-hydrazido(2-) complexes with a $M(H)(NNH_2)$ moiety and hydrazido (1-) complexes with a $M(NHNH_2)$ moiety (Section 1.4), and complexes with a NNH_3^+ ligand. These products are very sensitive to the metal, the co-ligands, the acid and solvent used. The hydrazinium complex is a presumed intermediate in the route of production of ammonia (Section 1.2.5).

The imido ligand can also be alkylated. Treatment of the molybdenum complex in Equation 1.29 with excess methyl bromide results in methylation of one imido N atom only [129].

$$cis\text{-}[Mo(NPh)_2(dtc)_2] + 3MeBr \dashrightarrow [MoBr_2(NPh)(dtc)_2] + NMe_3PhBr \qquad (1.29)$$

The complex $[Cp^*_2V(NPh)]$ undergoes methylation with loss of one Cp^* [120]. Intramolecular alkylation of imido ligands is also known [185-186].

1.3.5.2 Metathesis Reactions

The replacement of an oxo by an imido ligand is generally not thermodynamically favoured. Conversely, the reactions with aldehydes are typical reactions for imido complexes [181].

$$M{=}N{-}R + R'CH{=}O \text{ ----------> } M{=}O + R'CH{=}NR \qquad (1.30)$$

Hydrazido(2-) complexes react with aldehydes and ketones at the β- rather than that the α-nitrogen atom, as shown in Eq. 1.31 [187-188].

$$M{=}N{-}NH_2 + R_2C{=}O \text{ ----------> } M{=}N{-}N{=}CR_2 + H_2O \qquad (1.31)$$

This is probably due to the dπ-pπ interaction in hydrazido(2-) complexes decreasing the electron density on the αN atom relative to the unligated NH_2 group. However, under appropriate conditions [189] the αN atom can be induced to react with a carbonyl compound.

1.3.5.3 Reactions with Nucleophiles

The hydrogen bonded to the N atom of imido ligands exhibits enhanced acidity due to the ligand-to-metal π donation. Deprotonation of these species produces nitrido complexes. The enhanced acidity is also observed in the βH atoms (Fig. 1.6) of some alkylimido complexes of the more electronegative transition metals, such as rhenium in Eq. 1.32 [190].

$$[ReCl_3(NCH_3)L_2] + 2Py \text{ --------> } [ReCl_2(NCH_2)(Py)L_2] + Py{\cdot}HCl \qquad (1.32)$$

$$(L{=}PPh_3,\ PMePh_2,\ PEtPh_2)$$

Although the product was not structurally characterized, the alkylidenamido moiety is suggested to have a linear structure [191], implying a three-electron donor ligand like

nitrosyl.

The βH atoms of hydrazido molybdenum and tungsten complexes also show some acidity. The kinetic studies indicate that the deprotonation of tungsten complexes [192] is 10^5 times slower than that molybdenum analogue [193].

1.3.5.4 α Cleavage Reactions

The cleavage of the α bond of imido is a useful route to synthesise the corresponding nitrido complexes. Under appropriate conditions, a hydrazido ligand NNH_2 undergoes N-N bond cleavage leading to the formation of ammonia. A selection of results from such reactions is summarized in Table 1.4. In terms of the protonation mechanism of dinitrogen complexes (Section 1.2.5), the N-N cleavage should also give nitrido or imido intermediates. However no imido or nitrido complexes have been isolated and identified from this type of reaction, probably due to the fast protonations of these intermediates.

The influence of the metal, the ancillary ligand, the reagent and solvent on the yield of ammonia has been discussed in Section 1.2.4. Recently, a steric effect on the formation of ammonia was observed in the studies of the isomeric exo and endo hydrazido complexes, $[Mo(NNH_2)(dpepp)PR_3]$, which are generated by protonation of the corresponding bis(dinitrogen) complexes and show different activity towards the ammonia formation [150]. The exo-hydrazide (phenyl group and hydrazido ligand mutually trans) is much more reactive than the endo one, probably owing to the lesser steric hindrance around the hydrazido ligand in the exo-isomer.

Certain dialkylhydrazido(2-) complexes also show the N-N cleavage upon the

Table 1.4 Yields of ammonia and hydrazine from hydrazido(2-) complexes of molybdenum and tungsten.

Complex	Reagent	Solvent	yield*			Ref
			NH_3	N_2H_4	N_2	
$[WCl_2(NNH_2)(PMe_2Ph)_3]$	H_2SO_4	MeOH	1.26	0.12		67
$[WBr_2(NNH_2)(PMe_2Ph)_3]$	H_2SO_4	MeOH	1.58	0.05	0.0	67
$[WI_2(NNH_2)(PMe_2Ph)_3]$	H_2SO_4	MeOH	1.88	0.04	0.0	67
$[WCl_2(NNH_2)(PMe_2Ph)_3]$	HCl	DME	0.47	0.50		41
$[MoCl_2(NNH_2)(PMe_2Ph)_3]$	H_2SO_4	MeOH	0.61	0.0	0.44	67
$[Mo(NNH_2)(quin)(PMe_2Ph)_3]I$	H_2SO_4	MeOH	0.55	0.0	0.17	67
$[MoCl_2(NNH_2)(PMe_2Ph)_3]$	HCl	DME	0.24	0.52		41
$[WHClBr(NNH_2)(PMe_2Ph)_3]Br$	H_2SO_4	MeOH	0.63	0.34		41
$[WHClBr(NNH_2)(PMe_2Ph)_3]Br$	HCl	DME	0.50	0.55		41
$[WHCl_2(NNH_2)(PMe_2Ph)]Cl$	H_2SO_4	MeOH	0.97	0.42		205
$[WHCl_3(NNH_2)(PMe_2Ph)_2]$	H_2SO_4	MeOH	0.60	0.25		205
$[WCl_2(NNH_2)(PMe_2Ph)_3]$	KOH	H_2O	1.40	0.14		67
$[WBr_2(NNH_2)(PMe_2Ph)_3]$	$NaBH_4$	THF	1.3	0.0		67

* Mol/M atom

treatment with acid or lithium aluminum hydride [194-195].

1.4 Other Possible Intermediates In N_2-Fixation

The possible intermediates in nitrogen fixation will be discussed based in the proposed mechanism represented in Scheme 1.1 or on the steps of protonation on the dinitrogen ligands.

1.4.1 Diazenido Complexes

The first protonation of ligating dinitrogen would give a diazenido complex with a NNH ligand, but this has not been isolated directly probably due to the rapid second protonation [196]. Careful deprotonation of hydrazido(2-) complexes $[MX(NNH_2)(dppe)_2]X$ by weak base gives rise to diazenido complexes $[MX(NNH)(dppe)_2]$ [149]. These complexes show a strong band in the 1820-1940 cm^{-1} in IR spectra assigned to ν(NN) which is somewhat higher than that expected for a structure with a bent NNH group. The complexes with X=Cl or Br do not exhibit any bands assigned to ν(NH). Later studies suggest that these diazenido complexes may be hydrido dinitrogen complexes [197]. However many aryl- or alkyldiazenido complexes have been synthesized. In general, they adopt singly bent or doubly bent geometries, which can be distinguished by measuring ^{15}N NMR chemical shifts [198].

Although diazenido ligands have lower polarity than the dinitrogen analogue with a charge difference between nitrogen atoms of about 0.1 units [2], they undergo

electrophilic attack. Doubly bent diazenido ligands are always protonated at the αN to form diazene ligands (NHNR). While singly bent diazenido ligands are protonated at either αN or βN atoms, depending on the nature of the metal and coligands [199], to give rise to diazenido or hydrazido(2-) ligands, respectively.

1.4.2 Diazene Complexes

The diazene moiety has been postulated to be one of the intermediates in nitrogen fixing reactions. Three structures adopted by diazene ligands with their related complexes are shown below [2, 200]. However, no diazene complexes have been obtained directly from the conversion of coordinated dinitrogen, and no stoichiometric conversion to hydrazine or ammonia has been demonstrated [201].

$[ReCl(NHNC_6H_4F)(PEt_3)_2]^+$

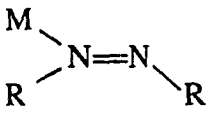

$[Ni(NPhNPh)(^tBuNC)_2]$

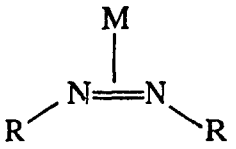

$[\{Ru(PPh_3)(dttd)\}_2(\mu\text{-}N_2H_2)]$

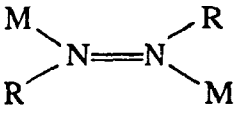

The protonation of the bridging diazenido tungsten complexes lead to the formation of bridging hydrazido(2-) complexes with $W\text{-}NH_2\text{-}NH_2\text{-}W$ moieties.

1.4.3 Hydride-Hydrazido(2-) Complexes

The mechanism of hydrazine formation from hydrazido(2-) complexes originally was believed to involve the third protonation on the αN to give a hydrazido(1-) moiety $NHNH_2$ [202]. Complexes $[WX_2(NNH_2)(PMe_2Ph)_3]$ (X=Cl, Br) were treated with halogen acids, or *trans*-$[W(N_2)_2(PMePh_2)_4]$ was treated with HCl in dichloromethane to give hydrazido(1-) complexes. This was supported by theoretical studies [203] and X-ray crystallography [204]. However, later X-ray structure [41] and ^1H, ^{15}N NMR [205] studies unambiguously demonstrated that the third protonation occurs on the metals producing two hydride-hydrazido(2-) complexes, $[WHX_2(NNH_2)(PMe_2Ph)_3]X$ and $[WHCl_3(NNH_2)(PMePh_2)_2]$. In one of the former complexes (X_2=Cl and Br), inter- and intramolecular hydrogen bonds exist between the N-hydrogen atoms and the halide ions. Further protonation of these hydride-hydrazido(2-) complexes produces hydrazine in relatively high yields, whereas protonation of the hydrazido(2-) complexes $[MX_2(NNH_2)(PMe_2Ph)_3]$ (X=Cl or Br) produces ammonia in high yield under similar protonation conditions (see Table 1.4). This clearly indicates that a hydride-hydrazido(2-) complex is the intermediate following the hydrazido(2-) complex and is probably on the route to hydrazine.

1.4.4 Hydrazido(1-) Complexes

True hydrazido(1-) complexes $MNHNH_2$ correspond to the third protonation of a ligating dinitrogen. Two bonding structures have been identified.

In $[Cp_2W(NH_2NAr)]X$ (Ar=Ph, *p*-C_6H_4F; X=BF_4, PF_6), the ligand binds to the metal through both nitrogen atoms in a side-on mode [160]. The unidentate structure has been found in rhenium, molybdenum and tungsten compounds [161, 206]. They release hydrazine under acid conditions. The complex $[Mo(NNMePh)(NHNMePh)(S_2CNMe_2)_2]^+$, which comes from the protonation of complex $[Mo(NNMePh)_2(S_2CNMe_2)_2]$ with an equivalent of HCl, contains both end-on hydrazido(2-) and side-on hydrazido(1-) ligands [204]. Addition of an excess of acid gives $[MoCl_2(NNMePh)(S_2CNMe_2)_2]$ and liberates hydrazine $PhMeNNH_2$ quantitatively. This suggests that the αN in hydrazido(1-) protonates somewhat more easily than the αN located on hydrazido(2-) ligand.

1.5 FeMoS Cluster

Since the discovery of the FeMo-cofactor in nitrogenase, inorganic chemists have made great efforts to synthesis and characterize FeMoS clusters in order to understand the

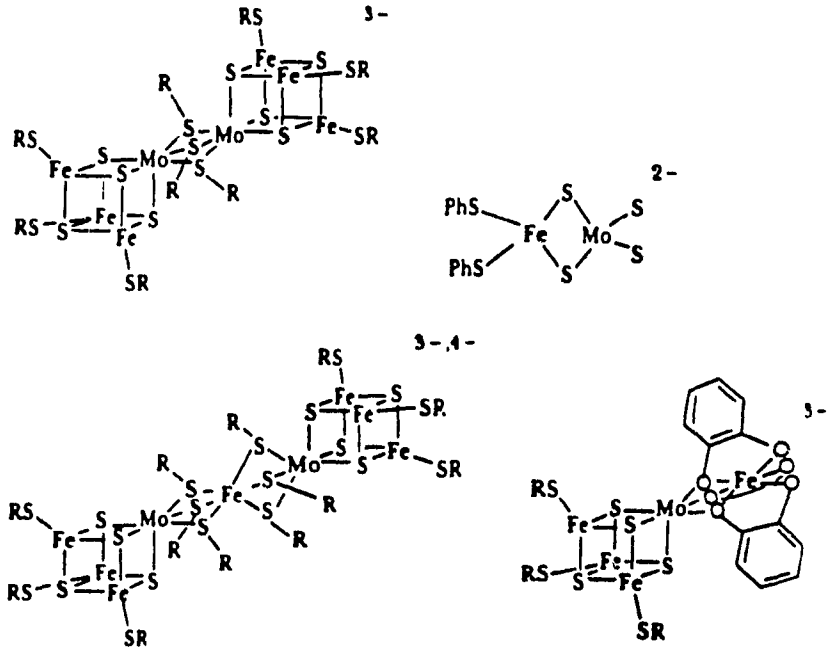

Fig. 1.7 Some possible models for the FeMo-cofactor.

chemical behaviour of the FeMo-cofactor [207-219]. Some clusters that have been prepared and studied as a possible models for the FeMo-cofactor are shown in Fig. 1.7. The original problems [219] in syntheses are the lack of systematic methods and poor yields, and the apparent lower ratio of Mo:Fe:S as compared to the true cofactor (the ratio in cofactor has not been definitely identified). So far there are only two general strategies adopted in the preparation, in which a homonuclear cluster is synthesized first and then converted to a heteronuclear one by metal group displacement. The other is "heterometallic condensation" to form a bimetallic cluster directly from two different metal complexes. In the other hand, many clusters with higher Mo:Fe:S ratio have been synthesized [5, 210].

The redox behaviour of the FeMoS clusters varies from type to type. The electrochemical studies reveal that several redox processes exist and the redox potentials of a cluster are sensitive to the environment of the metals, the hydrophilic or hydrophobic nature of the clusters, the solvent, the pH and hydrogen bonding [5, 207, 216, 218]. In the $[MoFe_3S_4(Me_2dtc)_5]$ cluster case, the redox process of $Fe^{3+} \rightleftharpoons Fe^{2+}$ is reversible with a potential about -0.4V (SCE), while the two more negative redox processes (potentials fall in the range of -0.9 to 1.2V) are irreversible [218]. The EPR and Mössbauer studies on the $MoFe_4S_6$ cluster indicate that the coordination of Mo to the Fe_4S_6 core has little influence on the electronic distribution within the Fe-S cage [214].

Tanaka et al [211] successfully reduced pentylazide n-$C_5H_{11}N_3$ in a cubane-like cluster $[MoFe_3S_4(SC_6H_4$-p-n-$C_8H_{17})_3(O_2C_6Cl_4)L]^{2-}$ (L=solvent) solution to amine n-$C_5H_{11}NH_2$, hydrazine and ammonia corresponding to 2e, 6e and 8e reduction processes respectively. The catalytic reduction of NO_3^- giving NH_3 *via* NO_2^- and NH_2OH has also

been achieved by using a $[Mo_2Fe_6S_8(SPh)_9]^{3-}$ modified glassy carbon electrode in water [209].

Based on their studies on a butterfly MoFe cluster containing a π bond four-electron-donating carbonyl ligand, Gibson et al. [212] proposed a structural model for the active site of the nitrogenase, although they failed to protonate it and have not obtained dinitrogen cluster. Their model involves a butterfly-like $MoFe_3$ fragment containing a π-bonded N_2 molecule. The protonation-reduction needed to produce two NH_3 molecules

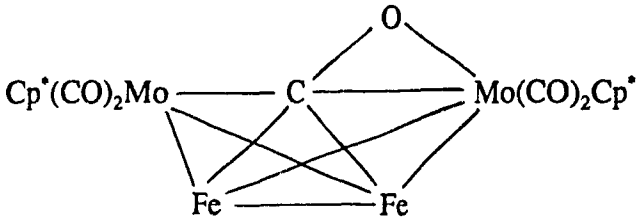

from the η^2-coordinated N_2 ligand is presumed to include a proton-induced N-N bond cleavage to give one NH_3 molecule and an intermediate butterfly-like $MoFe_3(\mu_4\text{-}N)$ fragment of an FeMo core.

A cluster [213] containing two hydrazido(2-) ligands shows very similar Mo-N, N-N distance and Mo-N-N angles with those listed in Table 1.3. Some other clusters, containing vanadium, magnesium, cobalt, copper and rhenium are also synthesized and studied [208, 216-217, 219-220]. Unfortunately there are no models that have any functional realism, although some notable EXAFS similarities have been observed. For example, none of the models duplicate the electrochemistry of the real FeMo cofactor [5].

CHAPTER II

PURPOSE AND MODEL DESIGN

2.1 Purpose

In terms of the step by step protonation-reduction of ligating dinitrogen to ammonia discussed in Chapter I, the hydrazido(2-) complexes represent an important stage existing in the course of N_2-fixation. Although chemists have put a great effort into the study of the mechanism of the subsequent protonation and reduction of many hydrazido(2-) complexes under various conditions, it is still far from clear owing to the difficulty in the isolation of the post-hydrazido intermediates, such as nitrido and imido complexes, and the limitations of the characterization techniques. The formation of ammonia or/and hydrazine from certain hydrazido complexes is very dependent on the coordination environment and reaction conditions. In H_2SO_4/MeOH media, the tungsten hydrazido complex $[WX_2(NNH_2)(PMe_2Ph)_3]$ (X=Cl, Br, I) gives ammonia stoichiometrically (see Table 1.4), while the analogous molybdenum hydrazido complex $[MoCl_2(NNH_2)(PMe_2Ph)_3]$ undergoes a disproportionation reaction (Section 1.2.5) giving rise to ammonia and N_2 gas. This suggests that the βN atom on the hydrazido tungsten complex is still relatively negatively charged or that the lone pair of βN is principally localized on βN itself and ready for the further electrophilic attack by a proton to give a $WN\text{-}NH_3^+$ species. The third protonation on βN is a key step to promote the cleavage of the N-N bond resulting in the quantitative formation of ammonia. This may be due to the strong interaction between the pπ orbitals of αN and the dπ orbitals of tungsten, and

the electron releasing capability of tungsten. If the third protonation gives a hydride species, instead of ammonia, hydrazine will be the main product.

In contrast, the molybdenum complex undergoes a disproportionation reaction at the hydrazido(2-) stage in the same conditions. This implies that the electrons required for the further quantitative reduction of a hydrazido complex to give ammonia come from an external source rather than from molybdenum itself, and a weaker Mo-N interaction relative to the W-N interaction.

In biological nitrogen fixation, the required electrons are supplied by the FeS protein and the required energy is offerred by the hydrolysis of MgATP to MgADP and phosphate. In inorganic chemical conditions, the question of how to supply electrons to the metal centre, especially to the molybdenum centre, and how to carry on the further protonation on the βN to promote the cleavage of the N-N bond are under investigation. The information from imido and hydrazido ligands bonded to transition metals, and their protonation, is not only important to the understanding of the function of the active site in the natural nitrogenase, but also to the design of an effective catalysis for the conversion of dinitrogen into nitrogen hydrides and organonitrogen compounds under mild conditions. However, so far, no optimum of hydrazido and imido complex models and the conditions for their reduction-protonation have been found.

It was proposed, in my project, to synthesize several imido(2-) and hydrazido(2-) molybdenum complexes as potential models, to characterize these complexes, and then to study their reduction- protonation behaviour.

2.2 A Potential Model in N_2-Fixation

The potential model which was proposed for the study of the imido(2-) and hydrazido(2) complexes is shown below. It contains a six coordinated molybdenum which is surrounded pseudooctahedrally by four sulfur atoms, one nitrogen atom and one ligand.

[Mo(NR)(dttd)(L)] where:

$(dttd)^{2-}$=2,3:8,9,-dibenzo-1,4,7,10-tetrathiadecane(2-),

R=Me, Ph for imido(2-) complexes,

R=NMe_2, NPh_2 for hydrazido(2-) complexes,

L=solvent or other ligand (depending on the preparation method and the precursor molybdenum compound used).

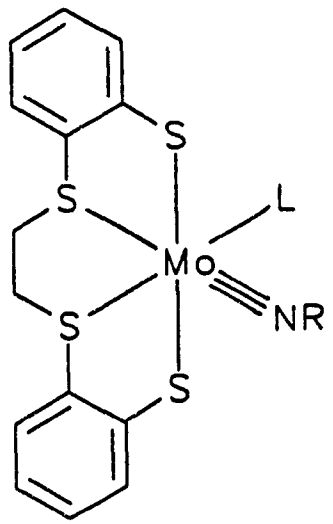

Fig. 2.1 The potential model in this thesis.

2.2.1 The Molybdenum Centre

The transition metal molybdenum is used as the metal centre of the potential

model, since the active site of nitrogenase in nature contains a FeMo-cofactor, and it is widely believed that the dinitrogen molecule binds to at least the molybdenum. Although vanadium and tungsten have been found in some bacterial enzymes, they are far from common compared with molybdenum.

In inorganic nitrogen fixation chemistry, tungsten seems more successful than molybdenum in playing a functional role in bonding and reducing dinitrogen. However, in order to understand the mechanism of nitrogen fixation in nitrogenase and to find a way to produce nitrogen-containing fertilizer industrially under a mild conditions, the study of a potential model which possesses the similarity to the active site in natural nitrogenase, i.e. a molybdenum centre with a sulfur coordination sphere, is still the most attractive.

From the point of view of bonding theory, the formation of imido or hydrazido complexes with early transition metals is prefered, with a metal centre having a d^0~d^2 electron configuration in order to meet the requirement of empty $d\pi$ orbitals for the multiple bond formation. Thus for molybdenum, the oxidation state should be IV to VI. In the proposed model compounds, the oxidation state of molybdenum is at least IV, which matches the total negative valences on the ligands. In other words, Mo has two or fewer d elections, leaving at least two empty $d\pi$ orbitals, favouring the formation of a multiple Mo-N bonds.

The coordination number of the Mo centre is six. The six-coordinated imido and hydrazido molybdenum complexes normally adopt octahedral or pseudooctahedral geometries. It simplifies the analysis of these complexes in molecular orbital terms.

2.2.2 The Imido(2-) and Hydrazido(2-) Ligands

In accordance to the proposed N_2-fixation mechanism (Scheme 1.1), the hydrazido and imido intermediates should be of the type $M(NNH_2)$ and M(NH) respectively, that is, with N-bonded hydrogen. However, it is difficult to synthesize a complex containing a $(NNH_2)^{2-}$ or $(NH)^{2-}$ ligands. Usually they are obtained, in poor yields, by careful protonation of dinitrogen complexes and nitrido complexes. The majority of synthesized model compounds are organohydrazido$(NNRR')^{2-}$ and organoimido $(NR)^{2-}$ complexes, and studies using these organic derivatives have been successful in providing structural models for the proposed intermediates. Thus, instead of simple hydrazido and imido ligands, organic derivatives are proposed as the multiple bonded ligands in the model complexes.

At the hydrazido stage further protonation may occur at three possible sites: the metal centre, giving a hydride complex; the αN atom, giving a hydrazido(1-) complex and the βN atom, giving a $(MNNH_3^+)$ species. This greatly depends on the nature of the $(MNNR_2)$ moiety, that is, which site is more negatively charged and more nucleophilic. This also strongly depends on the coligands and the reaction condition. If an electron is supplied to the metal centre at this stage, what happens at the three sites is still a question. Doubtless the addition of an electron to a hydrazido complex will change the relative charge density on the three sites, and thus change their chemical behaviour.

In organoimido and organohydrazido complexes, the substituents (R groups) markedly affect the chemistry of the multiple bound ligands towards reduction and protonation (Section 1.3). In order to see the influence exerted by the substituents on the multiple bound ligand, four complexes were to be synthesized. They are [Mo(NMe)(dttd)(L)], [Mo(NPh)(dttd)(L)], [Mo$(NNMe_2)$(dttd)(L)] and

[$Mo(NNPh_2)$(dttd)(L)]. Hopefully the information obtained about the extent of the conjugation between the molybdenum and $(NR)^{2-}$ or $(NNR_2)^{2-}$ moieties from the crystal structures of these model complexes and their reactivities, would help chemists to understand the nature of the MoNR and $MoNNR_2$ species.

2.2.3 The (L) Ligand

The (L) ligand *cis* to the imido or hydrazido ligand in the model complexes is not only used to make up a six-coordination geometry for the metal centre, it is also used as a mobile ligand ready to move away under certain conditions, leaving behind an active five-coordination intermediate for the quantitative reduction-protonation of the hydrazido(2-) ligand. The requirement of a vacant site for the formation of ammonia is critical, and it must be *cis* to the hydrazido ligand for N-N cleavage and α-elimination (see Section 1.2.5). This has been demonstrated by the fact that the dinitrogen complexes with monophosphine ancillary ligands are protonated easily to produce ammonia stoichiometrically, while the dinitrogen complexes with bidentate phosphine ligands such as dppe stop at the hydrazido(2-) stage under the same reaction conditions.

As in many homogeneous catalytic systems, the mobile ligand L in the model complexes should be a neutral ligand such as a solvent molecule, or a mono phosphine ligand, or a sulfur-containing ligand. On the other hand, if the L ligand bears a negative valence, for example , it is a halide X^-, the oxidation state of the molybdenum centre should be five. This favours the formation of a multiple bond. Under certain reduction conditions [70, 92, 222] the halide ligand can be replaced by a neutral σ donor ligand to give the desired model complexes.

Although the (L) ligand is a mobile ligand, it exerts electronic and steric effects on the reactivity of the multiple bound ligand while it ligates to the metal centre. Therefore the selection of the (L) ligand merits careful consideration.

2.2.4 The dttd Ligand

Dttd can be treated as an anion which carries two negative charges before coordination to the molybdenum centre: it is a tetradentate ligand containing two thiolate and two thioether sulfur atoms.

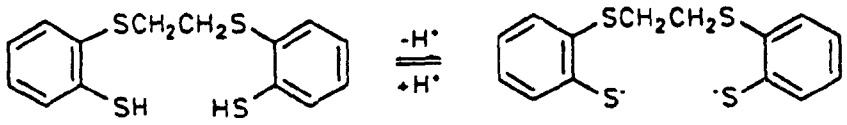

(2.1)

$(dttd{\cdot}H_2)$ $(dttd)^{2-}$

The six-coordinated transition metal centre complex with a dttd ligand usually adopts a pseudooctahedral or distorted octahedral geometry, in which the two thiolate S atoms take the *trans* position while the two thioether atoms take the *cis* position. Although there is another possible coordination geometry in which two thiolates take the *cis* positions, there are no examples showing this type of coordination.

Many metal-containing enzymes or proteins play an important role by using sulfur containing functional groups in biological processes, especially in the redox processes. Since there is no definitive structure of a Mo enzyme available, many studies have focused on the molybdenum complexes which possess one or more ligating sulfur atoms. A variety of sulfur containing ligands such as dithiolines, diakyldithiocarbamates, mono or dithiols, macrocyclic polythioethers and dttd have been used, because they may be able

to provide model complexes related to the natural enzymes [114, 127, 221, 227-229]. The special function of the coordinated sulfur in an active centre must derive from the nature of sulfur and the sulfur-metal bond.

Mo(IV) and Mo(V) show a strong affinity to sulfur containing ligands. This has been confirmed by the fact that only sulfur ligands coordinate to the molybdenum centre in the presence of oxygen donors in excess [221]. This is apparently due to the covalency of the sulfur-molybdenum bond. Electrochemical studies on molybdenum complexes suggest that the reduction of these complexes becomes easier and their redox reversibility is improved if the oxygen donors are replaced by sulfur donors [227]. This has been attributed to the electron rich nature and the large polarisibility of the ligating sulfur, resulting in electron delocalization.

As a σ-donor, sulfur is a moderately strong Lewis base. The coordination of sulfur containing ligands to a metal centre normally produces a thermostable complex. The ability of a donor to form a strong σ bond depends on several factors: the electronegativity, the polarizability, the size of the donor orbital, the energy level of this orbital and the overlap with the acceptor. Comparing of thioethers R_2S with R_3P and RCl, the σ donation capability of R_2S is lower than R_3P, but much higher than the RCl. This is partly related to the increasing electronegativity and the number of lone pair electrons on the donor atom. If one lone pair donates to the metal, the remaining lone pairs on the ligating atom are zero, one and two on going from R_3P, R_2S to RCl, respectively. The lone pairs induce repulsion between the ligand and the metal electrons, consequently, the σ-donation ability of the ligand decreases.

In free thioethers, the valence orbitals of the sulfur atom adopt sp^3 hybridization,

and there are two lone pairs on each sulfur atom. On coordination, one of the lone pairs can form a σ-donating bond with the metal. The other lone pair either remains in the nonbonding orbital, in this case it results in the electronic repulsion, or acts as a π donor to form a π bond with a suitable empty dπ orbital. Although the early transition metals have suitable empty d orbitals which may act as π acceptors, there is little evidence for this bonding in spite of some thermochemical data [230].

In addition to the filled valence orbitals in R_2S, the sulfur atom has empty 3d orbitals. Some of them may have the correct symmetry to take part in the π back donation from the metal to the ligand. This makes the sulfur atom a possible π-acceptor. The π back donation depends on the degree of overlap between dπ orbitals of sulfur and the metal, as well as the relative energy level of the orbitals involved. The observed bond lengths of M-S in low oxidation state transition metal complexes which are shorter than the sum of the covalent radii, are often used to illustrate the π back donation from metal to sulfur [228, 230]. However back donation has not been definitely confirmed. Even it exists, it is weaker than with tertiary phosphine ligands, which also have empty 3d orbitals and are generally regarded as good π-acceptors. This may be partly due to the sulfur's additional lone pair of electrons which prevents the back donation, although sulfur is more electronegative than phosphorus. The absence or weakness of π back donation, the moderate σ donor capability and the repulsion resulting from the presence of the nonbonding lone pairs on the sulfur atom make the sulfur containing ligands generally poor ligands with respect to phosphine ligands. However stronger bonding occurs with chelating or macrocyclic thioethers leading to the formation of low spin metal complexes.

In the proposed model complexes, the chelating ability of dttd on the Mo centre

leads to the formation of three five-membered rings. Each of them contains two carbon, two sulfur and the central metal atoms. This chelating effect combined with the moderately strong M-S bonds make the [Mo(dttd)] a stable fragment. This is of importance in model design, because the changes of the "participating" ligands, e.g. hydrazido and imido ligands during reduction and protonation are of interest.

Concerning the requirement for a vacant site during the reduction-protonation of a hydrazido ligand in Eq. 1.12, the hydrido and amido intermediates can be obtained from a six-coordination complex by replacement of the mobile ligand (L) by hydride or ammonia. Two mechanisms, e.g. SN1 and SN2, are usually used to describe the ligand substitution: Either the mobile ligand (L) moves away from the first coordination sphere leaving behind a five-coordination intermediate followed by fast coordination of the substituent, or the substituent coordinates to the metal centre first forming a seven-coordination intermediate followed by fast departure of the (L) ligand. In the proposed model complexes, if the (L) ligand is "metalophobic", the five-coordination intermediate stage is easy to achieve. On the other hand if the (L) ligand is "metalophilic" in nature, the substitution probably goes through a seven-coordination intermediate pathway. Since the nature of the (L) ligand on the model complexes is uncertain, the desired model complexes are required to have the possibility of adopting a seven-coordination.

Fortunately, the pseudooctahedral Mo(dttd) fragment is flexible enough for the further coordination of two or three coligands. X-ray structure analysis [225] on some Mo(dttd) complexes show that the metal centre can be seven-coordinated as well, confirming this flexibility. The Mo-S bonds and S-Mo-S angles vary, but within relatively narrow ranges indicating the easy conversion of six to seven coordination of

Mo(dttd) fragment without the Mo-S bonds being significantly weakened. Thus, it has been demonstrated that the complex $[Mo(NO)_2(dttd)]$ has unusual reactivity towards phosphines to form a seven-coordination complex [225]. The seven-coordination structure with a M(dttd) moiety can be derived from a six-coordination octahedral geometry by moving the central metal towards the edge defined by the two coligands.

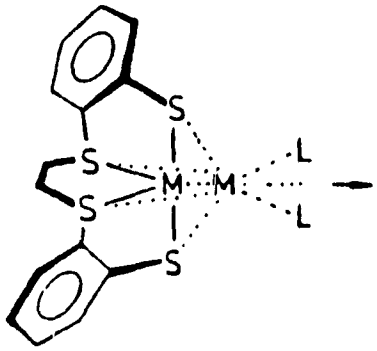

Fig. 2.2 The conversion of six coordination to seven coordination by moving the metal away from the centre.

Dttd is an unsaturated open chain ligand. Each of the two benzo groups connect to two sulfur atoms, which have lone pair elec -ons, at ortho positions. This arrangement favours delocalization of electrons on the molecule. During the redox reaction of the model complexes, dttd may be able to act as an electron buffer. Since there are lone pairs on the sulfur atoms after dttd coordinates to the metal centre, there are possibilities for the sulfur atoms to bridge two metal centres to form dimers or polymers. This has been demonstrated by the fact that many sulfur containing complexes are not monomers, while their phosphine analogues are monomers. For the two thioether sulfur atoms in dttd, there is only one lone pair electrons for each S atom and more steric hindrance around them

after coordination, thus they are less available to bridge. Because of the two thiolate sulfur atoms, each of which has two lone pairs and is not as crowded as the former after coordination, bridge formation is easily possible.

CHAPTER III

THE POTENTIAL MODEL:

SYNTHESIS, RESULTS AND DISCUSSION

Synthesis and characterization are two of the major parts in this thesis. Almost all of the compounds synthesized are air and moisture sensitive. Special care was taken during the preparation and characterization. In addition to the common glassware and equipment, schlenk tubes with a stopcock on the side arm, a vacuum/N_2 system, a dry-box and needle/syringe-vacuum/N_2 techniques were often used. Chemicals purchased were used directly without any further purification. Solvents were dried with sodium metal or metal hydrides. More details are given in Chapter VI. Scheme 3.1. summarizes the syntheses described in the following sections.

3.1 The Preparation of dttd·H_2

In the last 30 years, sulfur containing complexes have become more and more attractive for study due to their special functions in bio-systems and catalytic systems. However the synthesis of sulfur containing polydentate ligands seems difficult. Long procedures and the low yields are common problems in preparation and many desired S-containing ligands are commercial unavailable. For example [228], crown thioether [9]aneS_3 was synthesized in a yield of only 0.04% at the beginning in 1977, and the high yield synthesis was not reported until 1984. There is no exception for dttd·H_2 In the original literature, the yield of dttd·H_2 is reported as only 24% [231]. This is mainly due

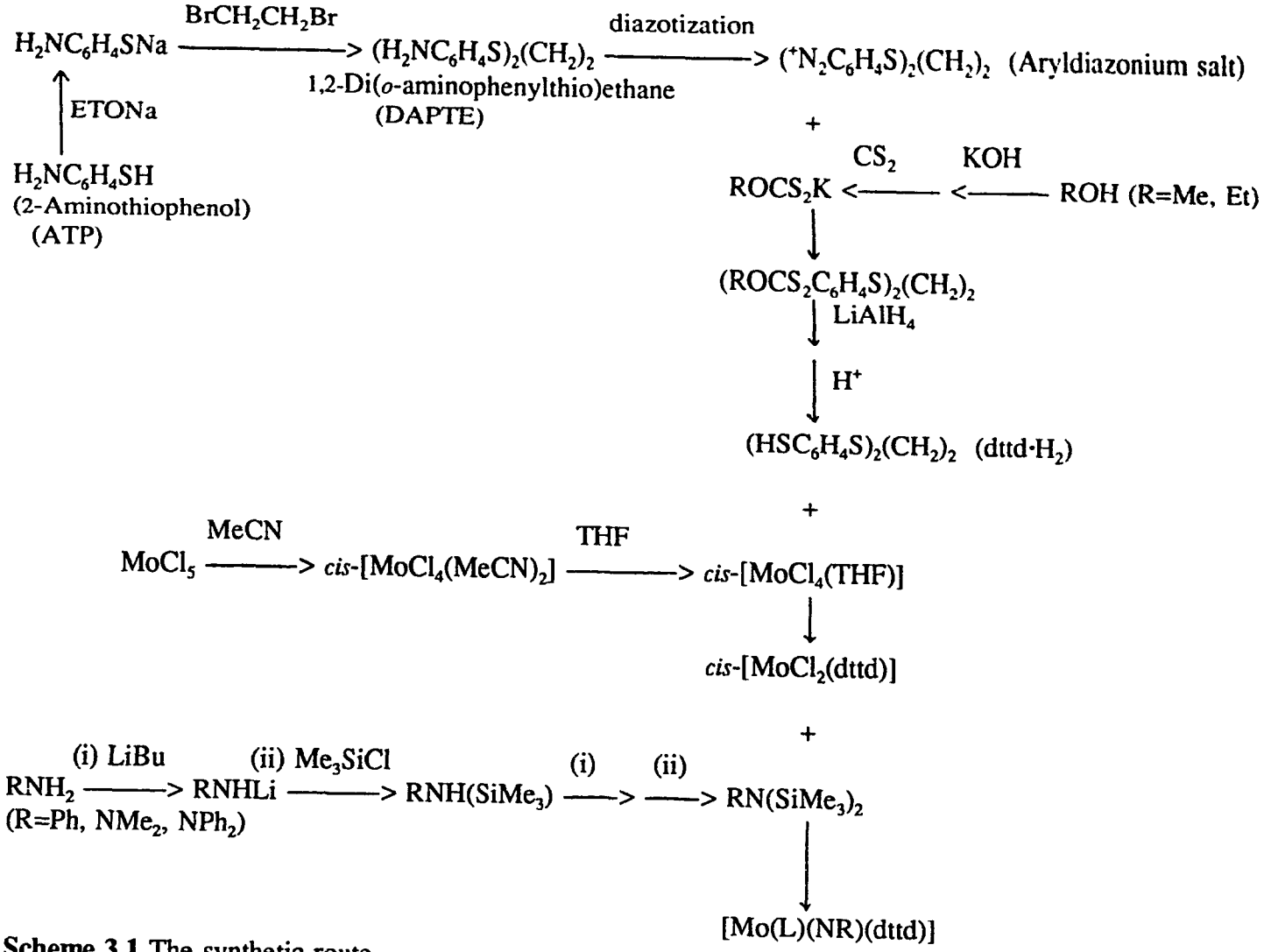

Scheme 3.1 The synthetic route.

to the long procedure, especially the diazotization-xanthanation-reduction synthetic method, which normally gives low yield. However, a higher yield (56%) is described in this thesis featuring an improved method, in which the diazotization was carried out in an aqueous system and the xanthanation was catalyzed by Ni^{2+}.

3.1.1 The Precursor of dttd·H_2

Xanthanation of aryldiazonium salts followed by reduction or hydrolysis gives thiophenol compounds. The precursor of dttd·H_2, 1,2-di(*o*-aminophenylthio)ethane (DAPTE) was synthesized according to the synthetic route illustrated in Scheme 3.1. The starting compound, 2-aminothiophenol (ATP) was treated first with EtONa followed by 1,2-dibromoethane resulting in the formation of DAPTE in a yield of 93%. The balanced equations are given below:

$$H_2NC_6H_4SH + EtONa \text{ ----------> } H_2NC_6H_4S^-Na^+ + EtOH \qquad (3.1)$$

$$2H_2NC_6H_4S^-Na^+ + BrCH_2CH_2Br \text{ -------> } \underset{\text{(DAPTE)}}{(H_2NC_6H_4S)_2(CH_2)_2} \qquad (3.2)$$

Thiols or mercaptans are compounds containing the -SH groups. They are stronger acids than their oxygen analogues. The acidity of thiophenol is comparable to H_2CO_3. The bond dissociation energy of the S-H bond (~80 Kcal/mole) of thiols is much less than that of the O-H bond of alcohols (~100KCal/mole). This is due to the large polarizability of sulfur atom, making it more nucleophilic than oxygen atom. On the other hand, a sulfur atom has a 3p orbital which is more diffuse than the oxygen 2p orbital. The overlap of H 1s with 3p is not as efficient as the overlap of H 1s with 2p. Thus the S-H bond dissociates more easily than the O-H bond. The reaction represented in Eq. 3.1 can be described as metathesis reaction, while the reaction in Eq. 3.2 is a typical nucleophilic

reaction of thiols.

The synthesized DAPTE was characterized by FTIR and ^{1}H NMR spectroscopy. In the FTIR spectrum (Fig. 3.1) two strong absorptions at 3350 and 3362 cm^{-1} indicate the presence of NH_2. Absorptions at 2970 and 2915 cm^{-1} are typical alkyl C-H stretching bands assigned to $-(CH_2)_2-$, and the 3051 band was assigned to aryl C-H. The S-H band of the parent *o*-aminothiophenol at 2520 cm^{-1} had disappeared in DAPTE spectrum which implies the presence of the bridge represented in Eq. 3.2. This connection by the $-(CH_2)_2-$ at sulfur atoms has been confirmed by the ^{1}H NMR spectrum.

In the ^{1}H NMR spectrum, Fig. 3.2, there are four sets of peaks. A singlet resonance at δ=2.89 ppm is assigned to $-(CH_2)_2-$ group. The second singlet resonance at δ=4.35 ppm was assigned to the two $-NH_2$ groups. The resonances of ring protons, split into two sets. They appear at δ=6.56-6.84 ppm and δ=7.00-7.46 ppm, and have been assigned to the protons at *o*-, *p*- to NH_2 and at *o*-, *p*- to SR respectively. The ratio of integration of these peaks is 1.06 : 1.01 : 1.00 : 1.03, suggesting a equal number to the three types of protons. The NH_2 resonance is broadened probably due to the proton-exchange of NH_2 with solvent. Compared with 2-aminothiophenol, which has one broadened singlet resonance at δ=3.68 ppm assigned to both SH and NH_2 protons, the resonance of amino protons shifts to lower field suggesting a lower basicity of amino group in DAPTE with respect to the aminothiophenol and a better conjugation of nitrogen lone pair with π electrons. This is because the SR groups are stronger electron withdrawing groups than SH, reducing the electron density on the rings.

There is a singlet for $-CH_2CH_2-$ proton resonance, because the four protons have identical chemical environment owing to the high symmetry of the molecule. Interestingly,

Fig. 3.1 FTIR spectrum of $(H_2NC_6H_4S)_2(CH_2)_2$ (DAPTE).

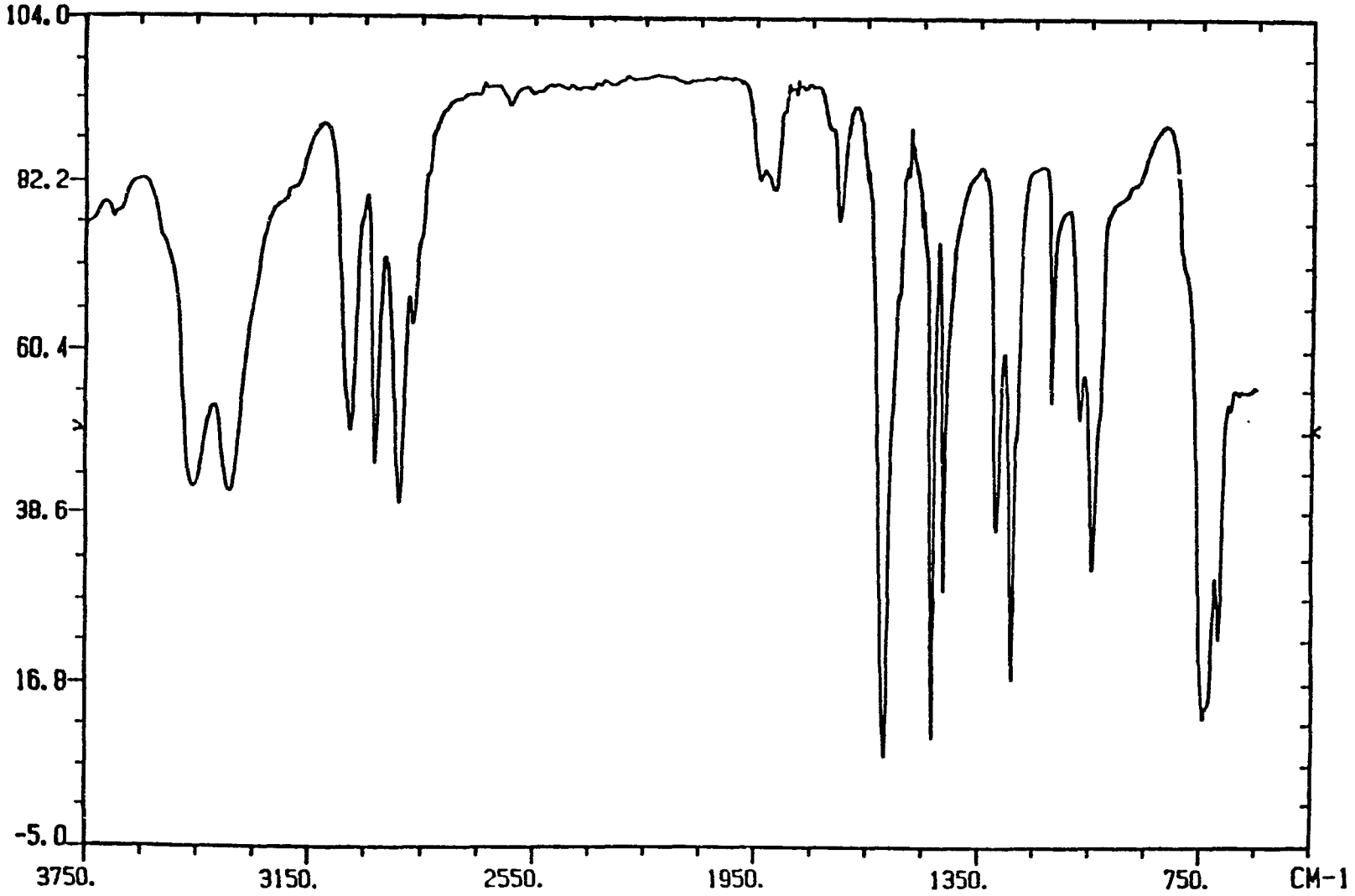

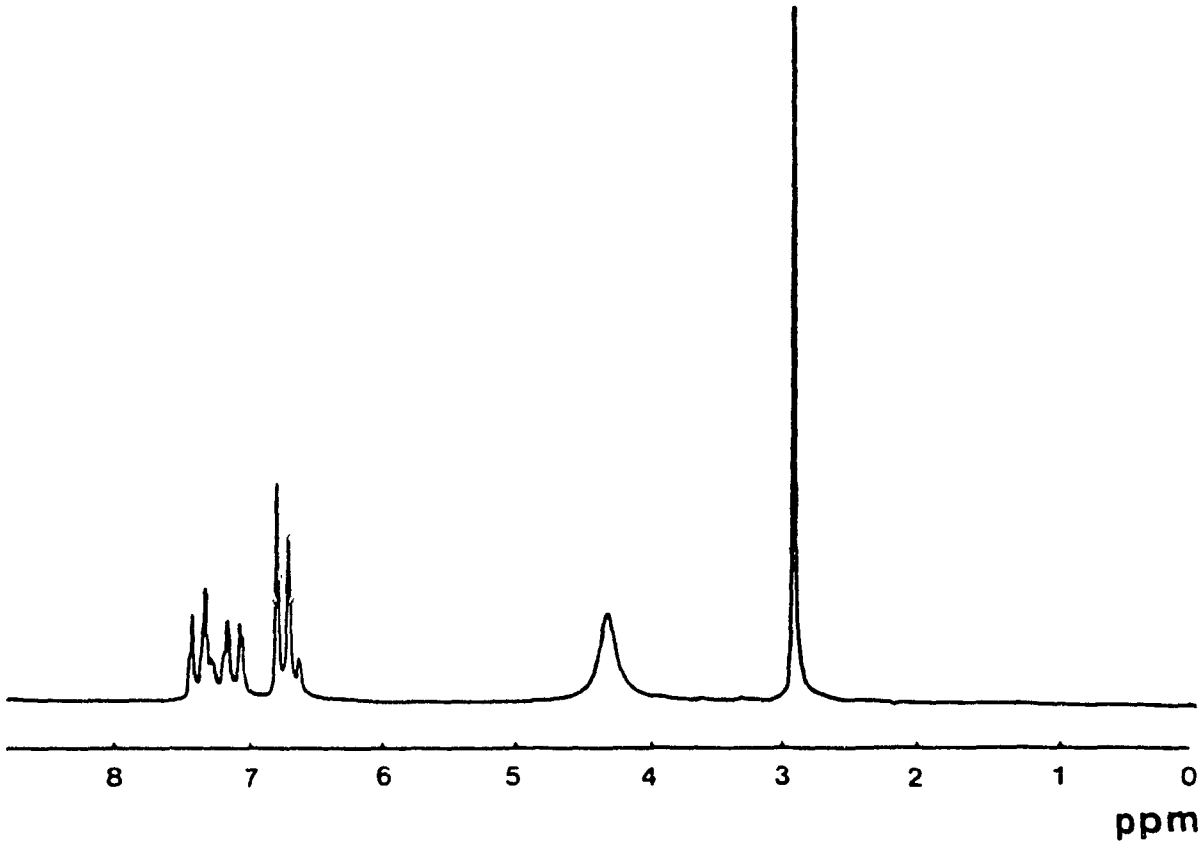

Fig. 3.2 ^{1}H NMR spectrum of $(H_2NC_6H_4S)_2(CH_2)_2$.

even after coordination, the $-CH_2CH_2-$ still shows a singlet in the case of $[Mo(dttd)(C_6H_4S_2)]$ [226].

3.1.2 Methylxanthate (CH_3OCS_2K)

Ethylxanthate is commercially available, but the yield of $dttd{\cdot}H_2$ using ethylxanthate in the xanthalation step is lower than that obtained by using methylxanthate perhaps due to the steric hindrance. Following the synthetic procedure in Vogel's "Textbook of Practical Organic Chemistry" (4th Ed., 1978, P588), methylxanthate was prepared and then characterized by ^1H NMR. The reactions are shown in Eq. 3.3 and 3.4.

$$CH_3OH + KOH \text{ ----------> } CH_3O^-K^+ + H_2O \quad (3.3)$$

$$CH_3O^-K^+ + CS_2 \text{ ----------> } CH_3OCS_2^-K^+ \quad (3.4)$$

Methylxanthate is very soluble in methanol. The initial yield recovered on cooling is about 55%. More can be obtained from the mother solution. Interestingly, it was found that more xanthate can be precipitated out at room temperature by adding ethanol to the methanol solution: the yield increases up to ~70%. No precipitate forms if pentane or dichloromethane is added. As expected the ^1H NMR spectrum of methylxanthate in Fig. 3.3 shows only a singlet at δ=3.77 ppm. This is in agreement with the fact that there is only one type of proton in methylxanthate and the resonance of the methyl protons shifts to quite low field due to the connection to a strong electron withdrawing group, $-OCS_2$.

3.1.3 Diazotization

Diazotization of an aromatic amine followed by xanthanation and hydrolysis or reduction are among the most common synthetic routes to thiophenols. Arenediazonium ions are

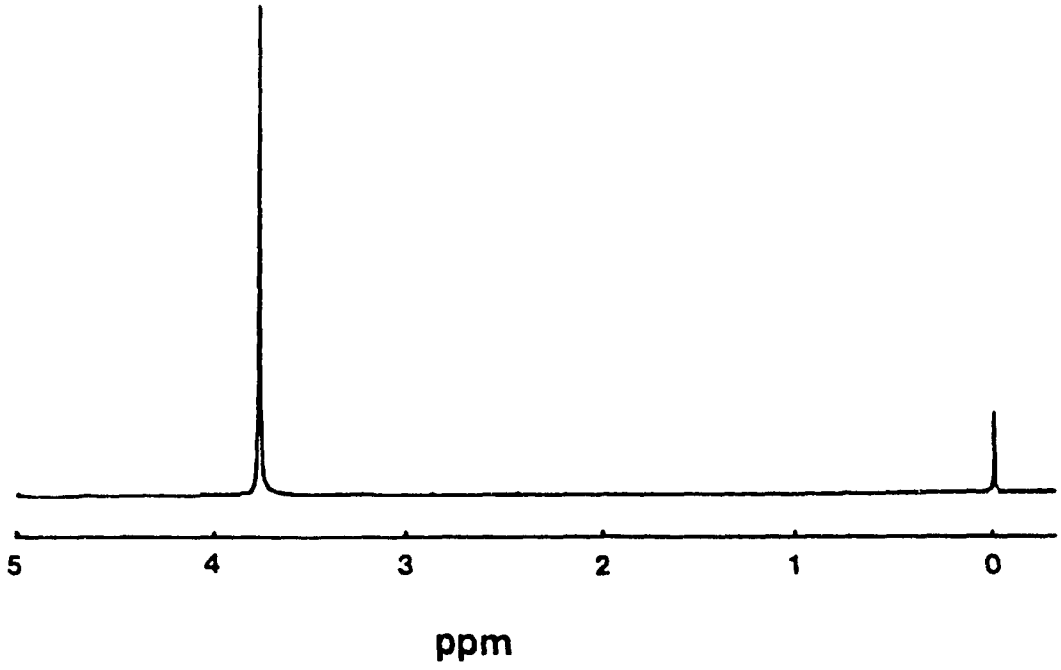

Fig. 3.3 ^{1}H NMR spectrum of potassium methylxanthate.

relatively stable with respect to alkanediazonium ions at low temperature. The reason for the relative instability of alkyldiazonium ions is the highly exothermic formation of alkyl cations and dinitrogen while the electronic resonance stabilizes the aryl compounds [232]. One of the electron pairs of the aromatic π system delocalizes towards the functional group, resulting in charge-separated resonance structures containing a double bond between the ring and the attached nitrogen. Only at high temperature do the arene diazonium ions evolve N_2 to form active aryl cations.

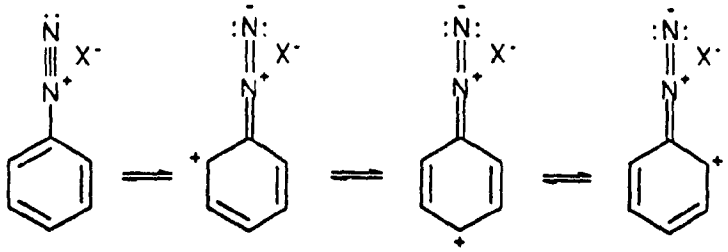

Fig. 3.4 Resonance in benzenediazonium cation.

In the literature [231] preparation of dttd·H_2, diazotization of DAPTE was carried out in a mixture of concentrated H_2SO_4 and $NaNO_2$ at ice-bath temperature. Then the arenediazonium salt was precipitated by addition of ether for the later xanthanation reaction. This method has disadvantages. The nitrous acid formed before diazotization is not stable, it is an intermediate oxidation state of nitrogen and a disproportionation reaction can occur to give nitric acid and nitric oxide.

$$3HNO_2 \text{ ----------> } 2NO + H_3O^+ + NO_3^- \qquad (3.5)$$

Furthermore, the arylamine DAPTE is hard to diazotize completely in concentrated acid media. This could be seen clearly in the IR spectrum of the crude product: two strong bands in the range 3200 to 3500 cm^{-1} were observed, attributable to undiazotized NH_2. (see Fig. 3.5).

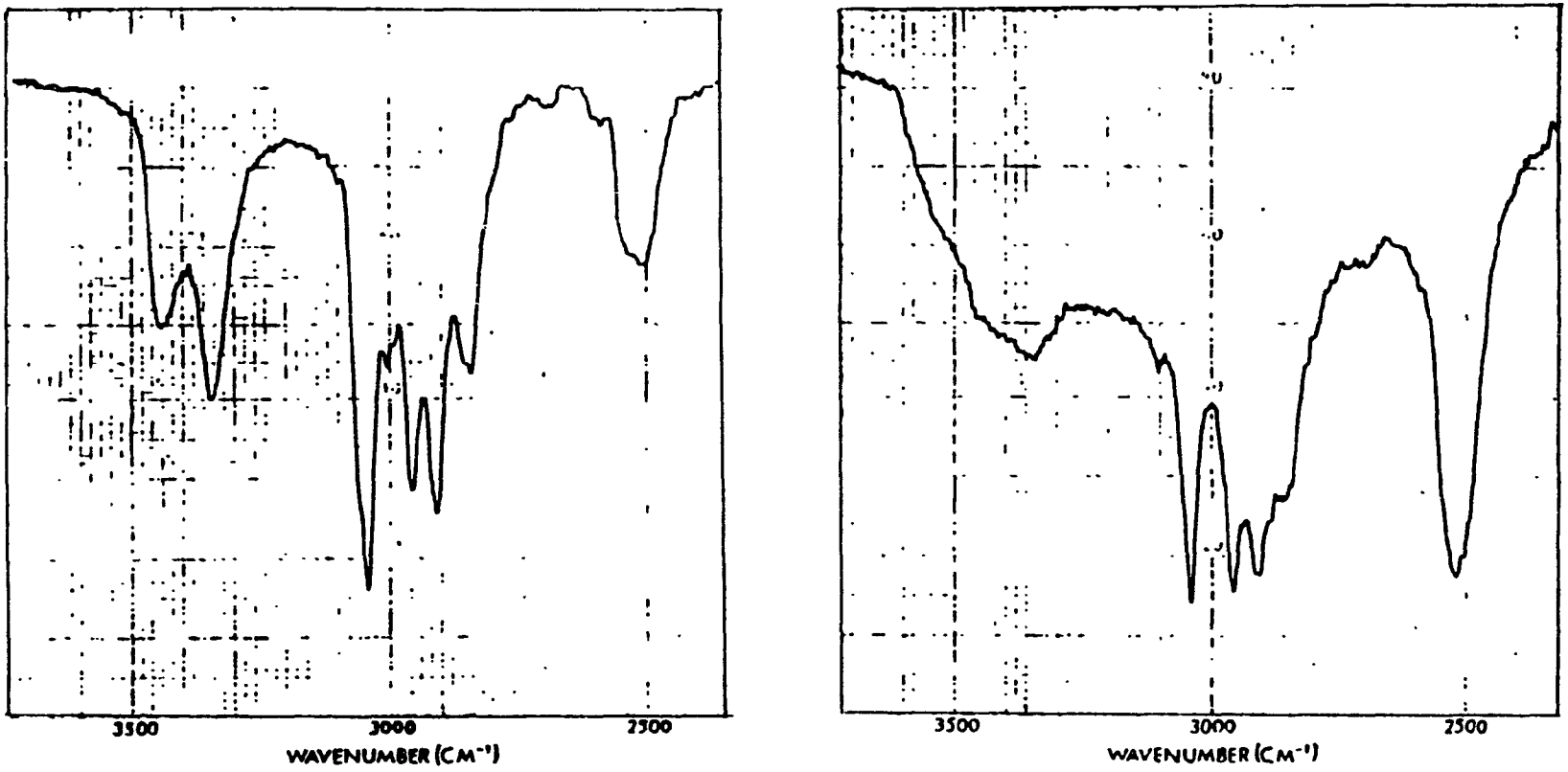

Fig. 3.5 The IR spectra of crude dttd·H_2 prepared following the procedure in the literature [231].

Left: N-H bands are shown in 3200~3500 cm^{-1}.

Right: O-H band (~3500 cm^{-1}) overlaps with the N-H bands.

In the procedure described in the experimental section, instead of using the concentrated sulfuric acid, dilute HCl was used. The aromatic amine disolves in the HCl solution. The nitrous acid is generated by dropwise addition of sodium nitrite solution to this solution. In this way, the problems of diazotization in concentrated acid are solved, and the conversion of the aromatic amine to the corresponding diazonium salt become fast and efficient. The produced diazonium salt solution was used immediately in xanthanation reaction. The stoichiometric reaction is shown in Eq. 3.6.

$$(H_2NC_6H_4S)_2(CH_2)_2 + 2NaNO_2 + 4HCl \text{ -----> } (Cl^-N_2^+C_6H_4S)_2(CH_2)_2 + 2NaCl + 4H_2O \qquad (3.6)$$

A simplified mechanism of diazotization is suggested by A. Streitwieser and C.H. Heathcock in "Introduction to Organic Chemistry" (1985):

$$HO\text{-}N{=}O + H^+ \longrightarrow H_2O^+\text{-}N{=}O \longrightarrow H_2O + {}^+N{=}O$$

$$Ar\text{-}NH_2 + {}^+NO \longrightarrow Ar\text{-}NH\text{-}N{=}O + H^+$$

$$\downarrow$$

$$Ar\text{-}NH\text{-}N{=}OH^+ \longleftrightarrow Ar\text{-}{}^+NH{=}N\text{-}OH$$

$$\downarrow$$

$$H_2O + Ar^+N{\equiv}N \longleftarrow Ar\text{-}N{=}N\text{-}OH_2^+ \longleftarrow Ar\text{-}N{=}N\text{-}OH + H^+$$

3.1.4 Xanthanation: An Improved Method

There are several ways to convert arenediazonium ions to thiophenols. Treatment of arenediazonium salts with $ROCS_2^-K^+$, Na_2S_x ($x \geq 2$) or $SC(NH_2)_2$ followed by hydrolysis or reduction resulting in the corresponding thiophenols. Among these routes, xanthanation is most commonly used. Diazonium ions are electrophiles, containing the best leaving

groups—molecular nitrogen in organic chemistry. There is a thermodynamic driving force for the decomposition of arenediazonium ions to phenylcations and nitrogen because of the stability of N_2. In the presence of nucleophiles, such as xanthate, $ROCS_2^-$, the arenediazonium xanthate ($(MeOCS_2^-N_2^+C_6H_4S)_2(CH_2)_2$ in this thesis) forms and this is followed by evolution of N_2 vigorously. Explosions resulting from heating the solutions of aryldiazonium salt and potassium ethyl xanthate have been reported. Therefore evolution of N_2 as soon as the diazonium xanthate is formed is desirable for safety. Sellmann et al [231] carried out xanthanation by adding isolated arenediazonium salt in portions to a concentrated potassium methyl xanthate solution at 80^0C. At such high temperature the arenediazonium salts are decomposed leading to the formation of aryl cations. These cations are very active and readily attacked by nucleophiles. This is because the empty orbital associated with the positive charge is one of the hybridized sp^2 orbitals of the ring carbon. This orbital is perpendicular to the π framework, so it cannot overlap with the π orbitals, thus the positive charge cannot be delocalized. Under the condition mentioned above, water as a nucleophile competes well with xanthate leading to the formation of phenols. This has been confirmed by the appearence of -OH band in the IR spectrum (Fig.3.5) of the crude dttd·H_2 obtained by this method. In order to maximize the possibility of the formation of $(MeOCS_2C_6H_4S)_2(CH_2)_2$, a huge excess of potassium methyl xanthate must be used.

It has been observed that dropwise addition of an aqueous solution of potassium methyl xanthate to a cold (0^0C) aqueous solution of diazotized orthanilic acid ($H_2NC_6H_4SO_3H$) results in the loss of nitrogen immediately when a trace of nickel ion is present in the stirred diazonium solution. The catalyst can be added as nickelous chloride

or simply by using a nichrome wire stirrer [233].

In this work, the xanthanation was catalyzed by Ni^{2+} at ~0^0C and nitrogen was liberated at 3~5^0C (Eq. 3.7).

$$(Cl^-N_2^+C_6H_4S)_2(CH_2)_2 + 2MeOCS_2K \xrightarrow[3\sim5^0C]{Ni^{2+}} (MeOCS_2C_6H_4S)_2(CH_2)_2 + 2N_2\uparrow + 2KCl \qquad (3.7)$$

The formation of the diazonium xanthate occurred as soon as the xanthate solution was added to the diazonium ion solution. It is insoluble and floats on the surface. Nitrogen was released when the temperature of the solution was increased from 0^0C to about 3^0C. The evolution of N_2 is an exothermic reaction and increases the temperature in some parts of the solution. Thus some crushed ice was added to keep the temperature below 5^0C. In this way, the xanthate was used quantitatively and the formation of the aryl cation was virtually eliminated. The brown coloured product, aryl methlyxanthate was extracted with ether and dried over anhydrous sodium sulfate for subsequent reduction.

3.1.5 The Formation of Dttd·H_2

The arylxanthate can be converted to the arylthiol either by reduction, or by hydrolysis in an alkaline medium. Reductions of arylxanthates by $LiAlH_4$ are usually used because thiols can be oxidized easily in basic solution. Good yields are often obtained especially with the hindered thiols. The aryl methxanthate obtained from Eq. 3.7 was reduced by $LiAlH_4$ in ether.

$$(MeOCS_2C_6H_4S)_2(CH_2)_2 + LiAlH_4 \xrightarrow{H^+} \underset{(dttd\cdot H_2)}{(HSC_6H_4S)_2(CH_2)_2} \qquad (3.8)$$

Lithium aluminium hydride reacts vigorously with traces of moisture to release hydrogen,

thus the ether used as solvent in the reduction must be dried previously. During the reduction course, the brown coloured aryl methylxanthate was reduced gradually. The raw product is a mixture of dttd·H_2, CH_3SH and CH_3OH. It is a brown coloured oil with very offensive odour. After purification a yellow coloured oil was usually obtained. On one occasion, a pale yellow coloured solid product was obtained, and it was characterized by FTIR and NMR spectroscopy as a "standard" for comparison with the other preparations.

In the FTIR spectrum of dttd·H_2 (Fig. 3.6), the stretching vibration of S-H was clearly seen at 2520 cm^{-1}; the same position as the S-H stretching band in 2-aminothiophenol. The absence of the NH_2 bands in 3300-3500 cm^{-1} and the aromatic C-N band at 1305 cm^{-1} in $(H_2NC_6H_4S)_2(CH_2)_2$ spectrum indicated the purity of dttd·H_2. The aromatic and aliphatic C-H stretching bands are at 3049, 2966 and 2914 cm^{-1}; almost the same as the precursor. The spectrum also displayed typical absorption patterns of a substituted aromatic in the region of 1650-2000 cm^{-1}; a combination of the C-H in-plane and out-of-plane bending deformations. The absorptions of the aromatic C=C stretching fall in the region of 1550-1600 cm^{-1}. The strong absorption at 743 cm^{-1} was assigned to the C-H bending (out-of-plane) of the 1,2-substituted phenyl rings. The in-plane deformation bands should be in the region of 960-1270 cm^{-1}. The frequency of these deformation bands is sensitive to change of substitutent. The presence of electron-donating substituents on an aromatic nucleus causes these absorptions to shift to lower frequency. For example the absorption at 743 cm^{-1} in dttd·H_2 shifts to 733 cm^{-1} in the arylamine precursor compound owing to the lone pair electrons on amine groups joining the π conjugation. A weak band at 703 cm^{-1} was assigned to ν(C-S) according to the C-S stretching (702 cm^{-1}) assigned in a -S-C=C-S- unit [224].

Fig. 3.6 FTIR spectrum of dttd·H_2.

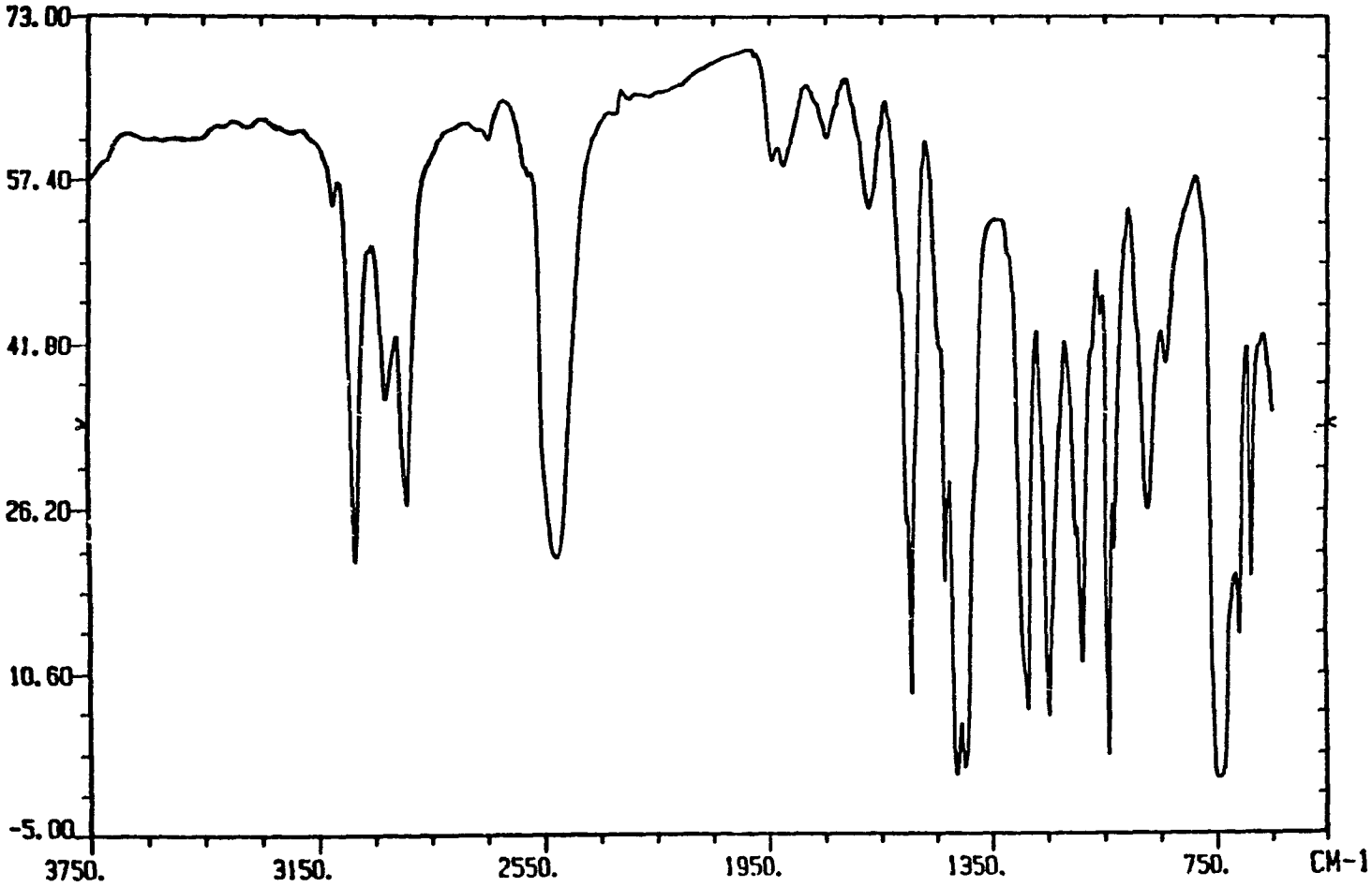

Fig. 3.7 ^{1}H NMR spectrum of dttd·H_2.

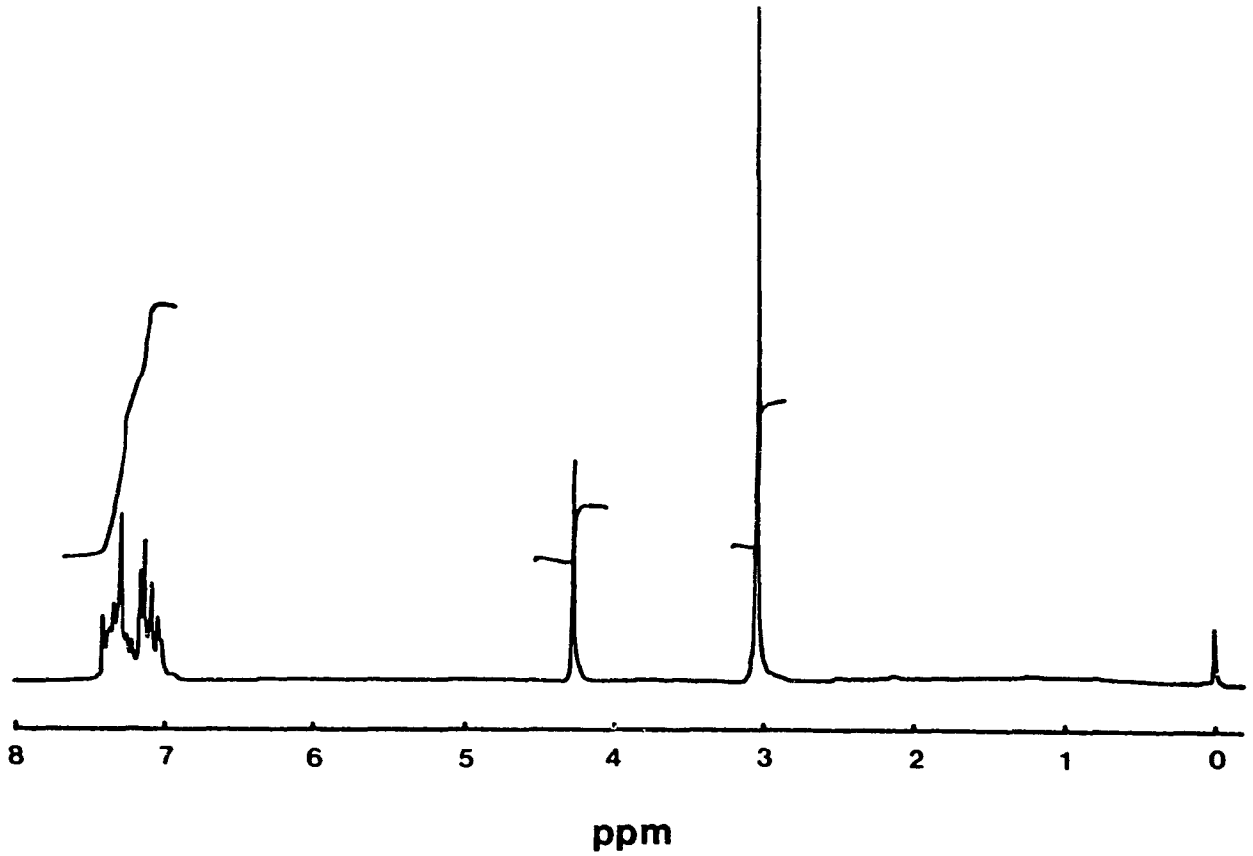

The ^1H NMR spectrum in Fig. 3.7 showed the same resonance pattern to that of arylamine precursor, two singlets and two multiplets. The singlet at δ=3.03 ppm belongs to the resonance of -$(CH_2)_2$-. It shifts 0.16 ppm down field corresponding to -CH_2CH_2-in the precursor. The second singlet (δ=4.26 ppm) was assigned to the -SH group. The chemical shift is comparable to the NH_2 resonance (δ=4.35 ppm) in the precursor, but not being broadened. This implies that the proton exchange of SH with solvent is much slower than that of NH_2, because the lone pairs on sulfur atom cannot form strong hydrogen bonds with solvent molecules, while the lone pair on the nitrogen atom readily does. The two multiplets which appear at δ=6.98-7.16 and 7.20-7.44 ppm were assigned to the proton resonances of the rings. The ratio of integration of these peaks is consistent with the number of protons in dttd·H_2. (Dttd·H_2 was also examined by 400 MHz ^1H NMR spectroscopy. The chemical shifts changed a little but not the resonance pattern.)

3.1.6 The Precursor Complex [Mo(dttd)Cl_2]: Preparation and FTIR

The imido(2-) and hydrazido(2-) molybdenum model complexes can be obtained by the reactions of the ligand precursors with a molybdenum(IV) complex bearing a dttd and two *cis* chloride ligands. This precursor complex was synthesized following the procedure published by Kaul et al [226]. Molybdenum pentachloride $MoCl_5$ was first reduced to a Mo(IV) complex by simply stirring $MoCl_5$ in acetonitrile (Eq. 3.10).

$$MoCl_5 + CH_3CN \text{ (excess)} \text{ ----> } [MoCl_4(CH_3CN)_2] + \text{"organic chlorides)} \quad (3.10)$$

The product obtained is a fine brown powder in a yield of 81%. It is air sensitive and slightly soluble in acetonitrile. This complex is a convenient precursor for the synthesis of many molybdenum(IV) complexes by replacement of the relatively labile acetonitrile

groups with other ligands.

The FTIR spectrum (Fig. 3.8) shows two medium intensity bands at 2307 and 2285 cm^{-1} assigned to ν(C≡N), and a strong band at 334 cm^{-1} assigned to ν(Mo-Cl) [238]. Compared to the free acetonitrile C≡N stretching bands which appear at 2266 and 2235 cm^{-1}, the coordinated MeCN shows a C≡N stretching vibration 40-50 cm^{-1} higher. The increase in frequency after coordination has been attributed to the σ^* character of the ligating lone-pair in free acetonitrile molecules. After coordination the lone pair delocalizes towards the metal centre and the strength of C≡N is enhanced. Two other bands positioned at 428 and 416 cm^{-1} were also assigned to the ligating acetonitrile. This was confirmed by the absence of these bands in the $MoCl_4(THF)_2$ FTIR spectrum. However it has not been established whether these bands are due to the ν(Mo-N) stretching vibration or to the σ(C-CN) deformation.

The coordination of dttd to the molybdenum centre was conducted in THF solution. Complex $[MoCl_4(MeCN)_2]$ was first converted to $[MoCl_4(THF)_2]$ in THF according to the Equation 3.11.

$$[MoCl_4(MeCN)_2] + 2THF \text{ --------> } [MoCl_4(THF)_2] + 2MeCN \qquad (3.11)$$

The yellow product was recovered in a yield of 73% and characterized by FTIR (Fig. 3.9). The spectrum displays a medium band at 988 cm^{-1} and a strong one at 820 cm^{-1}. These two bands are attributed to ν(C-O-C) of the coordinated THF. They shift to lower frequency with respect to free THF due to the transfer of electron density from oxygen to the metal centre, thus weakening the C-O-C bond.

It is noteworthy that the Mo-Cl band in the complex $[MoCl_4(MeCN)_2]$ splits into two bands positioned at 342 and 282 cm^{-1} in $[MoCl_4(THF)_2]$ spectrum. The geometrical

Fig. 3.8 FTIR spectrum of $[MoCl_4(MeCN)_2]$ (nujol mull).

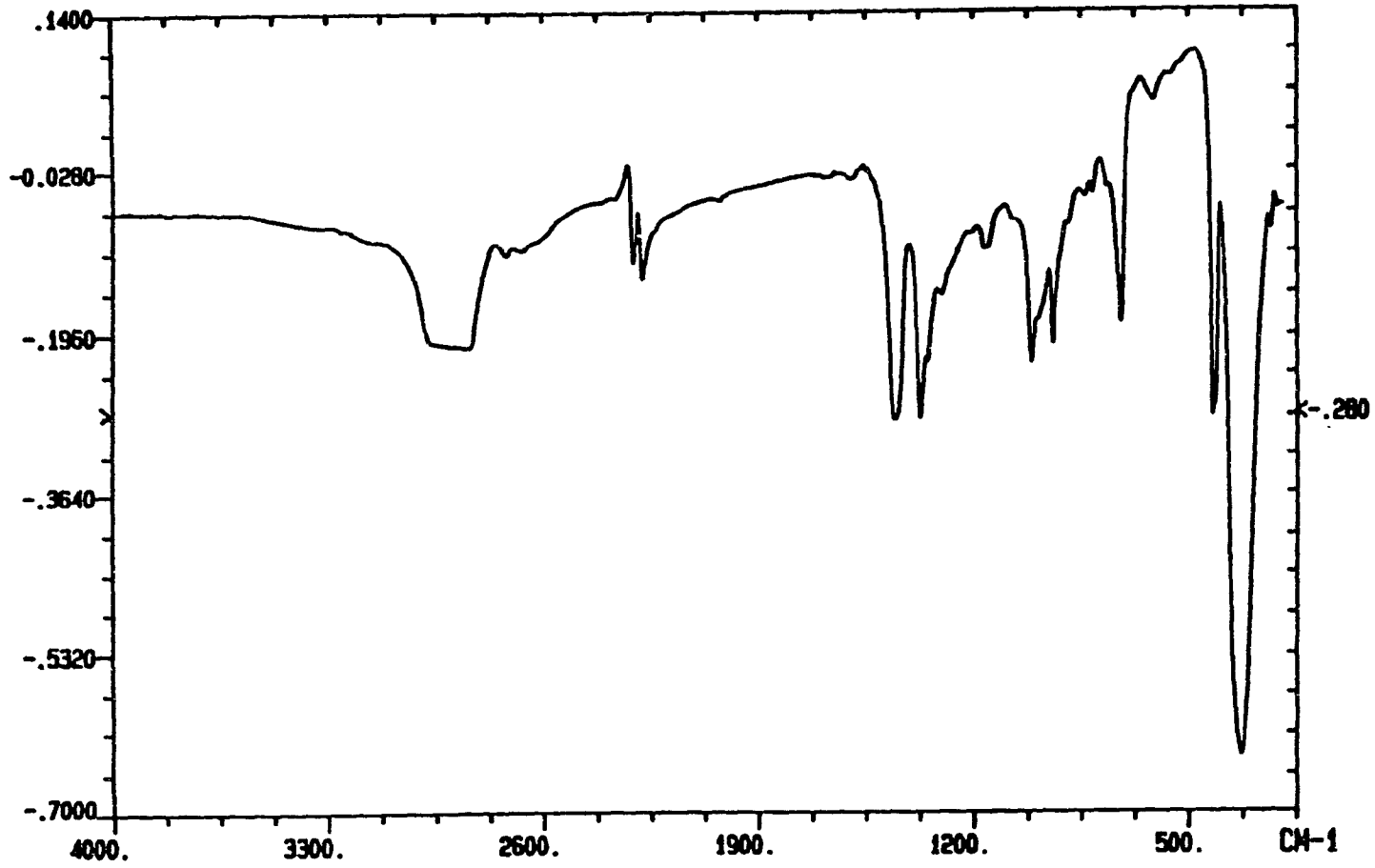

Fig. 3.9 FTIR spectrum of $MoCl_4(THF)_2$] (nujol mull).

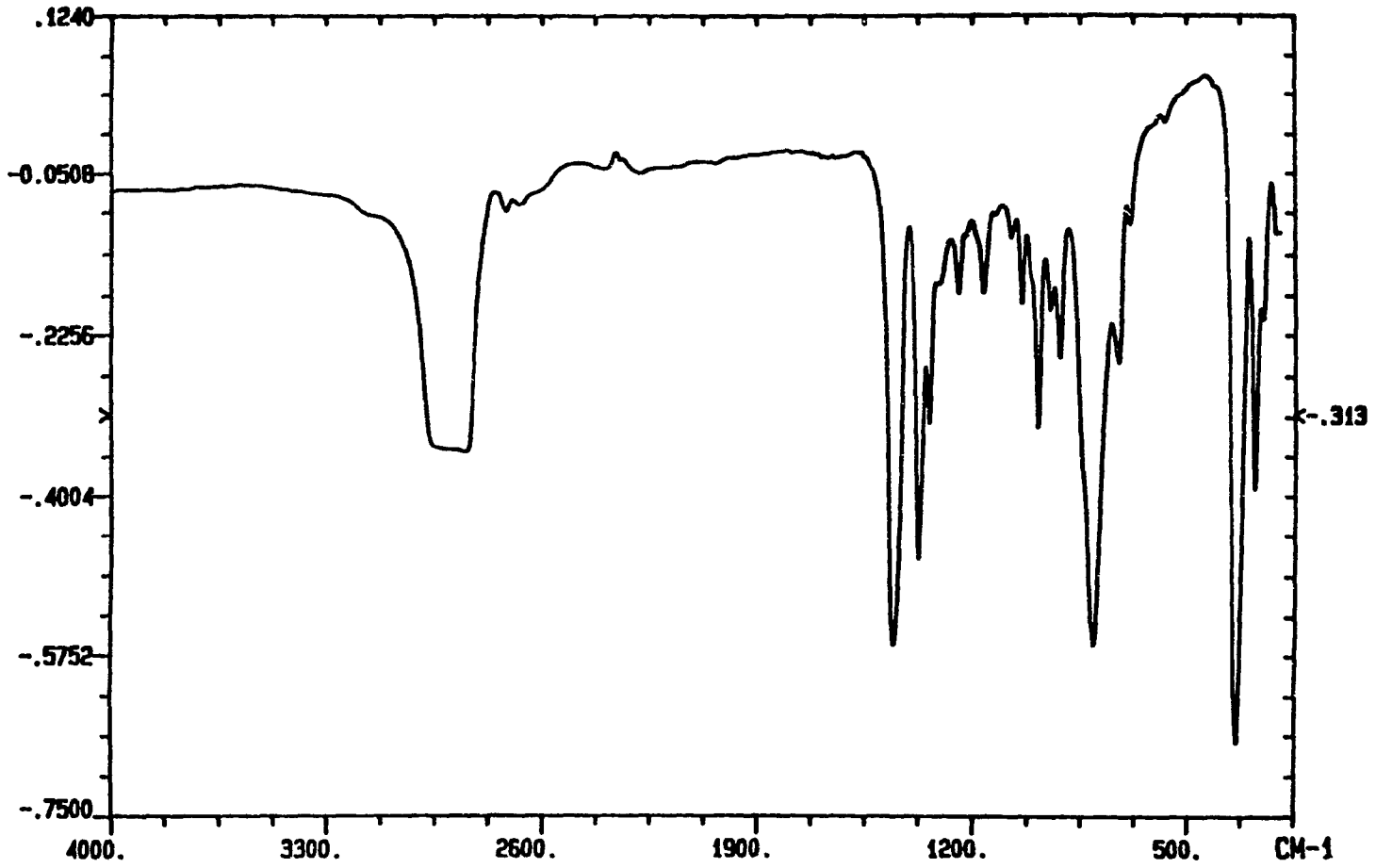

configuration of $[MoCl_4(THF)_2]$ can be deduced using these bands. In the case of octahedral MY_4Z_2 complexes [238], the *trans* isomer has D_{4h} symmetry. Although there are three possible M-Y stretching modes, only one (Eu) is infrared active. Thus the spectrum of *trans*-$[MoCl_4(THF)_2]$ complex should only show one Mo-Cl stretching band. On the other hand, the *cis* isomer of MY_4Z_2 has C_{2v} symmetry. It gives four M-Y stretching modes, and all of them are infrared active. Therefore the spectrum of a *cis*-$[MoCl_4(THF)_2]$ complex might show more than one (maximum 4) Mo-Cl stretching bands. In the spectrum (Fig. 3.9) two Mo-Cl bands were observed suggesting a *cis* geometry. This geometry, in which the two neutral THF ligands are mutually *cis*, is desirable for the formation of the precursor complex $[Mo(dttd)Cl_2]$, because the two thioether in dttd ligand take *cis* sites on coordination.

The precursor complex $[Mo(dttd)Cl_2]$ was formed by direct reaction of dttd·H_2 with $[MoCl_4(THF)_2]$ according to Eq. 3.12.

$$[MoCl_4(THF)_2] + dttd\cdot H_2 \xrightarrow{THF} [Mo(dttd)Cl_2] + 2HCl + 2THF \qquad (3.12)$$

Dttd·H_2/THF solution was added to a suspension of $[MoCl_4(THF)_2]$/THF. A little excess of dttd·H_2 was used, and the addition of dttd·H_2 was carried out very slowly, over a period of ~3 hours. The product, a black fine powder, precipitated from the reaction solution as the dttd·H_2 was added. A yield of 82% was recovered. $[Mo(dttd)Cl_2]$ is paramagnetic and stable in air for a limited time. It is slightly soluble in THF giving a violet solution, but is decomposed by more polar solvents such as DMSO or DMF.

The nujol mull FTIR spectrum of $[Mo(dttd)Cl_2]$ in Fig. 3.10 shows two strong bands at 330 and 308 cm^{-1} assigned to ν(Mo-Cl), and consistent with *cis* Cl ligands [226]. The band at 381 cm^{-1} was assigned to ν(Mo-S thiolate), because the symmetric and

Fig. 3.10 FTIR spectrum of [Mo(dttd)Cl_2] (nujol mull).

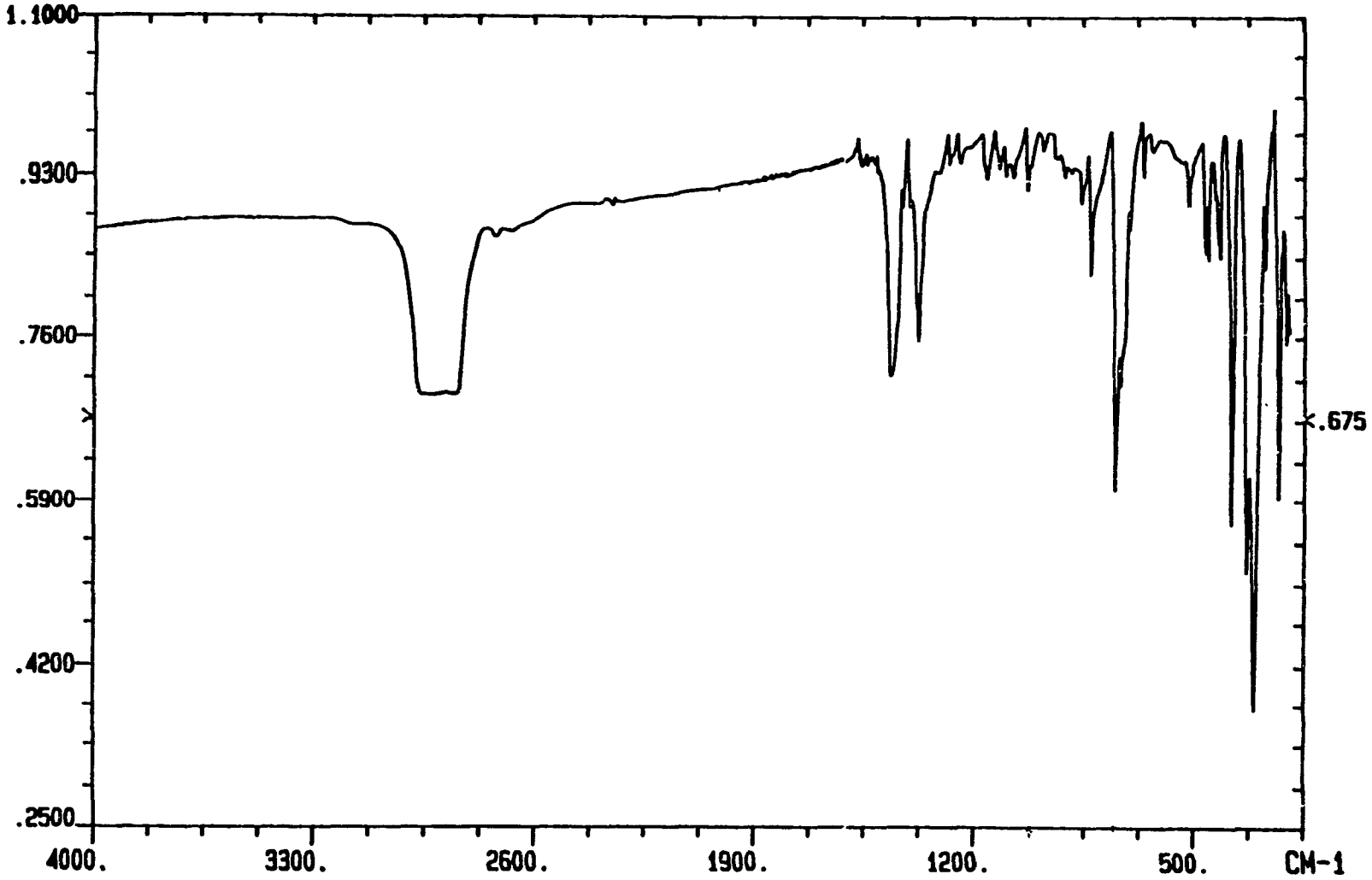

asymmetric ν(Mo-S thiolate) normally fall between 350-400 cm^{-1} [224]. The substituted benzene rings in the dttd ligand show their C=C stretching bands around 1555 cm^{-1} and deformation band at 741 cm^{-1}, almost unchanged in frequency with respect to free dttd·H_2. Like some other sulfur-containing complexes, several low intensity bands around 450 cm^{-1} are also shown in the spectrum. Two low frequency bands have not been assigned. Probably they are Mo-S thioether stretching bands, because the metal-thioether bands usually appear in the region of 350-200 cm^{-1}.

3.2 Bis(trimethylsilyl)amine and *N,N*-Bis(trimethylsilyl)hydrazine Compounds

As mentioned in Section 1.3.1, one of the preparative routes to metal ligand multiple bonds is to react the metal oxides or the metal halides with organic silyl compounds. This kind of reaction is driven thermodynamically by the formation of strong Si-O or Si-X (X=F, Cl) bonds. In this study, silylamine and silylhydrazine compounds were used as the precursors of imido(2-) and hydrazido(2-) ligands in reactions with [Mo(dttd)Cl_2)]. These precursors were:

N,N-bis(Trimethylsilyl)methylamine	$(Me_3Si)_2NMe$	**(1)**,
N,N-bis(trimethyl-silyl)aniline	$(Me_3Si)_2NPh$	**(2)**,
N,N-bis(trimethylsilyl)-*N',N'*-dimethylhydrazine	$(Me_3Si)_2NNMe_2$	**(3)**,
N,N-bis(trimethylsilyl)-*N',N'*-diphenylhydrazine	$(Me_3Si)_2NNPh_2$	**(4)**.

(2-4) were synthesized by a similar methods [234-235], (1) was purchased from Aldrich Chemical Co. and was used directly without further purification.

3.2.1 Preparation

The starting compounds for the preparation of (**2-4**) are $PhNH_2$, Me_2NNH_2 and $Ph_2NNH_2 \cdot HCl$ respectively. The substitutions of nitrogen-bonded hydrogens by trimethylsilyl groups were carried out step by step. Thus, the starting chemicals were first treated with one equivalent LiBu to form a RN^-HLi^+ species, then one equivalent trimethylsilylchloride was used to produce $RNH(SiMe_3)$. The second proton was replaced by trimethylsilyl in the same way. The products listed above were obtained by repeating these two steps.

Although the preparations follow the similar procedure, the solvents used are different. This is mainly due to the acidity of the substituted protons. Compared to the methylamine, the protons on the aniline are of higher acidity owing to the conjugation of the lone pair on N atom with the π system. This conjugation also decreases the basicity of this arylamine. Thus the substitutions were carried out in hexane and then ether for the first and second proton substitutions respectively. In the hydrazine cases, the first proton substitutions of dimethylhydrazine were performed in a hexane/ether medium. For the second step, THF was used. The proton substitutions of diphenylhydrazine were both carried out in THF necessitated by the higher basicity of the H_2N- unit in this compound which requires a more polarizing solvent. The literature preparation of this compound in benzene in a sealed tube [235] is much less effective.

3.2.2 IR and NMR Spectroscopy

The purified products were characterized by IR and ^1H NMR spectroscopy. All of the N-H stretching bands, which normally appear in the region 3400-3500 cm^{-1} in the IR

spectra disappeared, implying a complete substitution of hydrogen on the amine and hydrazine precursors by trimethylsilyl groups. Comparison with the IR spectrum of aniline, the spectrum of $(Me_3Si)_2NPh$ (2) displays additional C-H ($-CH_3$) absorptions between 2880-2980 cm^{-1} and three intense $-Si(CH_3)_3$ absorptions at 1240, 835 and 750 cm^{-1} which are comparable to the three typical absorptions of $-Si(CH_3)_3$ groups in bis(trimethylsilyl)acetylene IR spectrum [236]. However the last band (750 cm^{-1}) overlaps with one of the typical absorptions (755, 695 cm^{-1}) of the aromatic C-H out-of-plane vibration. The aromatic amine C-N stretching (1275 cm^{-1}, aniline) shifts to lower frequency (1250 cm^{-1}, compound (2)) which may be due to the heavy groups substituting N-hydrogen, or to lessened conjugation of the N atom with the ring.

The ^1H NMR spectrum of compound (2) shows two types of resonance corresponding to the two types of protons in (2). The resonance of protons on the two $SiMe_3$ groups are displayed as a singlet at δ=0.0 ppm, and the multiplet positioned at δ=6.8-7.2 ppm was assigned to the aromatic protons. The ratio of these two types of protons is 3.4:1. No other resonances were observed, indicating the purity of (2). The FTIR and ^1H NMR spectra of compound (2) are shown in Fig. 3.11 and Fig. 3.12.

The IR spectrum of (3) and (4) also display the typical $-SiMe_3$ IR bands at ~1245, 835 and 750 cm^{-1}. In compound (3) the last absorption is a sharp band, since there are no phenyl ring absorptions to overlap with it at ~750 cm^{-1} The methyl C-H stretching bands appear over a wide region, 2760-2980 cm^{-1}, while in compound (4), the methyl C-H bands are in the normal region of 2870-2980 cm^{-1}.

Interestingly, all the three spectra display a sharp medium intensity band positioned at 614 cm^{-1} for (2) and (3), and 616 cm^{-1} for ligand precursor (4). These bands

Fig. 3.11 FTIR spectrum of $(SiMe_3)_2NPh$.

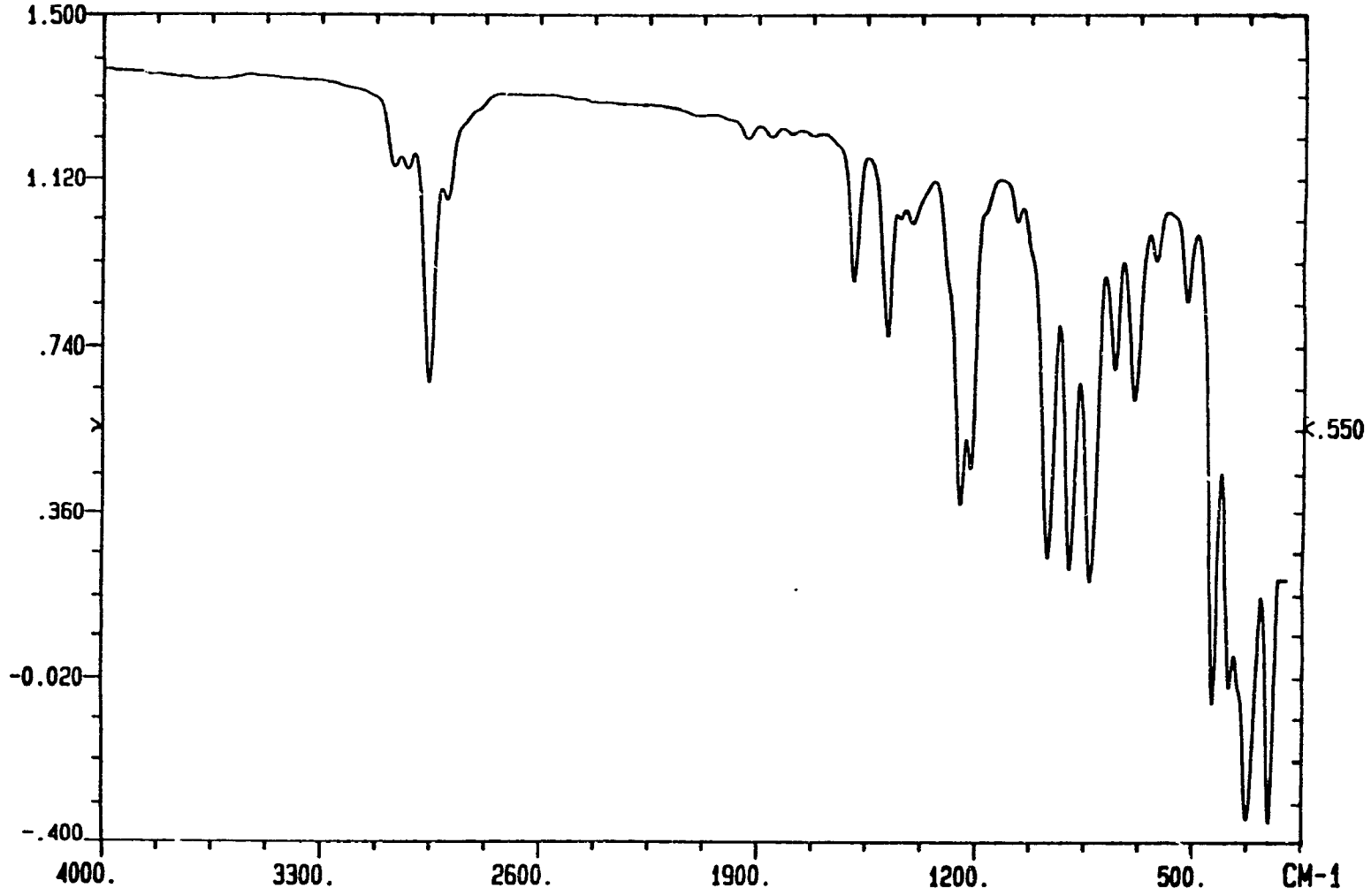

Fig. 3.12 ^{1}H NMR spectrum of $(SiMe_3)_2NPh$.

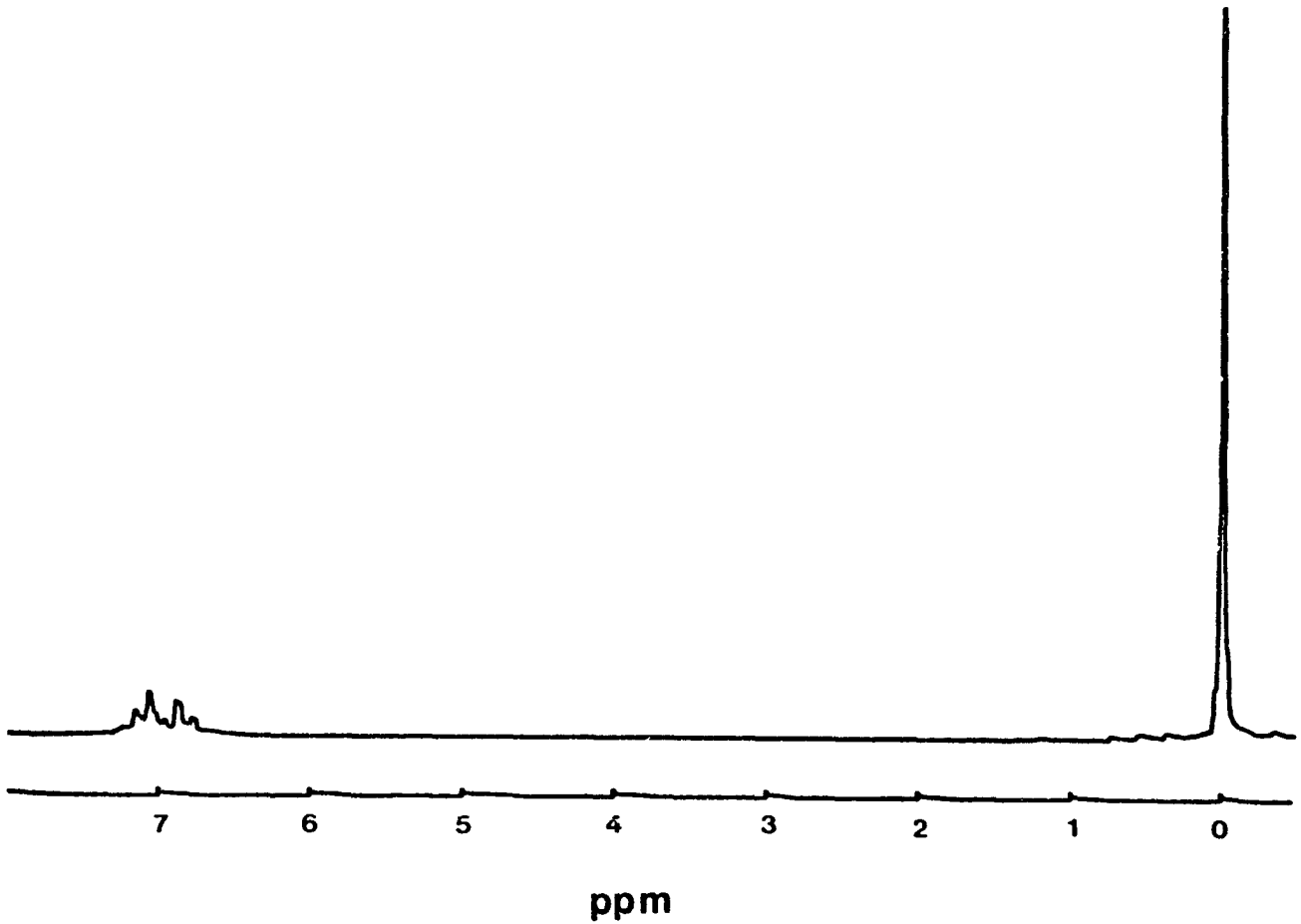

disappeared after ligation of these precursors to the Mo centres. Apparently, these bands are associated with N-$SiMe_3$ units. Since only three -$SiMe_3$ bands were reported [249], and there are no absorptions below 650 cm^{-1} in the spectra of Bis(trimethylsilyl)acetylene and Tetramethylsilane. These bands may be assigned to the vibrations of N-$SiMe_3$. It is rare to obtain information about N-Si absorptions from the IR region.

The ^1H NMR spectrum of (**3**) shows two singlets. One of them, at δ=0.13 ppm, was assigned to $SiMe_3$. The other one, at 2.37 ppm was assigned to NMe. The ^1H NMR spectrum of (**4**) shows a singlet at δ=0.11 ppm assigned to $SiMe_3$ and a multiplet at 7.2-7.3 assigned to C_6H_5. The small difference in methylsilyl chemical shifts in the two spectra is consistent with the basicity of the silyl-substituted nitrogen discussed in Section 3.3.1.

3.3 Synthesis and Characterization of the Imido(2-) and Hydrazido(2-) Model Complexes

Four model complexes have been synthesized and characterized. The results, especially the crystal structure of [$MoCl(NNPh)_2$(dttd)] indicate that they are indeed imido(2-) and hydrazido(2-) molybdenum complexes, although every of them has a chloride ligand.

3.3.1 Synthesis

The model complexes [MoCl(NMe)(dttd)] (**1**), [MoCl(NPh)(dttd)] (**2**), [$MoCl(NNMe_2)$(dttd)] (**3**) and [$MoCl(NNPh_2)$(dttd)] (**4**) were synthesized in the same manner. Excess ligand precursor was mixed with a slurry of [$MoCl_2$(dttd)]/THF in the

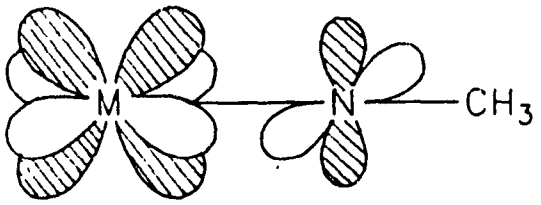

(1)

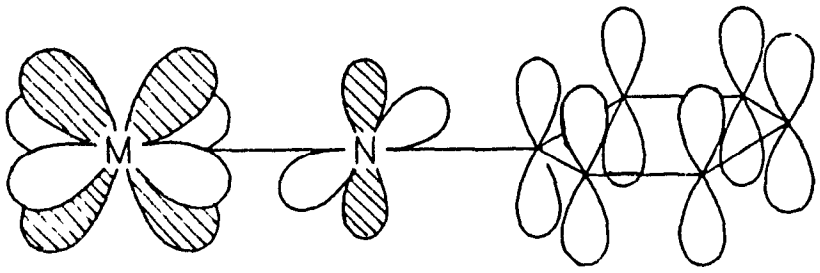

(2)

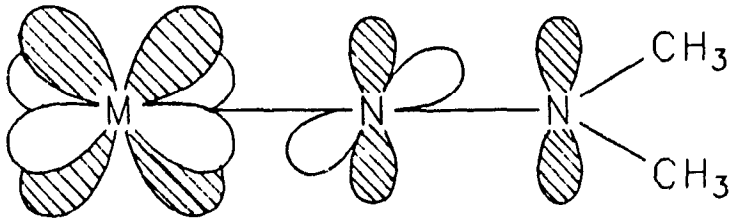

(3)

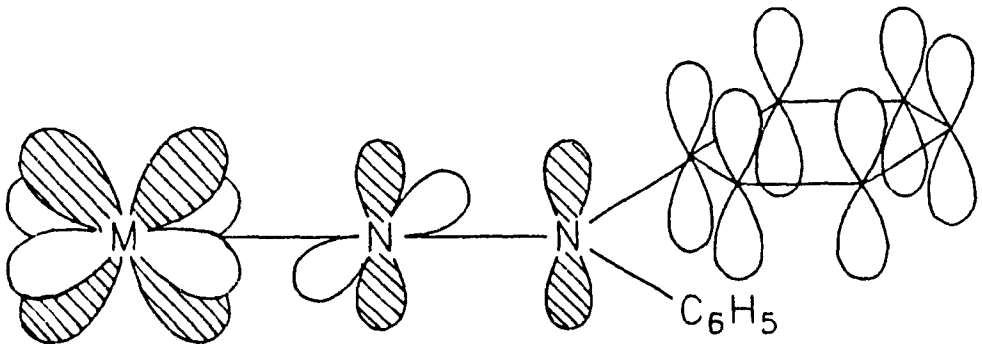

(4)

Fig. 3.13 Orbital interactions in **(1)** MoNMe, **(2)** MoNPh, **(3)** $MoNNMe_2$, **(4)** $MoNNPh_2$ fragments.

dry-box. The mixture was heated and stirred under N_2. The crude products gave brown, green and violet bands on TLC trial plates. The compounds were separated by silica gel chromatography and only the violet bands gave crystalline products which were subsequently identified to be imido and hydrazido molybdenum(V) complexes. Although each of the four complexes contains the same MoCl(dttd) core with a Mo-N multiple bond, the yield, the reaction rate, the amount of ligand precursor used, the reaction temperature and time required are quite different.

The final products are 17e molybdenum (V) complexes as shown in Eq. 3.13.

$$[MoCl_2(dttd)] + (Me_3Si)_2NR \text{ --------> } [MoCl(NR)(dttd)] \qquad (3.13)$$

$$R=Me,\ Ph,\ NMe_2,\ NPh_2$$

It seems that these reactions are not the simple metathesis reactions described in Section 1.3.1, since the Mo(IV) precursors have been oxidized to Mo(V) and one chloride ligand remains. It is not a simple redox reaction either and the mechanism is still in question. However, the differences can be explained in terms of electronic effects.

This type of reaction depends on the basicity of the αN atom in the multiple bonded ligands. In the =NMe fragment, the lone pairs of N atom can only interact with an empty dπ orbital, as illustrated in Fig. 1.13, thus =NMe is a strongly nucleophile ligand favoured by a high oxidation state metal core. In contrast, in =NPh the lone pairs can conjugate with the aromatic π system, consequently the electron density on the N atom is decreased. In the hydrazido cases, the strong interaction of the lone pairs on αN and βN in $=NNMe_2$ moiety reduces the interaction between αN lone pairs with the empty dπ orbitals. On the other hand the conjugation of the lone pair on βN with the phenyl rings in the $=NNPh_2$ unit reduces the interaction between the two N atoms, leaving the

αN as a moderate nucleophile. These orbital interactions are shown in Fig. 1.13.

3.3.2 Characterization

3.3.2.1 IR Spectroscopy

The IR spectra of the four model complexes were obtained by using nujol mull samples between CsI plates. All of the spectra show the absence of the intense -$SiMe_3$ bands which would appear at ~1245, ~835 and ~750 cm^{-1} in the ligand precursor spectra. They confirm the presence of the dttd ligands. The deformation bands of 1,2-substituted benzene rings and C=C stretching vibrations are clearly observed at ~730-760 and ~1565 cm^{-1} respectively. The νMo-S thiolate) appears at ~380 cm^{-1}. Several bands appear in the region close to ν(Mo-Cl), although there is only one chloride ligand on the model complexes. Some of them may be due to the absorption of ν(Mo-S thioether), because the two thioethers are no longer equivalent in [$MoCl_2$(dttd)] owing to the formation of the Mo≡N multiple bond: ν(M-S thioether) bands are usually assigned in a region of 350-200 cm^{-1}.

The assignment of Mo-N stretching vibrations in these spectra is a problem because of coupling with other modes such as N-R stretching modes, other metal-ligand modes and/or with the vibration modes of the R group. ^{15}N isotopic labelling studies of some phenylimido complexes [240] show a band in the region of 1310-1360 cm^{-1}, which shifts to a lower frequency by 20-30 cm^{-1} on ^{15}N substitution. Although this is a band associated with the phenylimido ligand (=NPh), whether it represents ν(M-N) or ν(N-C) or some combination of the two is still not clear, because aromatic amines show also their N-C stretching bands in the range of 1250-1370 cm^{-1}. It seems to depend on with which of the

Table 3.1 The IR bands of model complexes in the region of 1360-850 cm^{-1}.

$[MoCl_2(dttd)]$	$[MoCl(NMe)(dttd)]$	$[MoCl(NPh)(dttd)]$	$[MoCl(NNMe_2)(dttd)]$	$[MoCl(NNPh_2)(dttd)]$
852	855	860	875	860
905	900	910	905	903
936	-	-	945	930
975	-	978	-	-
982	-	-	-	-
1015	1015	1020	1020	1018
1025	1030	1030	1030	1030
1055	-	-	-	-
1092	1093	1095	1095	1093
1112	-	-	-	-
1120	1120	1125	1120	1120
1153	1150	-	1155	1150
1160	-	1160	1165	1165
-	1175	-	-	1175
1235	-	-	-	-
1240	1238	1240	1238	1238
-	1250	-	-	-
-	1255	1260	1257	1255
1270	-	-	-	-
-	-	1305	-	1308
-	-	-	-	1320

Fig. 3.14 FTIR spectrum of [MoCl(NMe)(dttd)] (nujol mull).

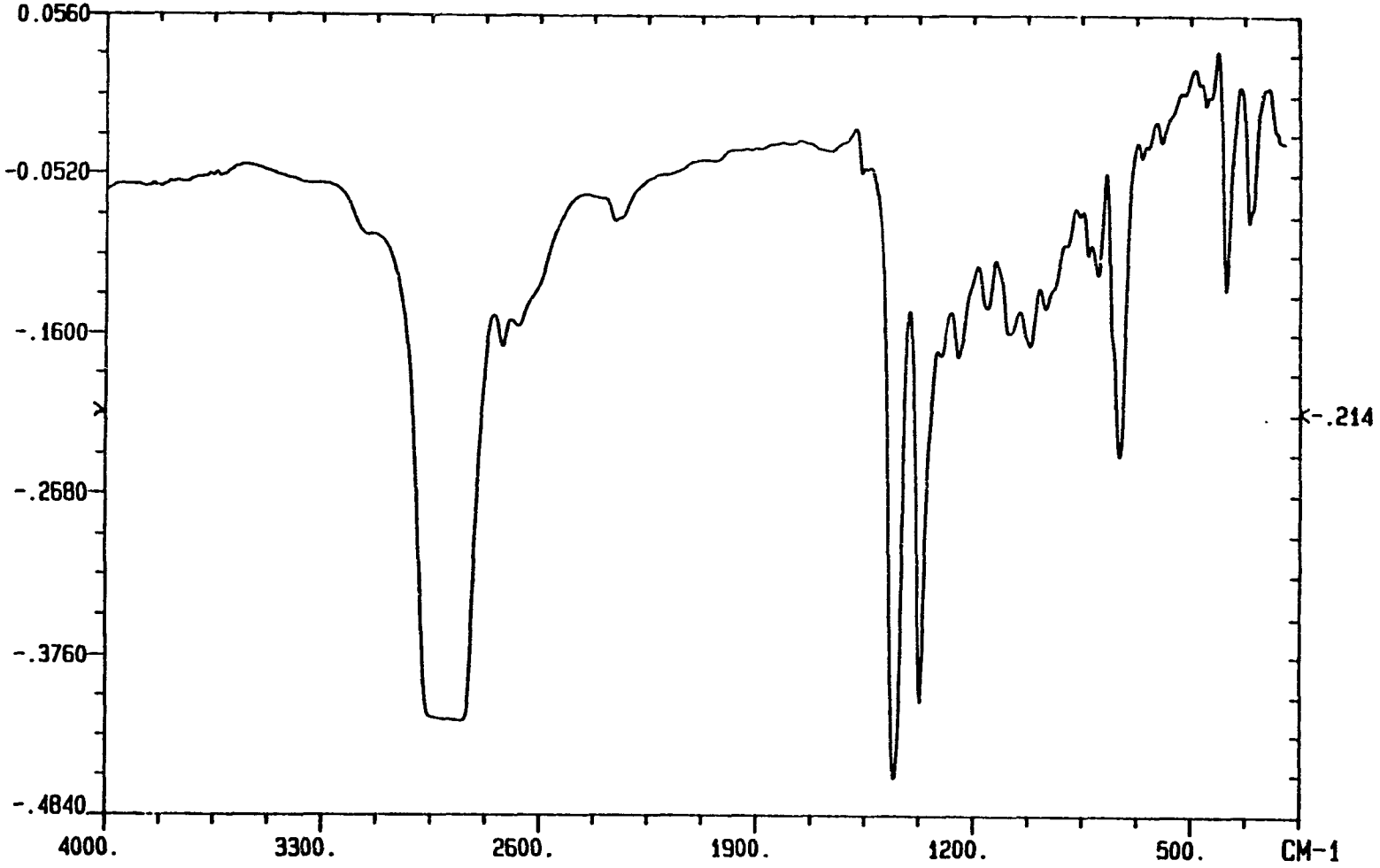

Fig. 3.15 FTIR spectrum of [MoCl(NPh)(dttd)] (nujol mull).

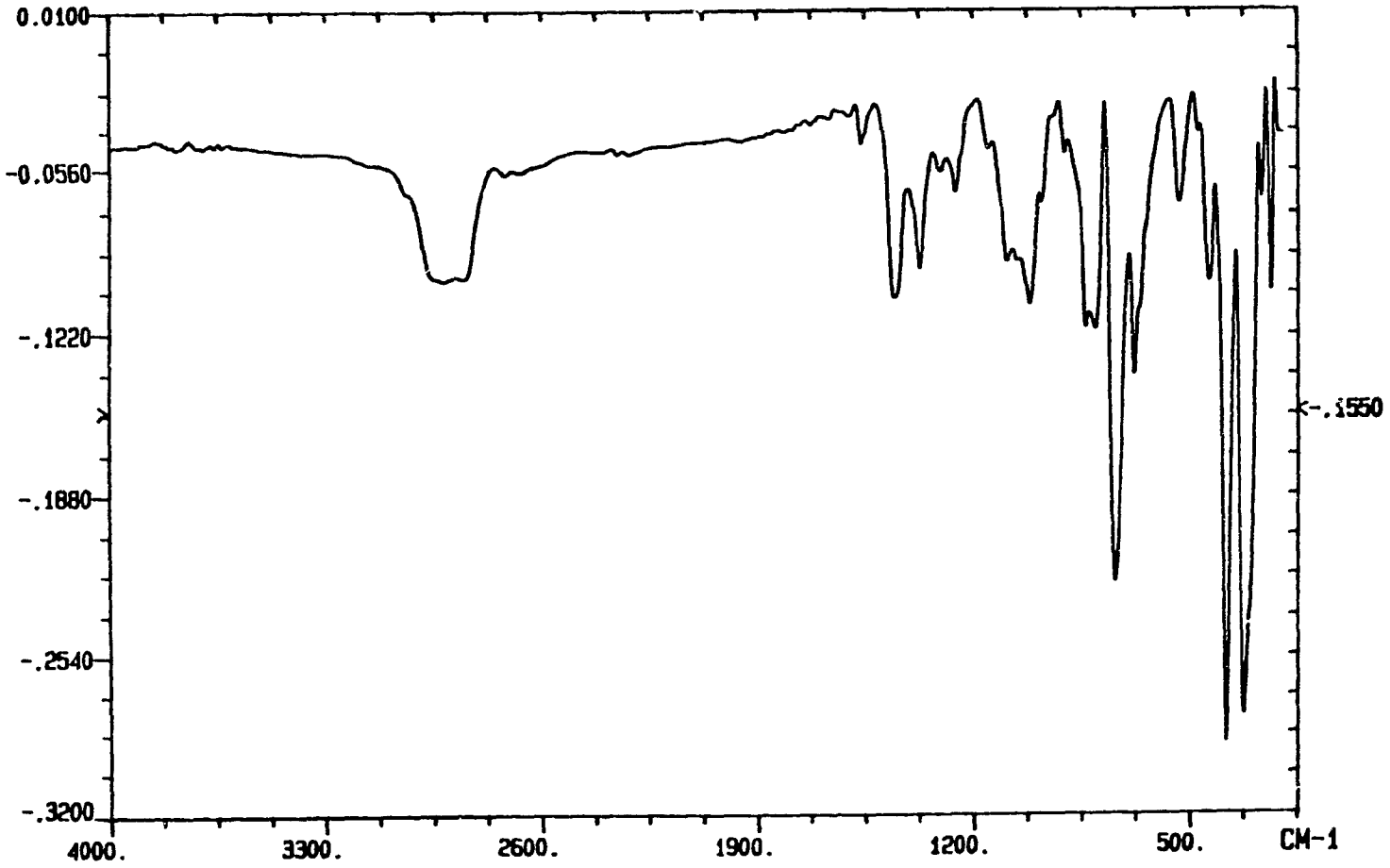

Table 3.2 FTIR bands (cm^{-1}) of model complexes (1) and (2).

[MoCl(NMe)(dttd)]	[MoCl(NPh)(dttd)]
1252 (m)*	1258 (w)*
1160 (m)	1160 (w)
1083 (m)	1088 (m)
1018 (m)	1020 (m)
975 (m)	978 (w)
904 (w)	908 (w)
834 (m)	842 (m)
800 (m)	810 (m)
758 (s,sh)*	742 (s)
670 (w)	680 (m)
645 (w)	660 (m,sh)
538 (w)	543 (w)
476 (w)	475 (w)
452 (w)	-
435 (w)	440 (m)
388 (s)	384 (s)
316 (s)	329 (s)
300 (s,sh)	306 (s,sh)
-	267 (w)
229 (m)	238 (m)
-	215 (w)

* w: weak. m: medium, s: strong, sh: shoulder.

metal dπ orbitals or aromatic π systems the N lone pairs interact. It is also difficult to assign a M-N stretching band below 1220 cm^{-1} for alkylimido complexes because alkylamines exhibit N-C stretching modes in the 1020-1220 cm^{-1} region.

The M-N stretching frequency is influenced by substitution on the N atom owing to the vibrational coupling. This has been observed in imido complexes $[Cl_3V(NX)]$: on going from X=Cl to Br and I, the ν(V-N) stretch decreases from 1170 to 1032 to 963 cm^{-1} with the ν(N-X) decreasing from 510 to 435 to 390 cm^{-1}. Compared to Br and I, Cl is the most electronegative. It should lead to a reduction in the bond order of M-N. However ν(V-N) in $[Cl_3V(NCl)]$ shows the highest frequency suggesting the V-N stretching frequency is dependent on the mass of X. If X is an organic substituent, the ν(M-N) goes to even higher frequencies, generally between 1200 and 1300 cm^{-1}.

An opposite point of view has also been given [241]. It suggested, based on the studies of $[Cp^*_2V(NR)]$ (R=C_6H_5, $C_6H_3Me_2$), that the 934 cm^{-1} band is due to the V-N stretching while the 1330 band corresponds to the N-C stretching mode. This has been confirmed by two facts: When R is dimethyl substituted phenyl, the V-N bond is shortened (Table 1.3) but the N-C bond is lengthened due to the lessened conjugation between the lone pair on N atom and aromatic π system. In fact ν(N-C) drops to 1293 cm^{-1}. This assignment also agrees with the ranking of the multiple bond order: M(N) > M(O) > M(NR). The ν(M-N) in nitrido complexes normally appears in the range of 948-1135 cm^{-1}. Molybdenum nitrido and oxo complexes exhibit ν(Mo-N) and ν(Mo-O) around 948-1109 and 900-1000 cm^{-1}, respectively.

Based on the two arguments above, the Mo-N stretching bands of the model complexes should appear in the 1360-850 cm^{-1} region. All of the bands in this region are

listed in Table 3.1. Even compared with the spectrum of [$MoCl_2$(dttd)], it is still hard to assign any one of these bands to ν(Mo-N). This is because: a) the Mo-N bond strength of the four complexes should be different if conjugation discussed in Section 1.3.2 is taken into account. This difference has been demonstrated in UV-VIS studies. The strength of Mo-N decreases in the order $MoNNPh_2$ > MoNMe ≈ ($MoNNMe_2$) > MoNPh. b) the coupling of vibrations in Mo-N-R fragment makes the assignment complicated. Nevertheless the bands positioned at 1305 cm^{-1} for phenylimido and 1308, 1320 cm^{-1} for diphenyl hydrazido complexes can be assigned to MoNPh and $MoNNPh_2$ respectively. The bands at 945 cm^{-1} for $MoNNMe_2$ and 930 cm^{-1} for $MoNNPh_2$ may be related to N-N vibrations since there are no bands around this region in the spectra of the imido complexes, and the N-N interaction is stronger in $NNMe_2$ than in $NNPh_2$ due to the conjugation (see Section 3.5.2) [242]. Both MoNMe and $MoNNPh_2$ show bands at 1175 cm^{-1}, which may be related to the MoNR units, where there is no or little conjugation between N and R, and the Mo-N bonds are relatively strong. There is one band at 1250 cm^{-1} for MoNMe only, which may be a combination vibration of Mo-N and N-Me. MoNPh shows an extra band at 978 cm^{-1}, perhaps related to the Mo-N bonds. However, further studies are required for a definite assignment to MoNR, in particular studies with ^{15}N isotope substitution.

The two FTIR spectra and band wavenumbers of methylimido and phenylimido molybdenum complexes are shown in Fig. 3.14, 3.15 and Table 3.2.

3.3.2.2 UV-Visible Spectroscopy [239]

Based on the ligand field description of multiple bonded complexes, the five d

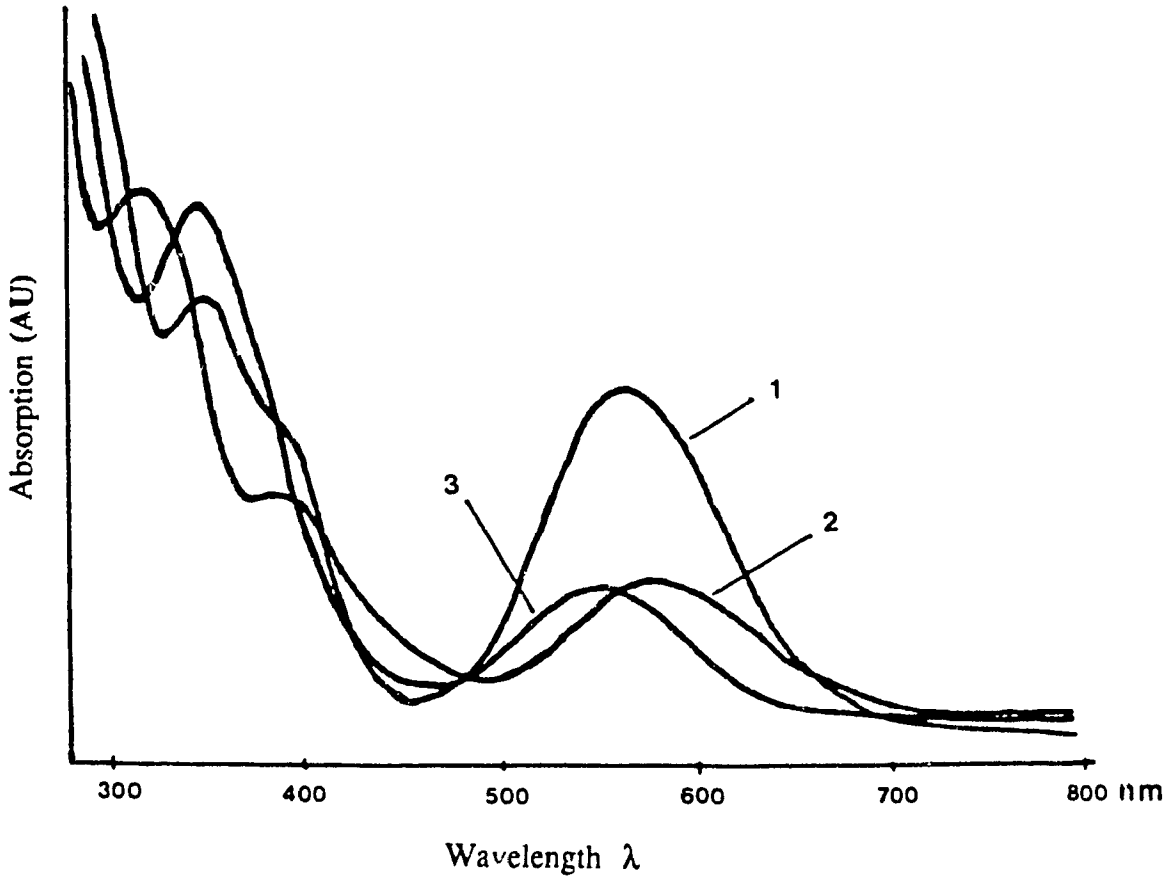

Fig. 3.16 UV-VIS spectra of the model complexes

(1) [MoCl(NMe)(dttd)], **(2)** [MoCl(NPh)(dttd)],

(3) [MoCl($NNPh_2$)(dttd)].

orbitals split, in the manner of increasing orbital energy, d_{xy}, degenerate d_{xz} and d_{yz}, $d_{x^2-y^2}$ and d_{z^2} if z axis is taken along the multiple bonds, (see Section 1.3.3, Fig.1.3 and 1.4). Electron spin resonance studies of d^1 vanadium and molybdenum complexes suggest that this electron primarily occupies a nondegenerate orbital perpendicular to the M-L multiple bond, that is the d_{xy} orbital. In electronic spectra of oxo and nitrido complexes, the lowest absorption band observed in the spectra of d^1 and d^2 complexes has been assigned to the $d_{xy} \rightarrow d_{xz}$, d_{yz} or $n \rightarrow \pi^*$ transition. It can also be described as metal-to-ligand charge transfer, since the π^* orbitals have significant ligand character.

In the UV-VIS (300-800 nm) spectra of [MoCl(NMe)(dttd)] (**1**), [MoCl(NPh)(dttd)] (**2**) and [MoCl($NNPh_2$)(dttd)] (**4**), the lowest energy bands are clearly seen, positioned at 565, 576 and 550 nm for (**1**), (**2**) and (**4**) respectively. (see Fig. 16). According to the ligand field description, these bands are essentially due to the absorptions of $n \rightarrow \pi^*$ or $d_{xy} \rightarrow d_{xz}$, d_{yz} transitions. The $n \rightarrow \sigma^*$ or $d_{xy} \rightarrow d_{x^2-y^2}$, d_{z^2} transitions, which correspond to the ligand field splitting energies (10 D_q in O_h symmetry) cannot be seen clearly, but they must be in higher energy levels. If we consider that the $n \rightarrow \sigma^*$ transition of $MoCl_6^{3-}$ occurs at 526 nm, and the chloride ligands, by comparison with a multiple bonding ligand and the chelate sulfur ligand in the model compounds, normally produce a much weaker ligand field, the assignment argued above is reasonable.

Although the energy differences among the three bands are small, they still can be used to compare the strength of the multiple bonds. Complex (**3**) has $n \rightarrow \pi^*$ transition at 550 nm (the highest energy band of the three) suggesting the strongest interaction between molybdenum and diphenylhydrazido ligand. This interaction, especially the π-interaction component, enlarges the energy gap between d_{xy} and d_{xz}, d_{yz}. While complex

(2) has the $n \rightarrow \pi^*$ transition at lowest energy (576 nm), thus the interaction between Mo and phenylimido ligand is the weakest. This is consistent with conjugation arguments. Since the lone pair on βN in complex (3) conjugates to the phenyl π system, the αN has its lone pair to interact principally with molybdenum dπ orbital. Thus a relatively strong multiple bond forms. On the contrary, the conjugation of lone pair with phenyl ring in complex (2) reduces the interaction on Mo-NPh, therefore a relatively weak multiple bond forms. Complex (1) has the absorption at 565 nm, consistent with a bond of medium strength and medium bond order.

Based on the conjugation arguments and the UV-VIS spectra obtained, the complex [$MoCl(NNMe_2)$(dttd)] (3) should have an absorption between 565-576 nm, and the four multiple bond strength order should be Mo=NPh < $Mo=NNMe_2$, Mo=NMe < $Mo=NNPh_2$.

The spectra of (1) and (2) also show other absorptions at 390 and 350 nm for (1) and at 390 and 316 nm for (2). While the spectrum of (3) shows one other intense absorption at 348 nm, the 390 nm band cannot be seen clearly. The spectroscopic studies on the oxo complex [$Mo(O)_2$(dttd)] [224] suggested that the O→Mo charge transfer (CT) occurs at 410 nm and the S→Mo CT occurs at 480 nm. Studies of [$MoCl_2$(dttd)] [226] have suggested that both the 470 and 492 nm bands are due to the S→Mo charge transfer. Although there are no bands observed at ~480 nm in the spectra of the model complexes, the ~390 nm band is probably due to the S→Mo charge transfer and the ~350 nm band is probably due to the N→Mo charge transfer.

The model Mo(V) complexes have been electrochemically and chemically reduced to Mo(III) species (see Section 3.3.2.3 and Chapter IV). The UV-VIS spectra (Fig. 3.17) of the Mo(III) species reduced from complexes (1) and (2) show absorptions at 608 and

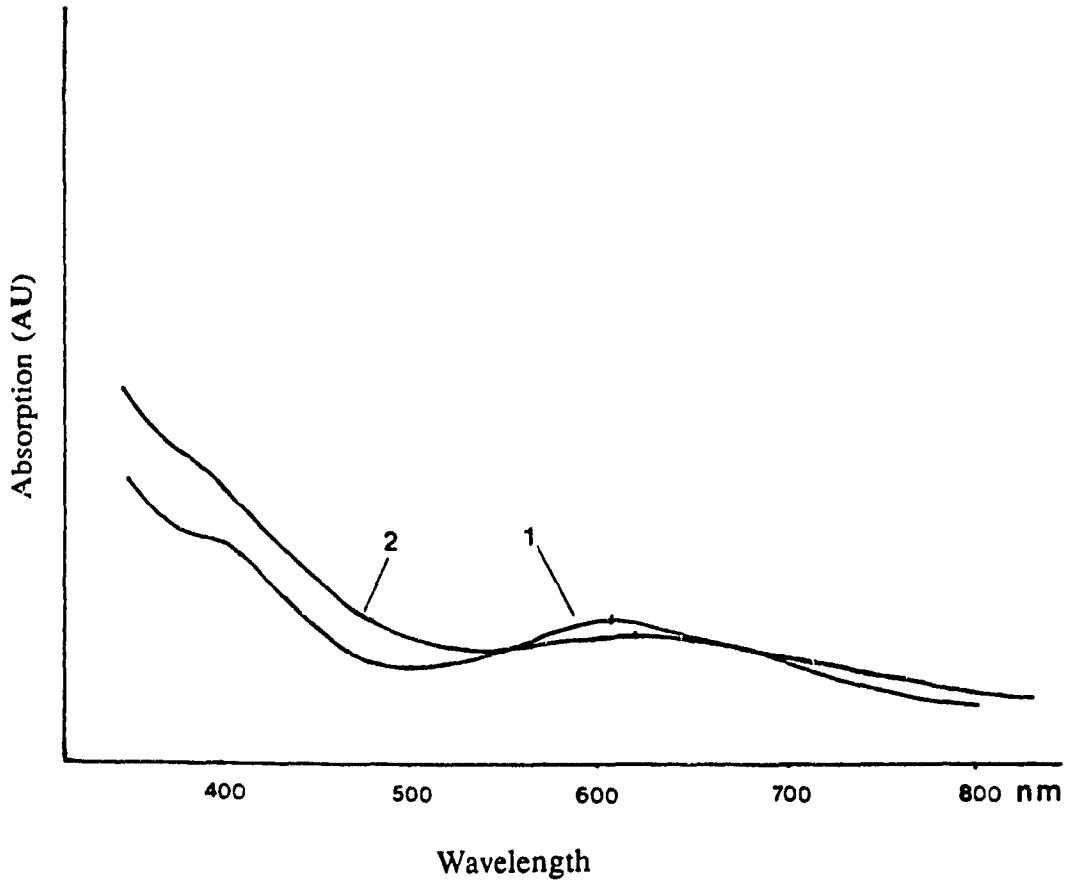

Fig. 3.17 UV-VIS spectra of Mo(III) species obtained from the reduction of (**1**) [MoCl(NMe)(dttd)] and (**2**) [MoCl(NPh)(dttd)] by Zn/Hg in CH_2Cl_2.

624 nm. Compared with the aborptions of complexes (**1**) and (**2**), these absorptions shifted more than 40 nm toward the low energy. This red shift suggested a much smaller transition energy required in the Mo(III) species than in the Mo(V) complexes. This is due to the weakening of the Mo-N multiple bonds, decreasing the ligand field. Consequently, the d -> d transitions are shifted to low energy.

3.3.2.3 Cyclic Voltammetry [239]

The redox properties of the model complexes were characterized by cyclic voltammetry, with the exception of the dimethylhydrazido(2-) molybdenum complex [MoCl(NNMe$_2$)(dttd)], due to the uncertainty of the purity. One of the voltammograms is shown in Fig. 3.18, and the results are listed in Table 3.3. All three complexes gave similar cyclic voltammograms. They only show one redox process between -0.1 and -1.8 V. The small shoulder in Fig.3.18 is probably due to an minor impurity. Little changes in ΔE were observed when the scan rate varied in the range of 50-600 mVs^{-1}. The peak separations ΔE (=E_{pa}-E_{pc}), 80 mV for complex (**1**), 100 mV for complex (**2**) and 50 mV for (**4**) indicates that these redox processes are irreversible according to the criterion, ΔE > 56/n mV, where n is the number of electrons involved in the redox process. Nevertheless repeated cycling did not change the amplitude of the waves (i_p). By using a diffusion coefficient of 10^{-6} cm^{2}s^{-1} for all three complexes, the observed peak currents (i_p) fit with those calculated for a two-electron process. This is also confirmed by subsequent coulometry experiments on complex (**1**) at a constant potential of -1.0 V. The currents required for complete reduction closely corresponds to a two electron processes. In a complete reduction, the violet coloured Mo(V)complexes were reduced to green coloured

Fig. 3.18 Voltammogram of [MoCl(NNPh$_2$)(dttd)].

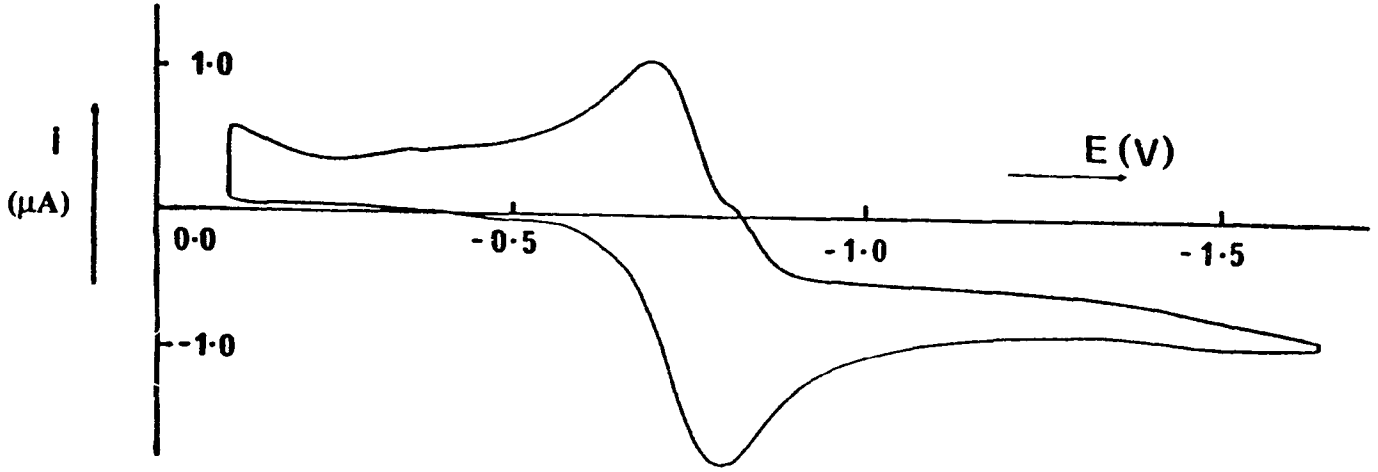

Table 3.3 Electrochemical parameters.

	Mo(dttd)Cl(NMe)	Mo(dttd)Cl(NPh)	Mo(dttd)Cl($NNPh_2$)
E_{pc} (V)	-0.740	-0.660	-0.785
E_{pa} (V)	-0.660	-0.560	-0.735
$E_{1/2}$ (V)[a]	-0.700	-0.610	-0.760
ΔE (V)[b]	0.080	0.100	0.050
$i_{pa(obsd)}$ (μA)	4.70	4.65	4.50
$i_{pa(calcd)}$ $1e^-$ [c]	2.1	2.1	1.9
$i_{pa(calcd)}$ $2e^-$	6.1	6.1	5.3
$i_{pa(calcd)}$ $3e^-$	11.2	11.2	9.8
C (molarity) $x10^4$	5.6	5.6	5.0

a: Mean of E_{pc} and E_{pa}. b: E_{pa} - E_{pc}.

c: The anodic peak current was calculated using a diffusion coefficient of 10^{-6} cm^2, the concentration shown in the last line, and the specified number of electrons.

Mo(III) compounds.

In a typical continuous electron transfer process, as shown in Eq.3,14

$$A + N_1e \overset{E_1^0}{\rightleftharpoons} B + n_2 \overset{E_2^0}{\rightleftharpoons} C \qquad (3.14)$$

if ΔE^0 ($=E_2^0-E_1^0$)=0 and $n_1=n_2=1$, there is only one wave in the voltammogram, since both A and B are reduced at the same potential, and both of them are involved in one electron processes. The amplitude of the wave, i_p, is higher than that in a one electron process and lower than that in two electron process. The results in Table 3.4 clearly show that the observed i_{pa} are between one and two electron redox processes, suggesting a two-step one-electron continuous reduction of these complexes. Oxo Mo(dttd) complexes usually undergo a one electron reversible redox reaction. For example, [MoO_2(dttd)] undergoes $1e^-$ reversible redox reaction and $2e^-$ irreversible reaction to give [MoOCl(dttd)]$^-$. The oxo analogue of the model complexes [MoOCl(dttd)] also undergoes $1e^-$ reversible reaction [223].

The reduction products of imido and hydrazido complexes greatly depend on the solvents, as mentioned in Chapter I. In the presence of 10-fold excess of the proton donor $(CF_3)_2CHOH$, the position of the waves in voltammograms of the model complexes remained unchanged down to -1.5V suggesting that the redox potentials of these complexes are unaffected by protic solvents, at least $(CF_3)_2CHOH$. This also implies perhaps, that for these model Mo(V) complexes, protonation does not occur before or during the reduction in the presence of the alcohol.

The irreversibility of the redox process probably comes from an irreversible change in the linkage of the Mo-N multiple bonds in the redox reaction. In the ligand field description, the one electron of a Mo(V) complex occupies the lowest energy orbital d_{xy}.

During one electron reduction Mo(V) becomes Mo(IV), the $2e^-$ share the d_{xy} orbital since the large energy gap exists between d_{xy} and d_{xz}, d_{yz}, and the d^2 electron configuration is still acceptable for imido and hydrazido complexes. When Mo(IV) is reduced to Mo(III), the extra e^- enters $d\pi$ orbitals and activates the Mo-N multiple bonds. The irreversibility may also come from the cleavage of Mo-Cl bond and the formation of a sulfur bridge. This has been demonstrated in the reduction of complex (**1**) by zinc amalgam. The resulting product is a dimer which corresponds to two molecules of (**1**) bonding mutually, meanwhile one chloride and one imido ligand are eliminated under reduction condition (Section 5.2).

3.4 The Crystal Structure of [MoCl(NNPh$_2$)(dttd)] [239]

The use of IR spectroscopy as a technique for unambiguous structural analysis of the model complexes is not satisfactory. This has been demonstrated in determination of the ν(Mo-N) in Section 3.4.2.3, because for polyatomic molecules more than one vibration mode often contributes to a given band in a spectrum. Furthermore, data about geometries of these complexes, such as bond length and bond angle which are very important in characterization cannot be obtained. Although NMR is widely used in structure determination, it is not effective in dealing with paramagnetic compounds.

X-ray diffraction is one of the most powerful methods of structure determination, but suitable high quality single crystals are needed. Although the methylimido, phenylimido and diphenylhydrazido complexes were repeatedly recrystallized in various solvents, none of them gave high quality crystals for structural analysis. Fortunately, one crystal of the diphenylhydrazido complex was found whose diffraction multiplets could

be resolved. This complex crystallizes in the orthorhombic space group *Pbac*. The structure was determined by the heavy-atom method and refined to R_1=0.081 and R_2=0.102 for 1257 independent reflections. Eight molecules were found in a unit cell. The molecule structure is shown in Fig. 3.19, the selected bond distances and bond angles are listed in Table 3.4 and the crystallographic data are collected in Table 3.5.

3.4.1 Geometry

The molybdenum centre is pseudooctahedrally surrounded by four sulfur atoms of dttd, a chloride and the diphenylhydrazido ligand (see Fig. 3.19). As in the cases of other dttd transition metal complexes, the two thiolates sulphurs, S_1 and S_4, of dttd are arranged in sites *trans* to each other. The two thioether sulphur, S_2 and S_3, are mutually *cis*, and *cis* to the two thiolates. The chloride is *cis* to the hydrazido ligand, the thiolates and S_2, but *trans* to another thioether S_3. The hydrazido ligand is in a *cis* site to S_1, S_3, S_4 and the chloride, but *trans* to S_2. This geometry is consistent with the desired model described in Chapter II. The multiply bonded ligand likes to be *cis* to chloride and thiolate has also been found in oxo complexes containing a chloride and thiolate groups [223]. However, in the phosphine Mo complex, [MoCl(NNH_2)(triphos)(PR_3)], the chloride takes a site *trans* to the NNH_2.

3.4.2 Discussion

The distance of Mo-N_1 (1.751 Å) indicates the existence of a multiple bond. It is comparable to the Mo-N distances in other structure identified molybdenum hydrazido or organohydrazido complexes (1.69-1.82 Å in Table 1.3). The N_1-N_2 distance is 1.342 Å,

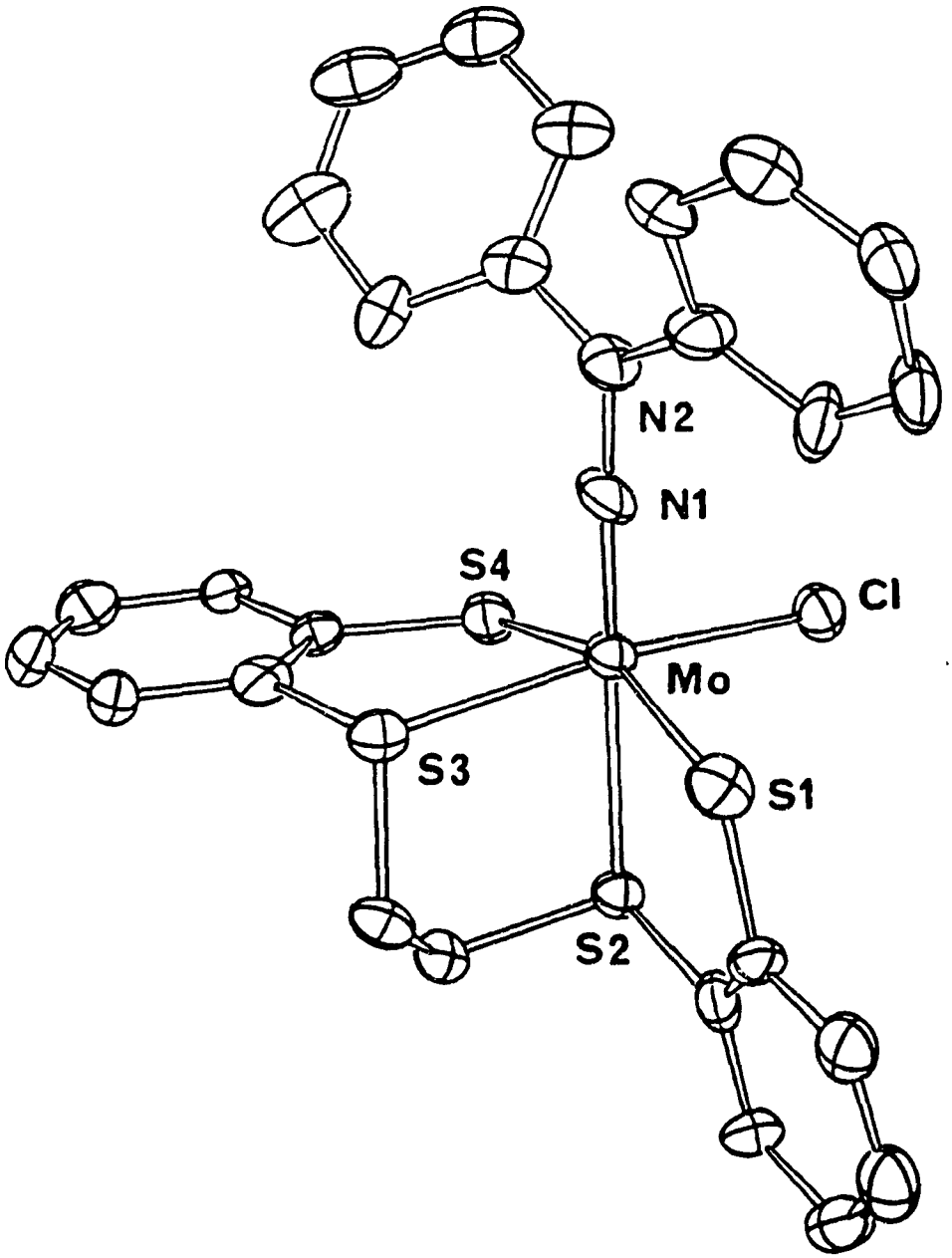

Fig. 3.19 Molecular structure of the complex [$MoCl(NNPh_2)(dttd)$].

Table 3.4 Bond lengths and bond angles of [$MoCl(NNPh_2)(dttd)$].

Bond Lengths (Å)*

MO - CL	2.408(7)	MO - S1	2.435(7)
MO - S2	2.608(6)	MO - S3	2.478(7)
MO - S4	2.414(7)	MO - N1	1.751(17)
S1 - C10	1.781(24)	S2 - C8	1.851(24)
S2 - C9	1.774(24)	S3 - C2	1.792(22)
S3 - C7	1.816(23)	S4 - C1	1.771(23)
C1 - C2	1.40(3)	C1 - C6	1.40(3)
C2 - C3	1.44(3)	C3 - C4	1.40(4)
C4 - C5	1.37(4)	C5 - C6	1.42(3)
C7 - C8	1.53(3)	C9 - C10	1.34(3)
C9 - C14	1.44(3)	C10 - C11	1.44(3)
C11 - C12	1.45(4)	C12 - C13	1.40(4)
C13 - C14	1.41(4)	N1 - N2	1.342(25)
N2 - C15	1.46(3)	C15 - C16	1.40(3)
C15 - C20	1.37(3)	C16 - C17	1.39(3)
C17 - C18	1.41(4)	C18 - C19	1.41(3)
C19 - C20	1.42(4)	N2 - C21	1.46(3)
C21 - C22	1.41(3)	C21 - C26	1.43(4)
C22 - C23	1.45(4)	C23 - C24	1.34(4)
C24 - C25	1.40(4)	C25 - C26	1.41(4)

Table 3.4 Continued

Bond Angles (deg)*			
CL - MO - S1	97.30(23)	CL - MO - S2	86.32(21)
CL - MO - S3	167.97(23)	CL - MO - S4	88.79(22)
CL - MO - N1	96.1(7)	S1 - MO - S2	80.24(21)
S1 - MO - S3	86.77(22)	S1 - MO - S4	158.55(23)
S1 - MO - N1	95.0(7)	S2 - MO - S3	83.21(20)
S2 - MO - S4	79.64(20)	S2 - MO - N1	175.0(7)
S3 - MO - S4	83.52(22)	S3 - MO - N1	94.8(6)
S4 - MO - N1	104.8(7)	MO - N1 - N2	172.7(17)
MO - S1 - C10	108.5(8)	MO - S2 - C8	101.6(7)
MO - S2 - C9	105.2(8)	C8 - S2 - C9	101.9(10)
MO - S3 - C2	104.8(8)	MO - S3 - C7	104.4(8)
C2 - S3 - C7	102.7(11)	MO - S4 - C1	106.7(7)
S4 - C1 - C2	122.2(16)	S4 - C1 - C6	118.0(16)
C2 - C1 - C6	119.6(20)	S3 - C2 - C1	120.8(17)
S3 - C2 - C3	116.8(17)	C1 - C2 - C3	122.3(20)
C2 - C3 - C4	117.0(22)	C3 - C4 - C5	119.7(23)
C4 - C5 - C6	124.0(24)	C1 - C6 - C5	117.1(21)
S3 - C7 - C8	112.4(15)	S2 - C8 - C7	112.1(15)
S2 - C9 - C10	120.9(18)	S2 - C9 - C14	115.8(18)
C10 - C9 - C14	123.3(22)	S1 - C10 - C9	124.2(18)

Table 3.4 Bond Angles Continued

S1 - C10 - C11	112.8(19)	C9 - C10 - C11	122.7(22)
C11 - C12 - C13	123.7(23)	C12 - C13 - C14	119.6(23)
C9 - C14 - C13	116.7(24)	N2 - C15 - C16	117.9(19)
N2 - C15 - C20	118.2(20)	C16 - C15 - C20	123.8(21)
C15 - C16 - C17	117.0(22)	C16 - C17 - C18	121.7(23)
C17 - C18 - C19	119.5(23)	C18 - C19 - C20	119.6(23)
C15 - C20 - C19	118.2(22)	N2 - C21 - C22	115.1(22)
N2 - C21 - C26	118.9(20)	C22 - C21 - C26	126.0(23)
C21 - C22 - C23	115.4(23)	C22 · C23 - C24	119.9(24)
C23 - C24 - C25	123.(3)	C24 - C25 - C26	122.(3)
C21 - C26 - C25	113.3(23)	C15 - N2 - C21	126.2(17)
C15 - N2 - N1	116.9(18)	C21 - N2 - N1	116.7(18)

* The esd's given in parentheses refer to the least signigicant digit(s) of the preceding number.

Table 3.5 Crystallographic data for [MoCl(NNPh$_2$)(dttd)].

Crystal Parameters	
Formula: $C_{26}H_{22}ClMoN_2S_4$	fw = 622.12
Crystal system: orthorhombic	Space group: *Pbca*
a = 21.298(15) Å	$\alpha = 90°$
b = 14.056(10) Å	$\beta = 90°$
c = 17.732(11) Å	$\gamma = 90°$
V = 5308(11) Å^3	Z = 8
d_{calcd} = 1.55 g cm^{-1}	μ(Mo Kα) = 9.04 cm^{-1}
Colour: blue/black	Transmission 70 - 87%
Crystal size: 0.40 x 0.15 x 0.08 mm	Temp. = 22°

Table 3.5 Continued

Data Collection and Structure Refinement	
Diffractometer: Picker FACS-1	Radiation: Mo Kα
Monochromator: graphite	Scan method: θ/2θ
Scan speed: 2°/m	Data limits: 3.5<2θ<40°
Octants collected: +h +k +l, -h -k -l	Total reflections collected: 4949
Independent reflections collected: 2475	Unique data $F_o>2\sigma F_o$: 1257
Least-squares method: block diagonal	Absorption correction: yes
Parameters refined: 307	Data/parameter ratio = 4.0
$R_1 = 0.081$	$R_2 = 0.102$
Goodness of fit = 1.65	

$R_1 = \Sigma[||F_o| - |F_c||]/\Sigma|F_o|$

$R_2 = [\Sigma w(|F_o| - |F_c|)^2/\Sigma w|F_o|^2]^{1/2}$, where $w = 1/\sigma(F_c)$

Goodness of fit = $[\Sigma w(|F_o| - |F_c|)^2/(N_{obs} - N_{parm})]^{1/2}$

which falls just between MeN=NMe 1.23 Å and H_2N-NH_2 1.46 Å, suggesting a bond order of ~ 1.5, i.e. some double bond character. The almost linear Mo-N-N fragment ($\angle$Mo-N-N =172.7^0) indicates that N_1 atom adopts sp hybridization, while the coplanarity of N_1, N_2, C_{15} and C_{21} ($\angle C_{15}$-N_2-C_{21} + $\angle C_{15}$-N_2-N_1 + $\angle C_{21}$-N_2-N_1 = 359.8^0) unambiguously indicates sp^2 hybridization for the βN. The average distance (1.46Å) of N_2-C_{15} and N_2-C_{16} is shorter than the N-C bond length of aliphatic amine, ~1.48 Å. All these data suggest a σ+π interaction between Mo and αN and an extensive delocalization throughout the $MoNNPh_2$ unit. From a comparison of Mo-N and N-N distances of the diphenylhydrazido model complex with the dimethylhydrazido molybdenum complex [242], which has a Mo-N distance of 1.78 Å and a N-N distance of 1.30 Å, the effect of substituents on βN are clearly seen.

A linear $MNNR_2$ unit lies between one of the two canonical forms shown below:

A **B**

For low oxidation state molybdenum(IV) hydrazido(2-) complexes form **A** is preferred, while the high oxidation state Mo(VI) complexes would like to adopt form **B**, since in form **B** electron density drifts towards the metal. Based on the data, the diphenylhydrazido Mo(V) complex is closer to **B** rather than **A**, since βN in **A** is sp^3 hybridized while in **B** it is sp^2 hybridized, although the Mo oxidation state falls between IV and VI.

The average bond length of Mo-S(thiolate) bonds is 2.42 Å, shorter than the Mo-S(thioether) bonds (Mo-S_3, 2.48 Å). The large *trans* influence of the hydrazido ligand

exerted on S_2 can be seen clearly from the unusually long Mo-S_2 distance (2.61 Å), which is about 0.13 Å longer than its neighbour. Compared to molybdenum sulfur containing enzymes, these Mo-S bond lengths are longer than the Mo-S distances (2.37 Å) postulated from EXAFS results for FeMo-cofactor and significantly shorter than sulfite oxidase (2.82-2.86 Å).

There is a common feature for the Mo-S-C bond angles. All of them are less than the perfect sp^3 hybridization angle 109.47°. Otherwise the bond angles around sulfur are approximately tetrahedral. Distortions from the ideal tetrahedral angle are often seen in complexes where the metal and S atoms form part of a ring. Most Mo-S-C angles are small rather than larger than the tetrahedral angle, except in the case where the thioether S atom bridges to metal centres. This observation has been ascribed to either the large steric effect of lone pairs or an incomplete involvement of the s orbital in the sp^3 hybridization.

There are factors contributing to the distortion of the geometry from an octahedron associated with the dttd and the hydrazido ligands. In almost all of the reported dttd transition metal complexes, there is a tendency for the S atoms to be close to each other. This can be seen from the *cis* S-Mo-S angles, none of them is 90° and the *trans* S-Mo-S angles are less than 170^0. The small angles may be a reflection of the inherently short S-S distance in the sulfur containing ligands. For example, a 3.3 Å S-S distance is required for a dithioether to chelate a Mo(0) centre [230]. These angles are further squeezed if a multiply bonded ligand is present. In this molecule, the diphenylhydrazido ligand not only lengthens the Mo-S_2 distance, but also repels the ligands *cis* to it, owing to the "fat" multiple bond and the short $MoNNPh_2$ unit. This distortion has been visualized as a

movement of the metal atom towards the multiply bonded ligand and away from the centre of an ideal octahedral geometry.

CHAPTER IV

REDUCTION OF THE MODEL COMPLEXES

Chemical reductions of the model complexes have been carried out in order to gain insight into the protonation-reduction mechanism of hydrazido and imido intermediates in nitrogen fixation. Electrochemical experiments had indicated that these complexes should be reduceable by common reducing agents such as Zn and Na. It was hoped that information about mechanisms might be obtained from the structures of the intermediates and products during the reduction courses. However, among the characterization methods, only X-ray crystallography was particularly useful because of the paramagnetism of the compounds. Thus, not only reduction, but also crystallization for structure analysis was important.

Based on the discussion in section 1.2.5 and Scheme 1.1, the reduction-protonation reactions of the imido molybdenum complexes are pernaps easier to understand: The final products are amines, and the reduction and protonation steps should be carried out successively. The question is, which atom is protonated first: the nitrogen or the metal centre. This depends on the nature and electron density of the nitrogen and the central metal atom.

In the two canonical forms for imido complexes, as shown below, complexes which adopt form **C** should favour protonation on the nitrogen atom, while complexes which adopt form **D** may be only protonated after reduction. This behaviour had been shown by the Mo(V) model complexes, which are inert towards the proton donor $(CF_3)_3COH$ in electrochemical experiments (see Section 3.3.2.5). Moreover the electrochemical reduction

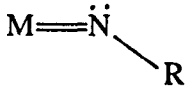

(C)

(D)

of the Mo(V) complexes did not stop at Mo(IV) but went directly to Mo(III). Undoubtably, this kind of reduction destroys the Mo-N multiple bond: imido and hydrazido molybdenum complexes appear only to exist in Mo(IV)-Mo(VI) systems and no Mo(III) imido or hydrazido complexes have been found so far.

In the case of hydrazido complexes, based on the discussion in Section 1.2.5 and Scheme 1.2, the protonation-reduction becomes complicated. Protonation occurs not only on the βN atom as expected, but also on the αN and the Mo centre. Complexes which adopt form **A** (Section 3.4.2), favour protonation on the βN atom, while for complexes which adopt form **B**, the protonation probably occurs on the metal centre, or does not occur at all before reduction.

The four model complexes prepared either take form **B** or take form **D**. There are no stereoactive lone pair electrons on the N atoms. Thus reduction is expected first.

The methyl- and phenylimido molybdenum (V) complexes could be reduced by zinc or sodium amalgam. In the absence of H^+, reduction by one equivalent of electrons gave a black-brownish solution, reduction by two equivalents gave a green solution. The dimethyl- and diphenylhydrazido Mo(V) complexes decomposed during the "$1e^-$" and "$2e^-$" reductions. The initial violet coloured solution became clear and the solute precipitated out as a fine brown power. When the reductions of these four compounds were carried out in the presence of H^+, all of them gave a similar brownish green solution for the "$1e^-$" reduction and a blue solution for the "$2e^-$" reduction. It seems that the reduction of all four model complexes in the presence of H^+ gave rise to a similar

product. For more detail see Section 4.4.

The reduction studies were principally concentrated on the methylimido Mo(V) complex, since the preparation of the other three model complexes was very time consuming and the yields were low.

4.1 Strategy of Reduction

The strategy of reduction was based on the kind of intermediates and products that might have been obtained. There were many possible products during the reduction courses. Several factors were considered:

- The reduction stoichiometry was tested with one or two equivalents of electrons.
- The reductions were carried out in the absence or presence of a phosphine ligand, to see whether the chloride ligand could be replaced by a phosphine under the reduction conditions, (the removal of a chloride ligand from a molybdenum centre under reduction conditions has been observed [70, 92]).
- The reduction was carried out with or without the presence of an acid;
- Large cations A^+ (A^+=PPh_4^+, NBu_4^+) were used in case the products were anionic, in the hope of getting suitable crystals. (Since the Mo(dttd) is a relatively rigid core, it was expected to be stable during the reduction.)

When the Mo(V) complexes are reduced, bonds might be broken to give either neutral or anionic complexes. The cleavage of Mo-S bonds seems unlikely since the

Scheme 4.1 The possible intermediates and products of one-electron reduction of [MoCl(NR)(dttd)] (R=Me).

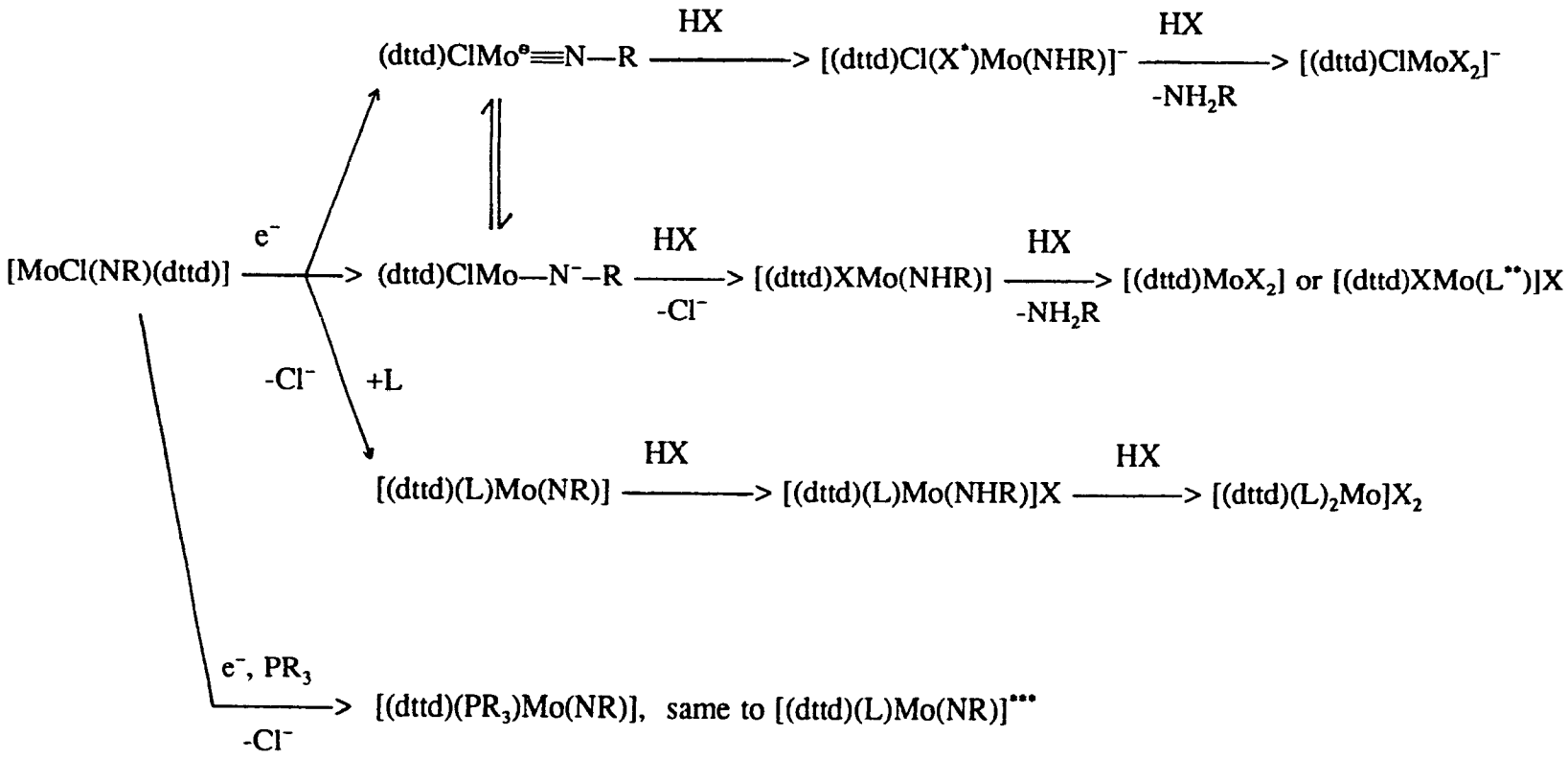

* X=anion, including Cl^-; ** L=solvent, monodentate phosphine or NH_2R; *** if L=PR_3.

Scheme 4.2 The possible intermediates and products of two-electron reduction of [MoCl(NR)(dttd)] (R=Me).

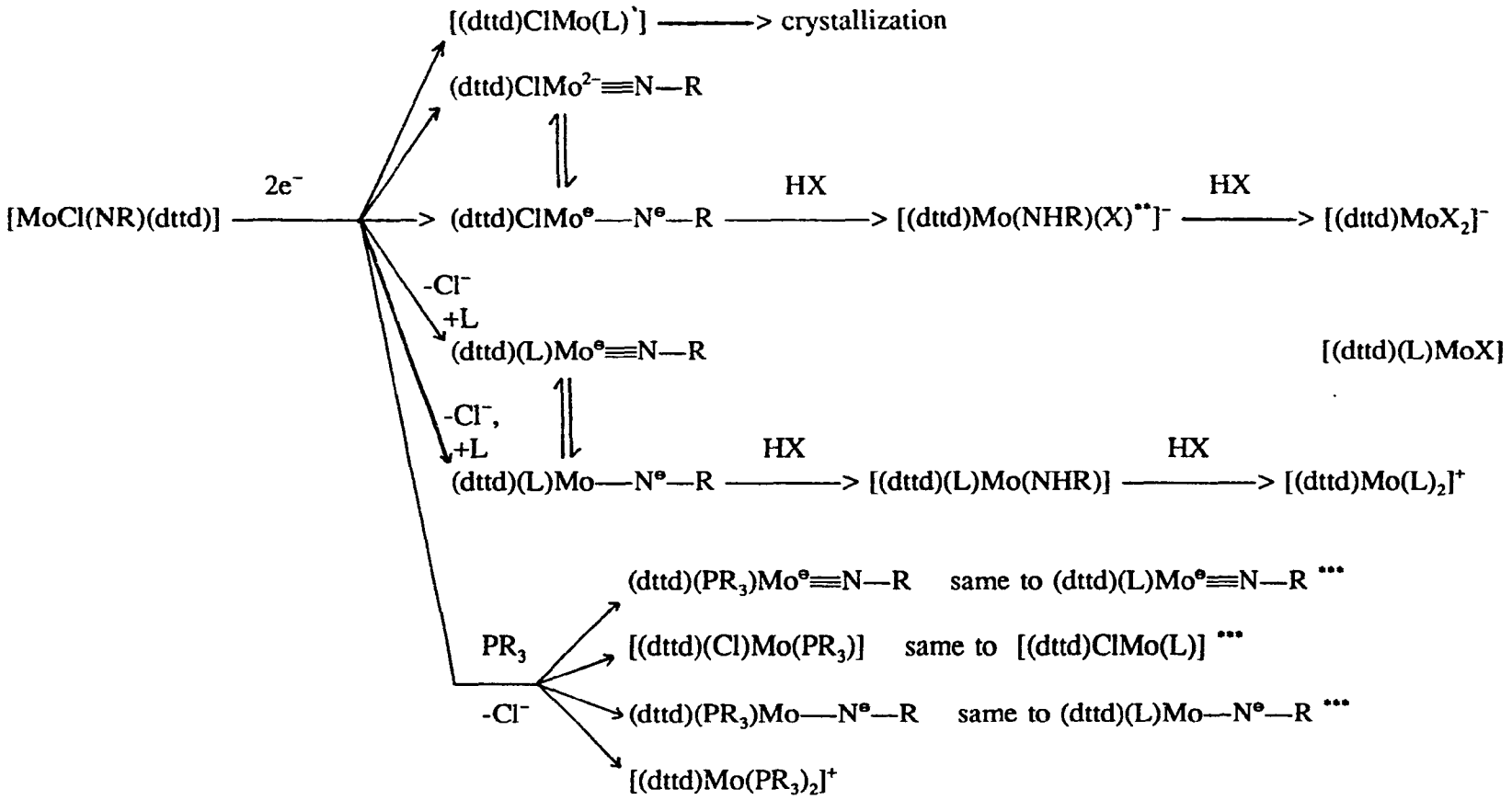

* L=solvent; ** X can also be a chloride; *** if L=PR_3

Mo(dttd) is a relatively rigid core, it is expected to be stable during the reductions. The possible "$1e^-$"and "$2e^-$" reduction intermediates and products are presented in Scheme 4.1 and 4.2, respectively.

In the case of "$1e^-$" Mo(V) -> Mo(IV) reduction, the possible neutral Mo(IV) complex might be [Mo(L)(NR)(dttd)] (L= solvent or monodentate organophosphine) derived from cleavage of the Mo-Cl bond. The possible anions might be either an anion in which the negative charge localizes on the metal centre and all of the Mo-L bonds remain unchanged, or an anion, such as (dttd)ClMo–$N^{\ominus}$–R derived from reduction of the Mo-N bond order, in which the negative charge principally localizes on the N atom. Although these possible products or intermediates possess a d^2 configuration, their behaviour and reactivities might be quite different. In the latter case, the lone pairs on the N atom make it a strong nucleophile. It has the potential to bridge to another metal centre to give a dimer or a polymer. In the presence of H^+, the N atom could be protonated to give a neutral complex [(dttd)ClMo(NHR)]. On the other hand, the protonation on the former anion complex, which has the negative charge on the metal centre, may produce a hydride.

If a one-electron reduction is carried out in the presence of phosphines, the chloride ligands might be replaced by phosphines leading to the formation of neutral species [(dttd)(NR)Mo(PR_3)]. Protonation on this complex with acid HB, if the protonation only occurs on the nitrogen atom, may give either complex cations such as [(dttd)(PR_3)Mo(NHR)]$^+B^-$, or neutral complexes such as [(dttd)Mo(B)(NHR)]. Further protonation, (if it occurs, although it is unlikely to be on the nitrogen atom only) may also give complex cations such as [(dttd)(PR_3)Mo(NH_2R)]$^{2+}B^-_2$, [(dttd)Mo(B)(NH_2R)]$^+B^-$ or a

neutral complex [(dttd)Mo$(B)_2$] and NH_2R. This neutral complex is just the precursor of the model complexes. If it reacted with silylamine or silylhydrazines to give the model complexes, a cycle would be completed.

In the case of a two-electron Mo(V) -> Mo(III) reduction (Scheme 4.2), the possible products are: anions (dttd)$ClMo^{2-}\equiv N-R$, in which all of the M-L bonds remain unchanged; anions (dttd)(L)$Mo^{\oplus}\equiv N-R$ (L=solvent), in which the Mo-Cl bond is broken; anions (dttd)$ClMo^{\oplus}-N^{\ominus}-R$, in which one of the Mo-N covalent bonds is broken; and anions (dttd)(L)$Mo-N^{\ominus}-R$, in which both of the Mo-Cl bond and one of the Mo-N covalent bonds are broken. A neutral product [(dttd)ClMo(L)] resulting from the complete cleavage of the Mo-N multiple bond may also be obtained. When the $2e^-$ reduction is carried out in the presence of phosphines, four other possible products may be obtained, they are: (dttd)$(PR_3)Mo^{\oplus}\equiv N-R$, [(dttd)ClMo$(PR_3)$], (dttd)$(PR_3)Mo-N^{\ominus}-R$ and [(dttd)Mo$(PR_3)_2]^+$. The last one seems unlikely due to the significant change in the coordination sphere.

Protonation of these products would give additional compounds. Protonation on the chloride ligand is unlikely and only protonation on nitrogen has been considered in Scheme 4.2.

Various attempts at crystallization and exchanges with large cations were carried out in the hope of trapping one or more of the various potential products.

4.2 One-Electron Reduction

The reduction reactions of [MoCl(NR)(dttd)] were carried out in THF and sodium amalgam was used as reducing agent because the precise content of sodium in the

amalgam is known. Crystallization of the "1e⁻" reduction product failed not only in THF, but also in CH_2Cl_2, CH_3CN and Et_2O. Exchange with large cations was attempted in a dry-box. The freshly reduced products were treated with tetrabutylammonium chloride or tetraphenylphosphonium chloride. Although some brown precipitate formed, no crystals were obtained from the concentrated black-brownish filtrate even after one week storage at -25°C.

Reduction of the model complexes in the presence of an equivalent of a monodentate organophosphine, such as PPh_3, $PMePh_2$, PMe_3 and PBu_3, also gave brownish-black solutions. No crystals were obtained even after one week standing at -25° C.

The one-equivalent-electron reductions were also carried out with the presence of a proton source, in one-to-one, two-fold proportions and in excess. In the presence of H^+, reduction of the molybdenum (V) complexes gave a brownish-green solution. Once again, no crystals were obtained.

Protonation experiments were also performed on the products which were reduced without H^+ or with phosphine according to Scheme 4.1. Large cation exchanges were tried at every possible anionic stage. No crystals were ever obtained from the one-electron reduction experiments. All of the reduced products are unstable: they decomposed gradually after one week storage in the refrigerator.

When a model complex undergoes one-electron reduction, it would either form an anion or a neutral complex as mentioned above. However, no positive results could be used to confirm the existence of one or the other of these possible species. The formation of a neutral complex is in question, since it is not necessary to break the Mo-Cl bond

when Mo(V) complexes are reduced to Mo(IV). The two electrons (d^2) can pair in the metal d_{xy} orbital (see Section 1.3.3). On the other hand, no stable Mo(IV) neutral complexes, such as [Mo(L)(NR)(dttd)], were isolated. It is not clear whether this neutral species can be produced in the Mo(V) -> Mo(IV) reduction system, or it is only an intermediate with a very short life-time, and being further reduced as soon as it forms. Also, the formation of the possible anions is in question, since no complexes, such as $[MoCl(NR)(dttd)]^-$ or [MoCl(NHR)(dttd)], were ever isolated. Even if they existed, they were not stable and were further reduced to Mo(III) species. This has been supported by the cyclic voltamograms in which there is no Mo(V)/Mo(IV) wave. The possible explanation may be the resultant Mo(IV) species possess the same or even higher redox potential than the Mo(V) compounds. Although chemical "$1e^-$" reductions were carried out quantitatively, the resulting product may be a mixture of Mo(V) and Mo(III) complexes.

The instability of the Mo(IV) anions is not surprising given the statistical data: in the established structural data collected by Nugent [245], there are only two anionic complexes $[Mo(NNPh)Mo(NNHPh)(S_2C_2H_4)_3(S_2C_2H_5)]^{2-}$ and $[\{Mo(NNPh)_2(\mu\text{-}OMe)(\mu\text{-}O_2MoO_2)\}_2]^{2-}$ among thirty-five molybdenum and tungsten imido and hydrazido complexes in which the metal centres possess d^2 electronic configurations and adopt octahedral geometries. However the second anion is not a hydrazido complex: actually it is a diazenido complex, and there may be only limited multiple bonding character between Mo and N when it adopts single bent bonding mode (see Section 1.4.1). The other 33 compounds are either neutral complexes or positively charged complex cations. This statistical data suggests that molybdenum(IV) imido and hydrazido complex anions are

not stable although their d^2 electronic configurations meet the requirement for two $d\pi$ orbitals for the formation of the Mo-N multiple bonds.

4.3 Two-Electron Reduction

The "two-electron" reductions of the model complexes were carried out under the same conditions as the "one-electron" reduction experiments. The reducing agents used were sodium amalgam and zinc amalgam. Sodium amalgam was used quantitatively, while the zinc amalgam was used in excess because the precise content of Zn in the amalgam was unknown due to the method of preparation (see experimental section). As expected the speed of reduction using Na/Hg is faster than that using Zn/Hg.

Protonation after the reduction, reduction in the presence of phosphines and large cation exchanges in every possible anionic stage were also performed according to Scheme 4.2. Several kinds of crystals were obtained. However only one of them was successfully analysized by X-ray crystallography. More details are given below.

4.3.1 Two-Electron Reduction with Zinc Amalgam

In order to know which valence bond would be broken during the $2e^-$ reduction, the Mo(V) model complexes were reduced by excess zinc amalgam without the presence of H^+ and phosphines. The hydrazido complexes were destroyed after they were mixed with Zn/Hg/THF. The imido complexes were successfully reduced to give a dark green solution for methylimido complex and a brownish green solution for the phenylimido complex. These solution were treated with PPh_4Cl, followed by treatment with $PMePh_2$. Crystals were obtained after 2 weeks storage at -10^0C. The compound could be

recrystallized, but some decomposition occured.

The reduction product of the methylimido complex gave black crystals with suitable size and shape for X-ray diffraction studies. One of the crystals was selected and sealed in a capillary tube with a diameter of 3 mm for X-ray crystallographic experiments.

The reduction product of the phenylimido complex gave large thin brownish crystals. They were relatively stable when exposed to air. Lack of strong spots in the alignment and zero-level photographs suggested that there may be no heavy atoms (molybdenum) in the unit cell. Thus no further analyses were performed on this compound.

4.3.2 Crystal Structure of [(dttd)Mo(μ-NMe)(μ-S-dttd)MoCl]· $3CH_2Cl_2$

The reduction product of methylimido molybdenum(V) complex crystallizes in a monoclinic space group $P2_1/c$. In this space group, the b axis was treated as the unique axis and the lattice constants are: a = 16.888(6) Å, b = 11.258(4) Å, c = 24.011(20) Å and β = 106.60(4)°. The structure was determined by heavy-atom method and refined to R_1 = 0.0742, R_2 = 0.1035 for 3658 reflections with $F_o > 3\sigma F_o$. Four molecules were found in a unit cell. Crystallographic data are collected in Table 4.1. The molecular structure of the dimer is shown in Fig. 4.1, and the bond lengths and bond angles are listed in Table 4.2.

4.3.2.1 Geometry

The molecule is a Mo(III)-Mo(IV) dimer with a metal-metal bond, a nitrogen and a sulfur bridge. The formation of this dimer can be described as two methylimido

Table 4.1 Crystallographic Data for [(dttd)Mo(μ-NMe)(μ-S-dttd)MoCl]·3CH_2Cl_2.

Crystal Parameters	
Formula: $C_{32}H_{33}Cl_7Mo_2NS_8$	fw = 1128.15
Crystal system: monoclinic	Space group: $P2_1/c$
a = 16.888(6) Å	α = 90°
b = 11.258(4) Å	β = 106.60(4)°
c = 24.011(20) Å	γ = 90°
V = 4374.8 Å^3	Z = 4
$d_{calcd.}$ = 1.713 g cm^{-1}	μ(Mo Kα) = 13.85 cm^{-1}
Colour: black	Transmission: 73 - 85%
Crystal size: 0.35 x 0.35 x 0.30 mm	Temp. = 22°

Table 4.1 Continued

Data Collection and Structure Refinement	
Diffractometer: Picker FACS-1	Radiation: Mo Kα
Monochromator: graphite	Scan method: θ/2θ
Scan speed: 2°/m	Data limits: 3.5<2θ<40°
Quadrant collected: +h +k +l,-h +k +l	Total reflections collected: 5721
Independent reflections collected: 5721	Unique data $F_o>3\sigma F_o$: 3658
Least-squares method: block diagonal	Absorption correction: yes
Parameters refined: 451	Data/parameter ratio = 8.1
R_1 = 0.0742	R_2 = 0.1035
Goodness of fit = 1.359	

$R_1 = \Sigma[||F_o| - |F_c||]/\Sigma|F_o|$

$R_2 = [\Sigma w(|F_o| - |F_c|)^2/\Sigma w|F_o|^2]^{1/2}$, where $w = 1/\sigma(|F_o|)$

Goodness of fit = $[\Sigma w(|F_o| - |F_c|)^2/(N_{obs} - N_{parm})]^{1/2}$

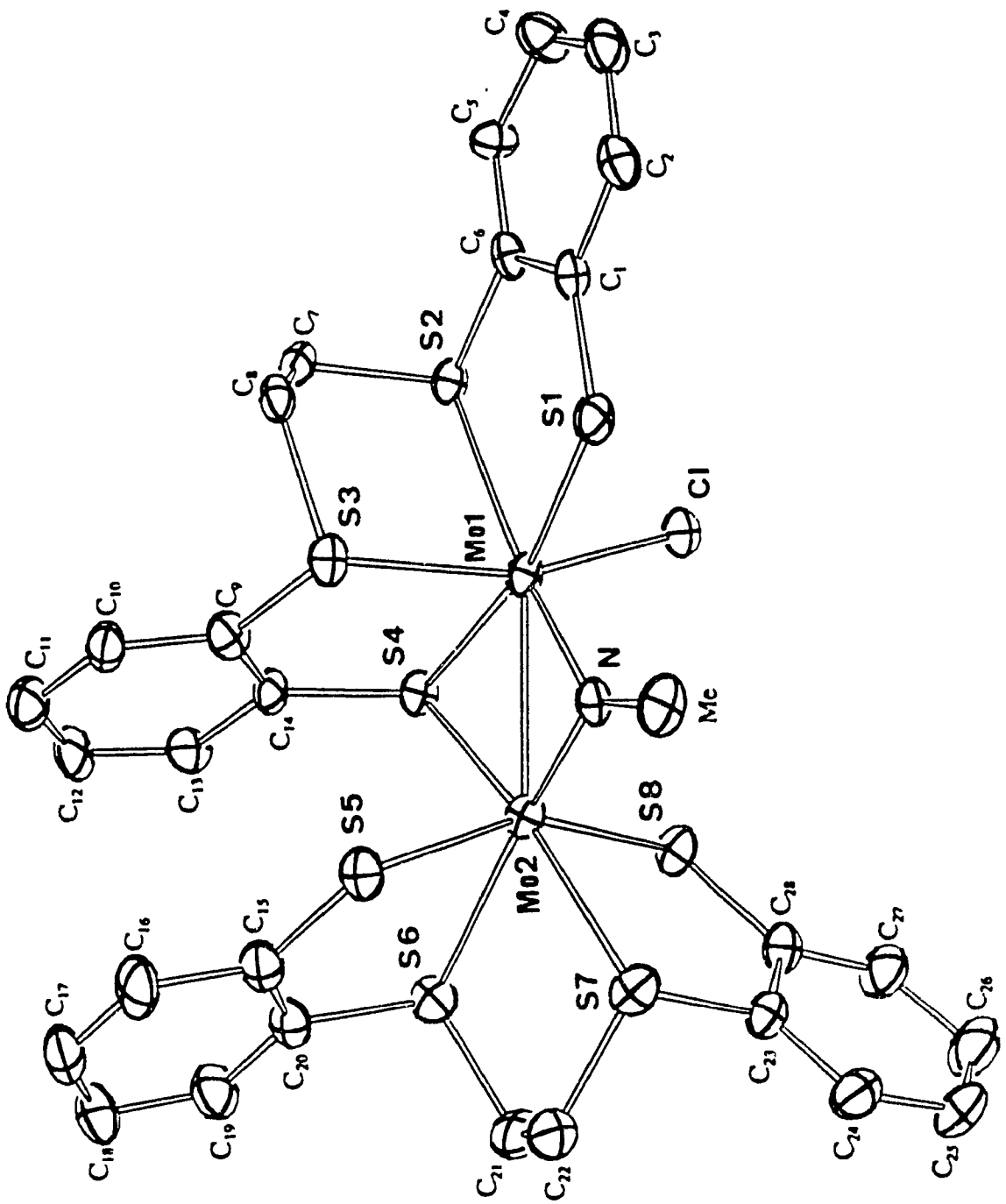

Fig. 4.1 The molecular structure of [(dttd)Mo(μ-NMe)(μ-S-dttd)MoCl]· $3CH_2Cl_2$.

Table 4.2 The bond lengths and bond angles of [(dttd)Mo(μ-NMe)(μ-S-dttd)MoCl]· $3CH_2Cl_2$.

Bond Lengthes (Å)*					
MO1	MO2	2.6097(20)	MO1	S1	2.475(3)
MO1	S4	2.438(3)	MO1	S2	2.583(3)
MO1	S3	2.503(4)	MO1	Cl	2.384(4)
MO1	N	1.974(10)	MO2	S4	2.441(3)
MO2	S5	2.478(4)	MO2	S7	2.530(4)
MO2	S6	2.608(4)	MO2	S8	2.415(4)
MO2	N	1.914(10)	S1	C1	1.739(13)
S4	C14	1.805(13)	S5	C15	1.769(15)
S2	C6	1.772(12)	S2	C7	1.836(13)
S3	C8	1.848(14)	S3	C9	1.761(13)
S7	C22	1.827(17)	S7	C23	1.781(13)
S6	C20	1.818(13)	S6	C21	1.850(17)
S8	C28	1.765(14)	C1	C2	1.469(18)
C1	C6	1.409(17)	C2	C3	1.383(21)
C3	C4	1.404(21)	C4	C5	1.402(20)
C5	C6	1.402(17)	C7	C8	1.510(18)
C9	C10	1.432(18)	C9	C14	1.439(19)
C10	C11	1.393(21)	C11	C12	1.459(25)
C12	C13	1.385(21)	C13	C14	1.413(17)

Table 4.2 Bond Lengths Continued

C15	C16	1.460(19)	C15	C20	1.362(20)
C16	C17	1.301(23)	C17	C18	1.40(3)
C18	C19	1.444(24)	C19	C20	1.381(21)
C21	C22	1.548(24)	C23	C24	1.392(20)
C23	C28	1.420(19)	C24	C25	1.382(22)
C25	C26	1.38(3)	C26	C27	1.42(3)
C27	C28	1.386(20)	ME	N	1.459(16)
ME1	CL1A	1.750(22)	ME1	CL1B	1.751(21)
CL1A	CL1B	2.860(9)	ME2	CL2A	1.82(3)
ME2	CL2B	1.70(3)	CL2A	CL2B	2.807(16)
ME3	CL3A	1.706(25)	ME3	CL3B	1.610(23)
CL3A	CL3B	2.901(13)			

Table 4.2 Continued

Bond Angles (deg.)*							
MO2	MO1	S1	131.69(9)	MO2	MO1	S4	57.72(9)
MO2	MO1	S2	145.72(9)	MO2	MO1	S3	93.78(10)
MO2	MO1	CL	101.15(11)	MO2	MO1	N	46.9(3)
S1	MO1	S4	166.62(12)	S1	MO1	S2	82.09(11)
S1	MO1	S3	85.79(12)	S1	MO1	CL	93.07(13)
S1	MO1	N	85.1(3)	S4	MO1	S2	88.00(11)
S4	MO1	S3	83.88(12)	S4	MO1	CL	93.90(13)
S4	MO1	N	104.5(3)	S2	MO1	S3	81.60(12)
S2	MO1	CL	79.27(13)	S2	MO1	N	167.1(3)
S3	MO1	CL	160.81(13)	S3	MO1	N	96.2(3)
CL	MO1	N	102.8(3)	MO1	MO2	S4	57.61(9)
MO1	MO2	S5	102.74(11)	MO1	MO2	S7	135.23(10)
MO1	MO2	S6	141.53(10)	MO1	MO2	S8	100.56(11)
MO1	MO2	N	48.8(3)	S4	MO2	S5	99.71(13)
S4	MO2	S7	166.38(12)	S4	MO2	S6	84.01(12)
S4	MO2	S8	90.87(13)	S4	MO2	N	106.3(3)
S5	MO2	S7	82.62(13)	S5	MO2	S6	79.49(13)
S5	MO2	S8	156.59(13)	S5	MO2	N	92.3(3)
S7	MO2	S6	83.23(13)	S7	MO2	S8	82.43(13)
S7	MO2	N	86.9(3)	S6	MO2	S8	80.94(13)

Table 4.2 Bond Angles Continued

S6	MO2	N	167.9(3)	S8	MO2	N	104.7(3)
MO1	S1	C1	105.4(4)	MO1	S4	MO2	64.68(9)
MO1	S4	C14	106.2(4)	MO2	S4	C14	107.1(4)
MO2	S5	C15	107.2(4)	MO1	S2	C6	104.9(4)
MO1	S2	C7	105.0(4)	C6	S2	C7	98.6(6)
MO1	S3	C8	105.0(4)	MO1	S3	C9	106.7(5)
C8	S3	C9	97.4(6)	MO2	S7	C22	105.2(5)
MO2	S7	C23	105.8(4)	C22	S7	C23	100.2(7)
MO2	S6	C20	105.2(5)	MO2	S6	C21	102.0(5)
C20	S6	C21	103.6(7)	MO2	S8	C28	108.0(4)
S1	C1	C2	117.5(9)	S1	C1	C6	126.7(10)
C2	C1	C6	115.7(11)	C1	C2	C3	121.3(12)
C2	C3	C4	119.9(13)	C3	C4	C5	121.0(13)
C4	C5	C6	118.9(12)	S2	C6	C1	119.4(10)
S2	C6	C5	117.6(9)	C1	C6	C5	123.0(11)
S2	C7	C8	112.2(8)	S3	C8	C7	112.3(8)
S3	C9	C10	118.8(10)	S3	C9	C14	120.5(9)
C10	C9	C14	120.5(12)	C9	C10	C11	120.5(13)
C10	C11	C12	118.1(13)	C11	C12	C13	121.3(12)
C12	C13	C14	121.0(13)	S4	C14	C9	122.5(9)
S4	C14	C13	119.2(10)	C9	C14	C13	118.3(11)
S5	C15	C16	120.5(11)	S5	C15	C20	124.9(10)

Table 4.2 Bond Angles Continued

C16	C15	C20	114.5(13)	C15	C16	C17	122.7(15)
C16	C17	C18	122.3(14)	C17	C18	C19	117.4(14)
C18	C19	C20	117.6(15)	S6	C20	C15	118.7(11)
S6	C20	C19	116.0(11)	C15	C20	C19	125.2(13)
S6	C21	C22	115.7(10)	S7	C22	C21	111.9(11)
S7	C23	C24	120.4(11)	S7	C23	C28	120.0(10)
C24	C23	C28	119.5(12)	C23	C24	C25	123.2(15)
C24	C25	C26	118.9(15)	C25	C26	C27	118.3(15)
C26	C27	C28	123.9(15)	S8	C28	C23	122.5(10)
S8	C28	C27	121.4(11)	C23	C28	C27	116.1(13)
MO1	N	MO2	84.3(4)	MO1	N	ME	137.5(9)
MO2	N	ME	138.0(9)	CL1A	ME1	CL1B	109.5(9)
ME1	CL1A	CL1B	35.2(6)	ME1	CL1B	CL1A	35.2(6)
CL2A	ME2	CL2B	106.1(15)	ME2	CL2A	CL2B	35.5(9)
ME2	CL2B	CL2A	38.4(10)	CL3A	ME3	CL3B	122.0(14)
ME3	CL3A	CL3B	28.1(7)	ME3	CL3B	CL3A	29.9(9)

* The esd's given in parentheses refer to the least significant digit(s) of the preceding number.

complexes [MoCl(NMe)(dttd)] losing one chloride and one imido ligand during the reduction, then connecting together through the sulfur and nitrogen bridges and the Mo-Mo bond. Each molybdenum atom is seven coordinated. Mo_1 is surrounded by one chloride, one amido and four sulfur atoms. While Mo_2 is coordinated by an amido and five sulfur atoms. Compared to other dttd-transition metal complexes, the framework of dttd ligands remains unchanged during the "$2e^-$" reduction except that one of the thiolate sulfur atoms forms a bridge to the other metal centre using a previously unshared electron pair. The thioethers are mutually *cis* and the thiolates are mutually *trans*.

Seven-coordinate complexes are not often found. Among them three geometries are common. They adopt either a pentagonal bipyramid derived from the octahedral geometry by addition to an edge, or a capped octahedron with the seventh ligand occupying the face of an octahedron, or a capped trigonal prism with the seventh ligand being above a rectangular face. Since the angles of N-Mo_1-Mo_2 (46.9^0), N-Mo_2-Mo_1 (48.8^0), S_4-Mo_1-Mo_2 (55.7^0) and S_4-Mo_2-Mo_1 (57.6^0) are much less than that of a pentagonal bipyramid geometry, in which these angles should be close to 72^0, this dimer is better described as two pseudooctahedra sharing one edge, that is the N-S_4 edge.

4.3.2.2 Results and Discussion

The following is a suggested mechanism for the formation of the dimer. The simplified possible mechanism of the formation of the dimer through the combination of the two possible intermediates is illustrated in Scheme 4.3.

During the "$2e^-$" reduction, two imido complexes lose one chloride and one imido ligand to form two different kinds of possible Mo(III) intermediates (see Section 4.1).

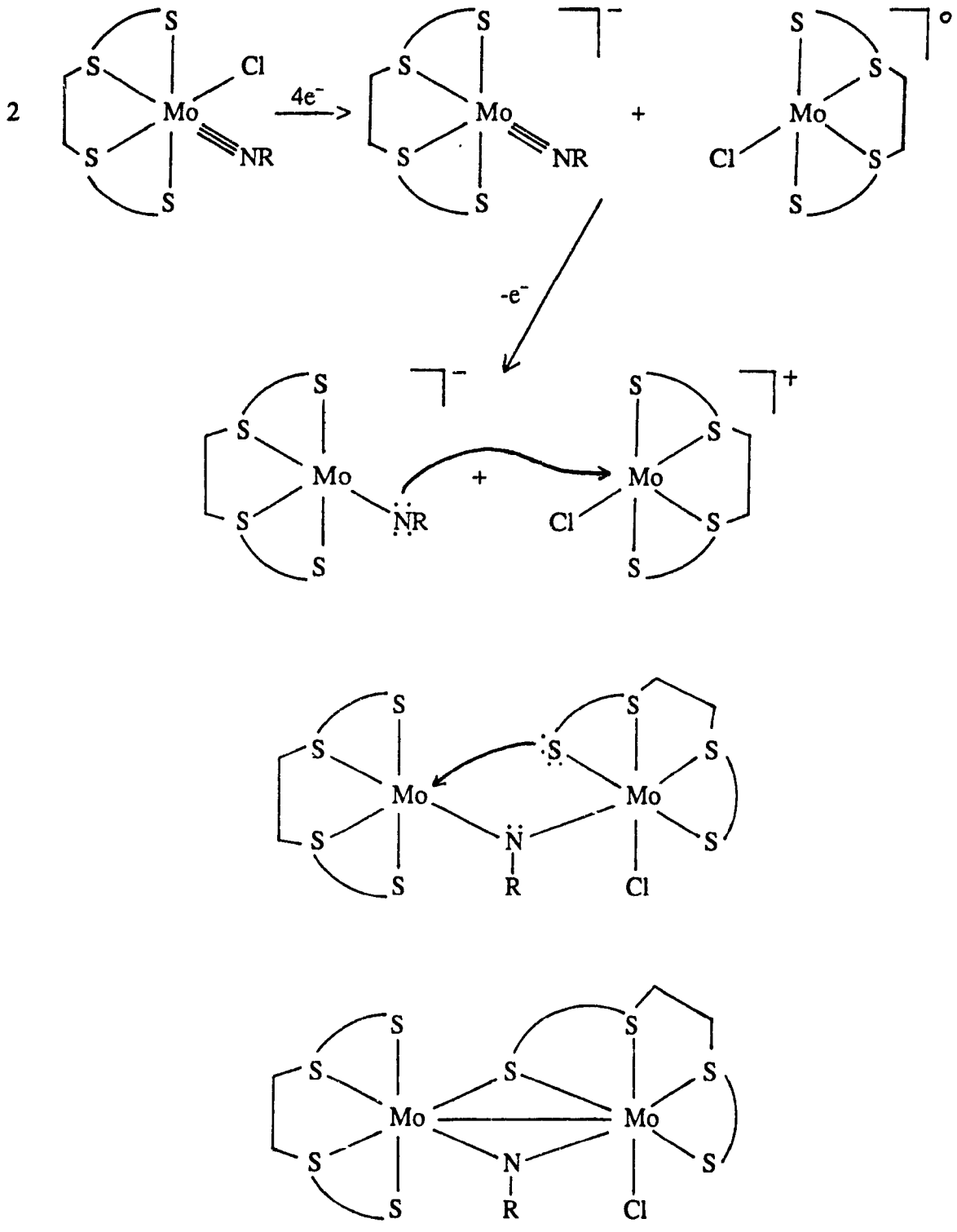

Scheme 4.3 The formation of the dimer (S S S S=dttd).

One is (dttd)(L)Mo—N$^{\bullet}$–R (L=solvent, phosphine), the other is [(dttd)ClMo(L)] (L=solvent, phosphine). When the Mo(V) centre accepts two electrons, the second one will occupy the π^* or the degenerate dπ orbitals, d_{xz} or d_{yz} (see Section 1.3.3). This occupation decreases the interaction between dπ and pπ orbitals of the ligating nitrogen, since this dπ electron is an anti-bonding electron which exerts large repulsion on the nitrogen pπ electrons. Consequently the π bond between nitrogen and molybdenum is cleaved, leading to the possible formation of (dttd)ClMo$^{\bullet}$—N$^{\bullet}$–R species.

These species are not stable, further cleavage of the Mo-L (L=Cl, N) bonds leads to the formation of the two possible intermediates. The (dttd)(L)Mo—N$^{\bullet}$–R species is derived from the further cleavage of the Mo-Cl bond to give an anion species, the other is derived from the cleavage of the σ Mo-N bond to give a neutral Mo(III) species, [(dttd)ClMo(L)], and RN^{2-} species. Since in the (dttd)ClMo$^{\bullet}$—N$^{\bullet}$–R species, there are free bonding electrons on the nitrogen atom and three dπ electron on the metal centre, the repulsion between molybdenum and nitrogen is enhanced, and the remained Mo-N bond is activated. As a result, the Mo-N σ bond can be broken, also. This Mo-N σ cleavage is also favoured by the formation of a neutral Mo(III) species.

In the two possible intermediates, (dttd)(L)Mo—N$^{\bullet}$–R is more active since the negative charge is associated with a bonding orbital, and the nitrogen atom becomes a strong nucleophile. It is ready to bind with another electrophilic metal centre to form a stable dimer.

The Mo-Cl distance in the dimer is 2.384(4) Å, about 0.024 Å shorter than that in the diphenylhydrazido complex, although in the dimer the molybdenum is seven coordinated and its oxidation state is lower. On the other hand, the thioether sulfur atom

trans to the chloride ligand is pushed away from the metal centre, leading to a 0.025 Å longer Mo-S_3 distance in the dimer than that in diphenylhydrazido complex (2.503(4) Å *vs.* 2.478(7) Å). The lengthening of the Mo-S_3 distance is probably due to the *trans* influence of the chloride, although the chloride ligand is positioned close to the lower end in the ligand *trans*-influence order.

The two molybdenum centres have a separation of 2.610(2) Å. This is somewhat shorter than the Mo-Mo distances in other molybdenum dimer complexes [245-247] probably due to the small Mo-N-Mo (84.3(4) deg.) and Mo-S-Mo (64.68(9) deg.) angles and the short Mo-N distances (average 1.944 Å). In a seven coordinated complex, the seventh ligand usually suffers repulsion from t_{2g} orbitals if the t_{2g} orbitals are filled with electrons. In the dimer if N-Mo_1-S_2 and N-Mo_2-S_6 are considered as two z axes, S_4-Mo_1-S_1 and S_4-Mo_2-S_7 as two y axes, Cl-Mo_1-S_3 and S_5-Mo_2-S_8 as two x axes, and the second Mo is treated as the seventh ligand, as illustrated in Fig. 4.2, the Mo-Mo should interact with d_{yz} orbitals not d_{xz} or d_{xy} orbitals. Although the two molybdenums are Mo(III) and Mo(IV) respectively and both have non-bonding d electrons, these prefer to stay in d_{xy} orbitals due to the relatively large energy gap, cause by π interaction, between d_{xy} and d_{xz}, d_{yz}. Thus little repulsion exists between the two Mo atoms or between the seventh ligand and the d electrons. This is agreement with the relatively short Mo-Mo distance with respect to the sum of the covalent radii.

However, it seems that the Mo-Mo distance in a dimer possessing an N bridge is not determined by the number of the non-bonding electrons in the d orbitals, that is the Mo-Mo distance is not, at least, closely related to the repulsion existing between the two Mo centres. Actually, this distance is determined by the Mo-N-Mo angle and Mo-N

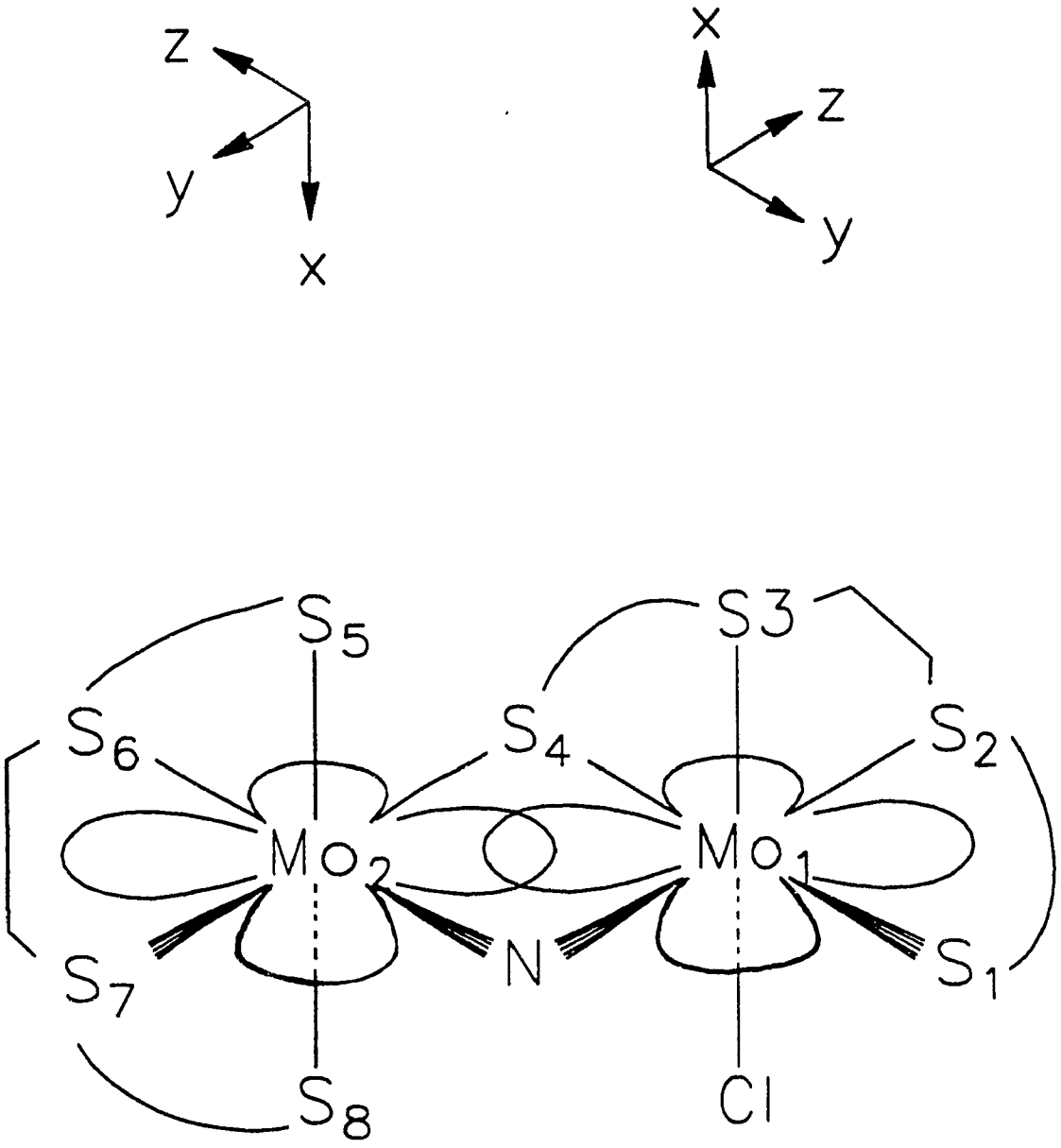

Fig. 4.2 The coordinate system for the Mo(III)-Mo(IV) dimer and the interaction of the d_{yz} orbitals between the two molybdenum centres.

distance which reflect the extent of Mo-N interaction. For example, in an Mo(V)-Mo(V) dimer [245], which possesses an Mo(μ-N)(μ-N)Mo unit as depicted in (**A**), since the Mo-N-Mo angles (average 86^0) are larger and Mo-N distance (average 1.96 Å) is longer than that in the Mo(III)-Mo(IV) dimer. The Mo(V)-Mo(V) distance (2.672 Å) is longer even though there are no non-bonding d electrons on the two metal centres.

On the contrary, if the Mo-Mo distance depends on the repulsion of the two relatively positive metal centres, the distance should be longer in the Mo(V)-Mo(V) case than in the Mo(III)-Mo(IV) case. However, in a Mo(III)-Mo(III) dimer complex with a framework (**B**) [247], the Mo-Mo has a distance (2.788 Å), also longer than the Mo(III)-

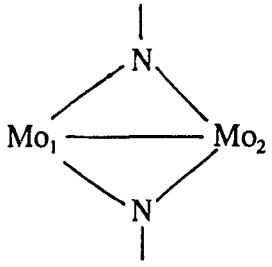

(A)

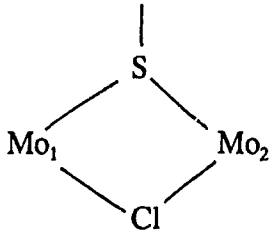

(B)

Mo(IV) even though the oxidation state is lower in the former. However, the former has larger bridge angles and longer Mo-bridging atom distances. Thus the Mo-Mo distance in a dimer greatly depends on the nature and geometry of the bridging atoms.

Because of the existence of Mo_1-Mo_2 interaction, the S_4-Mo-N angles are enlarged (average 105.4^0). Interestingly, the adjacent angles to $\angle S_4$-Mo-N such as $\angle S_2$-Mo_1-S_4, (88.0(11) deg.) and $\angle S_7$-Mo_2-N (86.9(3) deg.) are not compressed, but the angles positioned opposite $\angle S_4$-Mo-N, i.e. $\angle S_6$-Mo_2-S_7 (83.23(13) deg.) and $\angle S_1$-Mo_1-S_2 (82.09(11) deg.) are.

The bridging nitrogen atom in the dimer plays an important role in the geometry.

It spans the two molybdenum centres with an angle ($\angle Mo_1$-N-Mo_2) of 84.3(4) degree and an average N-Mo distance of 1.944 Å. This Mo-N distance is shorter than the sum of covalent-metallic radii of Mo (1.36) and N (0.74). It is also shorter than the Mo-N distances in the complex having fragment (**A**) and in [$Mo(NMe_2)_6$] (Mo-N=2.034 Å) [248]. On the other hand, the sum of the three angles around the bridging nitrogen atom in the Mo(III)-Mo(IV) dimer is 359.8^0 indicating planarity and therefore sp^2 hybridization of the nitrogen atom. The lone pair, in a pπ orbital of the nitrogen, is parallel to the two x axes and is perpendicular to the plane formed by Mo_1, Mo_2, N and C of the methyl group. This arrangement makes an opportunity to the lone pair electrons to interact with the d_{xz} orbitals of the metal atoms, and makes Mo-N bonds containing a π component. This π interaction is illustrated in Fig. 4.3.

Based on the discussion above, the molecular orbital diagrams for each molybdenum centre and the Mo(μ-N)Mo centre can be simply drawn qualitatively as in Fig. 4.4. Two of the five d electrons form a Mo-Mo bond through the d_{yz} orbitals, three non-bonding electrons of the dimer stay in the two d_{xy} orbitals and the two d_{xz} orbitals interact with nitrogen lone pair to form π bonds.

In the case of (**A**) [245], there are two nitrogen bridges, the average sum of the three angles around N is about 355^0, indicating the sp^2 hybridization of the N atom is not as perfect as that in the Mo(III)-Mo(IV) dimer. Thus the interactions between the lone pairs of N atoms and the dπ orbitals are decreased. This is reflected in the longer Mo-N distances. The d orbital energy level is drawn as in Fig.4.5. If the dimer **A** takes the same coordinate system as the Mo(III)-Mo(IV) dimer, the Mo(V)-Mo(V) bond forms through the d_{yz} orbitals, leaving empty d_{xz} and d_{xy} orbitals for the π interaction, if this interaction

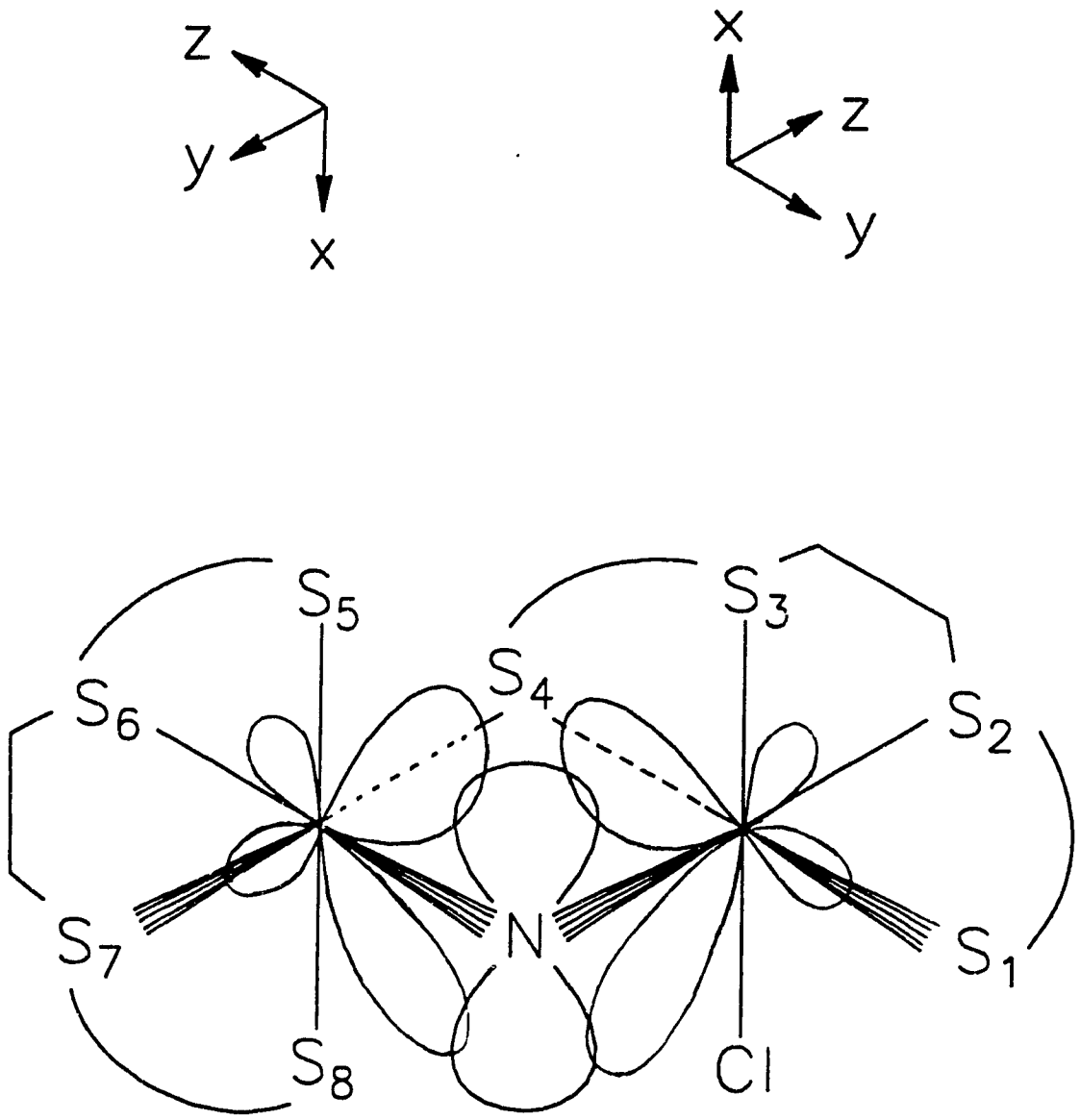

Fig. 4.3 The π interactions between the pπ orbital of the N atom and the d_{xz} orbitals of the two molybdenum centres.

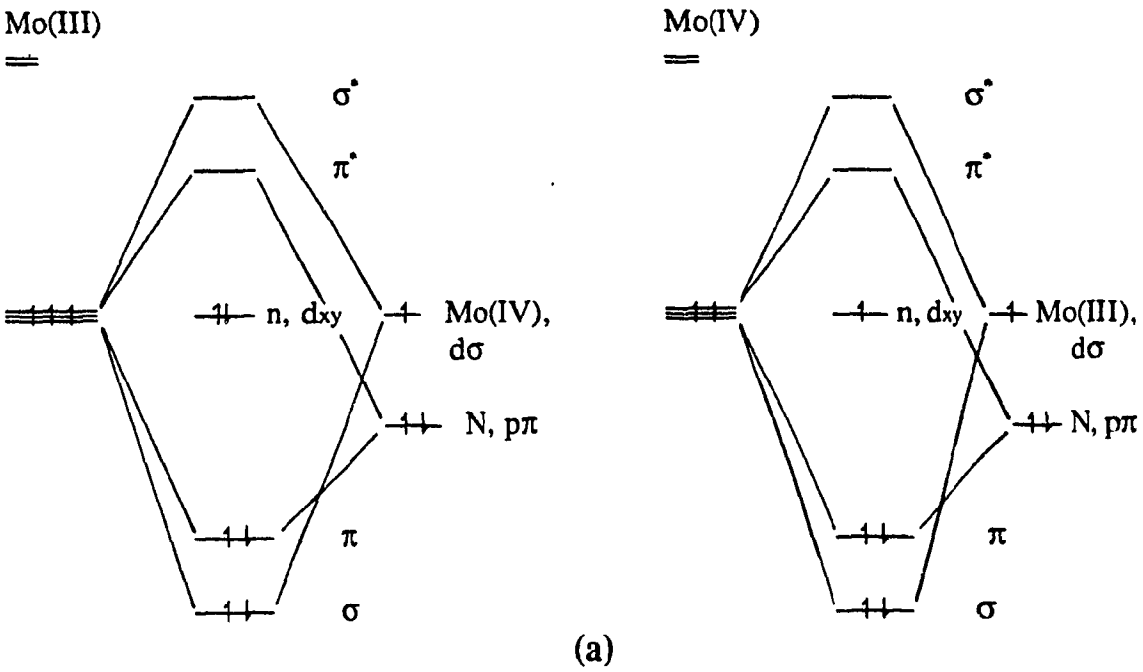

(a)

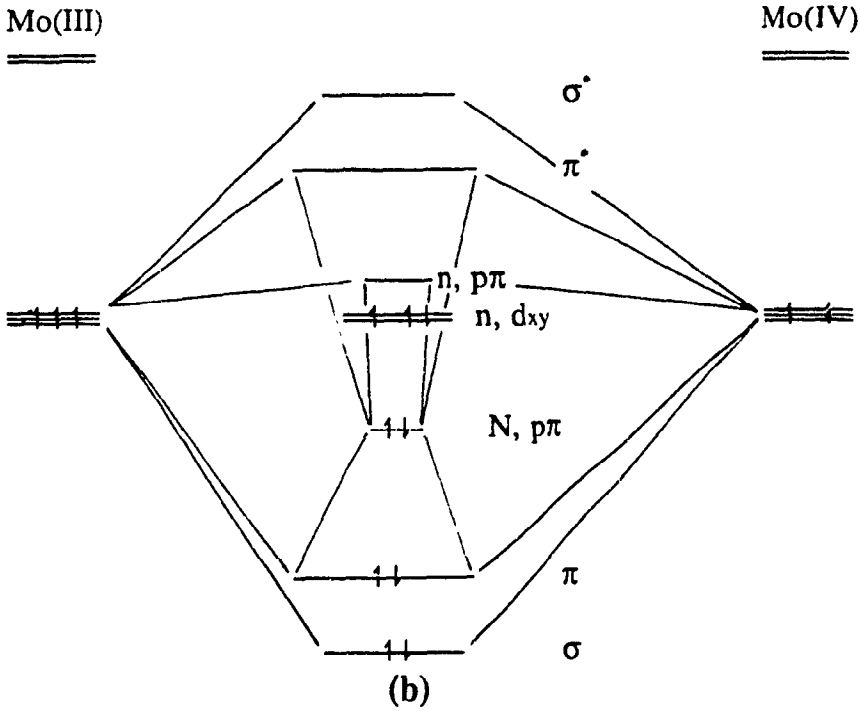

(b)

Fig. 4.4 Qualitative molecular orbital diagrams for each Mo centres (a) and the Mo(μ-N)Mo centre (b). The N pπ orbital is shown in red.

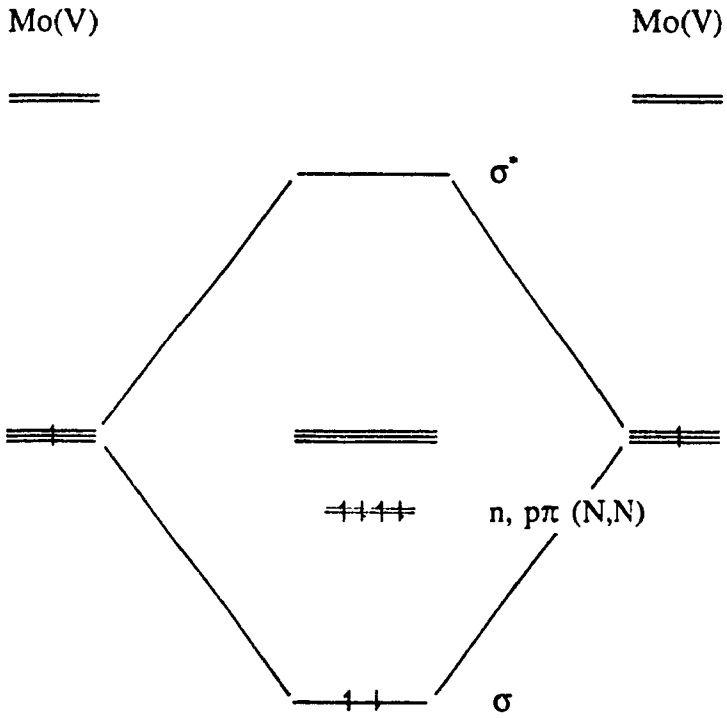

Fig. 4.5 Qualitative molecular orbital diagrams for the Mo(V)(μ-N)(μ-N)Mo(V) centre. The N nonbonding orbitals are in red.

exists.

The complex $[Mo(NMe_2)_6]$ [248] has the sum of the three angles around N exactly 360^0 ($\angle$Mo-N-C=126^0, $\angle$C-N-C=108^0), indicating a perfect sp^2 hybridization of the ligating nitrogen atoms. The interactions between the $d\pi$ orbitals and nitrogen lone pairs should be stronger than in the case of the Mo(III)-Mo(IV) dimer. However the complex $[Mo(NMe_2)_6]$ has a Mo-N distance of 2.034 Å, 0.09 Å longer than the average Mo-N distance in the Mo(III)-Mo(IV) dimer. This is because there are six lone pairs competing for the three empty d orbitals. Thus the complex $[Mo(NMe_2)_6]$ has the longest Mo-N bond among the three complexes. (While it has an N-C distance (1.462 Å) comparable to that in the Mo(III)-Mo(IV) dimer (1.459 Å)).

At this moment, it has to be emphasized that even though there may be π interactions in Mo-N units as discussed above, they are relatively weak, and cannot be compared with π interactions in imido and hydrazido complexes. However this kind of π interaction has been also suggested by the *trans*-influence and *cis*-repulsion of the nitrogen atom in the Mo(III)-Mo(IV) dimer, which is discussed in the following text.

Trans-influence and *cis*-repulsion have been treated as structural characteristics of multiply bonding ligands such as nitrido, oxo, imido, hydrazido, alkylidene and alkylidyne. A clear example has been seen in the structure of diphenylhydrazido molybdenum(V) complex $[MoCl(NNPh_2)(dttd)]$ in Fig. 3.15, and these two structural characteristics have been discussed in Section 3.5.

In the structure of the Mo(III)-Mo(IV) dimer (Fig. 4.1), two thioethers, S_2 and S_6 are *trans* to the amido ligand. Compared to two other thiothers, S_3 and S_7, the distances between Mo_1-S_2 (2.583(3) Å) and Mo_2-S_6 (2.608(4) Å) are about 0.08 Å longer than the

distances between Mo_1-S_3 (2.503(4) Å) and Mo_2-S_7 (2.530(4) Å). (Although the latter two Mo-thioether distances have been lengthened compared to Mo-S_3 (2.478(7) Å) in Fig. 3.15.) The distances of Mo_1-S_2 and Mo_2-S_6, which are comparable to the distance of Mo-S_2 (2.608(6) Å) in Fig. 3.15, are also symptomatic of a strong *trans*-influence, especially the distance of Mo_2-S_6, which is as long as Mo-S_2. Careful analysis of the structure leads to the conclusion that no other factors are responsible for such long Mo_1-S_2 and Mo_2-S_6 distances except the *trans*-influence of the amido ligand.

Another structural character reflecting the π interaction between nitrogen and molybdenum is the *cis*-repulsion. In model complex [MoCl(NNPh$_2$)(dttd)] (Fig. 3.15), the hydrazido ligand occupies a large space and pushes the ligands *cis* to it away. This can be clearly seen from the *cis* angles such as $\angle N_1$-Mo-Cl (96.1^0), $\angle N_1$-Mo-S_1 (95.0^0), $\angle N_1$-Mo-S_3 (94.8^0) and $\angle N_1$-Mo-S_4 (104.8^0) all of which are larger than 90°. In normal seven coordination a *cis* L-M-L angle should be equal or less than 90^0. However in the dimer, large angles are formed between the imido nitrogen, a metal centre and the *cis* ligands. They are $\angle$N-Mo_1-Cl (102.8(3)^0), $\angle$N-Mo_1-S_3 (96.2(3)^0), $\angle$N-Mo_2-S_5 (92.3(3)^0), and $\angle$N-Mo_2-S_8 (104.7(3)^0). Interestingly, all *cis* angles in the molecular structure of diphenylhydrazido molybdenum (Fig. 3.15) are larger than 90^0, but not all of the *cis* angles in the dimer (Fig. 4.1) are. For example, the angles $\angle$N-Mo_1-S_1 and $\angle$N-Mo_2-S_7 are only 85.1(3)^0 and 86.9(3)^0 respectively. This can be explained by the fact that the π interaction only exists between the pπ orbital of the nitrogen and one of the d orbitals, unlike the imido or hydrazido complexes in which two pπ orbitals of nitrogen interact with two dπ orbitals. If readers keep the coordinate system mentioned above in mind, this d orbital taking part in the π interaction with N lone pair should be d_{xz}. Thus the *cis*

ligands to the amido on the x axis such as Cl, S_3, S_5 and S_8 have been pushed away, while the *cis* ligands on the y axis such as S_1 and S_7 are not influenced.

Sulfur atoms are usually treated as sp^3 hybridized when they take part in bond formation. However in the dimer none of the eight sulfur atoms adopts a perfect sp^3 hybridization, just as in the case of [MoCl(NNPh$_2$)(dttd)], since the angles around S are less than $109^0 28'$. The distances of S_4-Mo_1 (2.438(3) Å) and S_4-Mo_2 (2.441(3) Å) are almost the same, and these two bond lengths are comparable to the Mo-thiolate distances, such as Mo_1-S_1 (2.475(3) Å), Mo_2-S_5 (2.478(4) Å) and Mo_2-S_8 (2.415(4) Å), and quite different from the Mo-thioether distance (at least 2.5 Å) in this dimer. Thus it is hard to say which molybdenum is Mo(III) and which is Mo(IV). However if the Mo(dttd) core was assumed to remain unchanged during the reduction reaction, i.e. no any Mo-S thiolate bonds being broken, the S_4-Mo_1 bond might be the covalent bond and Mo_1 could be in the oxidation state IV.

It is interesting to analyse the angles at carbon on the rings of the dttd ligands, especally the angles around C_1, C_6, C_9, C_{14}, C_{15}, C_{20}, C_{23} and C_{28}. If these carbons are perfectly sp^2 hybridized, the angles should be 120^0. But the carbons associated with thiolates have small internal ring angles, while the carbons associated with thioethers have large angles. For example, $\angle C_2$-C_1-C_6=115.7(11)^0 is about 7.2^0 smaller than $\angle C_1$-C_6-C_5 (123.0(11)^0). $\angle C_{16}$-C_{15}-C_{20}=114.5(13)^0, it is 10.7^0 smaller than $\angle C_{15}$-C_{20}-C_{19} (125.2(13)^0). Also, $\angle C_9$-C_{14}-C_{13} and $\angle C_{27}$-C_{28}-C_{23} are smaller than $\angle C_{10}$-C_9-C_{14} and $\angle C_{28}$-C_{23}-C_{24}, respectively. This kind of difference may be caused upon coordination of dttd to the metal centre, but why it occurs is still unclear.

C_7, C_8, C_{21} and C_{22} should be sp^3 hybridized, but all of them show angles larger

than $109^0 28'$, probably due to the distance required between S_2 and S_3, S_6 and S_7 for coordination (like C_7 and C_8 in the molecular structure of $[MoCl(NNPh_2)(dttd)]$ in Fig. 3.15).

Usually seven coordinated complexes are relatively unstable owing to the fact that the additional bond energy of the seventh bond is offset by the increased repulsion between ligands, by the weaker M-L bonds and the reduced crystal field stable energy as a result of nonoctahedral geometry. Indeed, the Mo-S bonds in the seven coordinated dimer are longer than that in the six coordinated monomer reflecting the weaker M-L bonds. Seven coordinated complexes normally have three geometrical isomers, and the interconversion between them are very easy since the energy barriers for this conversion is only about 0-4 kcal/mole. Thus, under most experimental conditions seven coordinated complexes are not stereochemically rigid. However polydentate ligands such as dttd favour the formation of complexes with coordination number seven. This has been demonstrated by the isolation of the complex [(dttd)Mo(μ-NMe)(μ-S-dttd)MoCl], and its stability is further enhanced by the formation of a dimer.

4.4 Reduction of the Model Complexes in the Presence of H^+

Three model complexes (all except $[MoCl(NNMe_2)(dttd)]$), were reduced in the presence of H^+. The proton sources used here were CF_3COOH, C_4H_9SH and C_6H_5SH. Reductions were carried out in the dry-box, with two equivalents of sodium (based on Mo in the complexes used) and one or two equivalent of H^+. No crystals were obtained when one equivalent of H^+ was used. When two equivalent of H^+ was used, all of the three model complexes seemed to give the same result: the three reduced products crystallized

in the same shape, the same colour, the same size and decomposed in an almost identical period.

When [MoCl(NMe)(dttd)] was reduced under such conditions, it gave a blue coloured solution. After filtration, the filtrate was concentrated and kept at 0^0C. During the crystallization, not only the reduced product crystallized, but also a white precipitate formed, and the amount of the precipitate increased with the increase of the amount of the crystals. It was very difficult to separate the crystals from the white precipitate, since both of them have almost the same solubilities in solvents such as CH_2Cl_2, CH_3CN and THF. The initial colour of the fine crystals observed after 24 hours kept under 0^0C is blue It changed to green after another 24 h, and the crystals decomposed gradually during one week. The decomposition rate of crystal obtained from the $2e^-$ reduction in the presence of CF_3COOH was relatively faster and the size of the crystals was smaller.

More experiments were carried out using thiols. When butanethiol was used, the crystal size is larger making for an easier purification. However the recrystallized crystals gave blank X-ray diffraction photographs.

On the other hand, when the reduction was carried out with thiophenol C_6H_5SH, the recrystallized product did give a diffraction pattern, although the crystal size was relatively small and the purification was quite difficult. This product crystallizes from THF in trigonal (rhombohedral) *R3m* space group. However the structural analysis failed probably due to the poor quality of the crystal. Some information obtained by using the heavy-atom method indicated that the molecule contains a sodium cation surrounded by six THF molecules and a molybdenum complex anion with a sulfur coordination sphere, without nitrogen or chloride. Details of the ligand structures were not resolved. Probably

the imido ligand was protonated to give an amine under these reduction conditions and then the Mo-N bonds were cleaved.

CHAPTER V

THE CASE FOR REMOVAL OF THE CHLORIDE LIGAND AND ATTEMPTS TO DO THIS

When the two model imido Mo(V) complexes were reduced and protonated, no impediment existed for them to give amines as the final products, since the Mo-N multiple bond-order was, in principle, reduced: this has been suggested by the UV-VIS spectra of the reduced Mo(III) species (see Section 3.3.2.4). In fact, the later crystallographic study (see Section 4.4) showed that there is probably no nitrogen in the coordination sphere of the molybdenum complex obtained from the two-equivalent-electron reduction/protonation of the model Mo(V) complexes.

According to the discussion in Section 1.2.5 and Scheme 1.2, protonation of hydrazido complexes produces either ammonia or hydrazine or both depending on which N atom is being protonated. If a hydrazido complex adopts canonical form **A** (see Section 3.4.2), protonation probably occurs on the βN atom to form a $MNN^{+}HR_2$ species, since the lone pair of βN is principally localized. This βN protonation promotes the cleavage of the N-N bond leading to the formation of two ammonia molecules as the final product. Conversely, for a hydrazido complex adopting canonical form **B**, since the lone pair of βN takes part in π delocalization towards the metal, making the βN relatively electropositive in character, the protonation probably occurs on the metal centre or on the αN rather than on βN. This non-βN protonation principally leads to the formation of hydrazine as the final product. In order to obtain ammonia from hydrazido complexes with the canonical form **B**, reduction should be carried out first to decrease the oxidation

state of the metal centre and increase the electron density on the βN atom.

Now the two model hydrazido Mo(V) complexes adopt form **B**. Reduction and protonation of these hydrazido Mo(V) complexes would probably give hydrazine as the main product. In order to get an amine, these complexes must be converted from form **B** to form **A**, that is by reducing the oxidation state of the molybdenum centre and increasing the electron density on βN atom. However, the reduction of the Mo(V) model complexes under electrochemical conditions is difficult to stop at Mo(IV), although the Mo(IV) imido and hydrazido complexes possess an $18e^-$ configuration. Rather, it continues to Mo(III), in which the Mo-N multiple bond is probably broken. Quantitative $1e^-$ reductions of the Mo(V) model complexes were attempted chemically, but they failed and no useful results were obtained.

Possibly, in a true $1e^-$ hydrazido Mo(V) -> Mo(IV) reduction, a neutral Mo(IV) species, such as [Mo(L)($NNPh_2$)(dttd)] (L=solvent, monodentate organophosphine), might have been derived from the cleavage of the Mo-Cl bond. This kind of neutral Mo(IV) complex was desired because:

- The Mo(IV) seems to be the lowest oxidation state among the stable Mo imido and hydrazido complexes, and it probably adopts canonical form **A**.
- It possesses an $18e^-$ configuration, and thus it should be relatively stable and the stability is required in subsequent isolation and characterization.
- The removal of the chloride ligand offers a vacant site which is required by the latter protonation on the αN and the elimination of the first amine molecule (see Section 1.2.5).

Other possible products of the $1e^-$ reduction of the hydrazido complexes are anions,

which can be formulated, in general, as $[MoCl(NNR_2)(dttd)]^-$. Their stabilities and reactivities would depend on which atom carries the negative charge: the metal centre (**a**); the thiolate sulfur atom (**b**) or the αN atom (**c**).

During the $1e^-$ reduction, if all of the covalent Mo-L (L=N, S, Cl) bonds orders remain unchanged, as in case (**a**), this electron would occupy one of the metal d orbitals, i.e. d_{xy} orbital, giving a d^2 configuration. The resulting Mo(IV) species is relatively electron rich with respect to its parent, and may adopt canonical form **A**.

If one of the covalent Mo-L (L=S, N) bonds is broken during the $1e^-$ reduction, as in case (**b**) and (**c**) the negative charge would localize on either one of the thiolate sulfur atom or the αN atom depending on which covalent bond, the Mo-S (thiolate) bond or the covalent Mo-N π bond is broken. Although the species obtained in case (**b**) and (**c**) are still formally Mo(IV) complexes with a d^2 configuration, their reactivities are quite different from the Mo(IV) complexes in case (**a**), because the thiolate sulfur atom or the αN atom, which bears the negative charge, becomes a strong nucleophile. The cleavage of the Mo-S (thiolate) bond in case (**b**) seems unlikely. This is because the molybdenum is "sulfophilic"; the Mo-S bond is a σ bond, and the chelate effect of the dttd on the metal centre increases the thermostability of the Mo-S bonds. However, the cleavage of the relatively weak covalent π bond of the Mo≡N linkage in case (**c**) seems possible. It gives an active (dttd)ClMo—$N^{\ominus}$–R species.

In this anion, the electron pairs can be donated to another electrophilic metal centre to form a bridge of form N-H bonds if protons are present. The protonation of the αN is preferred leading to the formation of hydrazine in further protonation/reduction. Thus the desired Mo(IV) products in the $1e^-$ Mo(V) -> Mo(IV) reduction are the neutral complexes

or the anions of type (a). However, these Mo(IV) species are not stable, the instabilities have been confirmed by the reduction experiments and the statistical data mentioned in section 4.2.

It seems then, that the pathway for conversion of the Mo(V) hydrazido complexes to Mo(IV) with the canonical form **A** through $1e^-$ reduction is not viable. The other way to have complexes with canonical form **A** is to synthesize neutral Mo(IV) complexes possessing dttd and hydrazido ligands, that is to synthesize starting model complexes which do not have chloride ligands.

In the reaction of $[MoCl_2(dttd)]$ with $(Me_3Si)_2NR$, only one chloride was removed from the metal centre. In order to get the second chloride off, monodentate organophosphines were added to the mixture of the reactants. However instead of the desired Mo(IV) product [Mo(NR)(dttd)(phos)], two products were obtained. They were separated on a silica gel column. The top band was orange coloured. The second one was violet coloured and identified to be [MoCl(NMe)(dttd)], the same that synthesized without the presence of phosphines. It seems that the phosphines, PR_3, not only cannot change the nature of the reaction represented in Eq. 3.13, but also competed with $(Me_3Si)_2NR$ for $[MoCl_2(dttd)]$ to give a new product. Although the orange compound crystallized to give dark red crystals, the structure analysis by X-ray crystallography was impossible due to unresolved multiple spots.

The IR spectrum of the orange compound shows the absence of Mo-Cl stretching vibrations around 320 nm. The mass spectrum of the product obtained from a mixture of $[MoCl_2(dttd)]$, $(Me_3Si)_2NMe$ and $PMePh_2$ shows three major sets of peaks with M/e around 778.0, 577.9 and 377.9 implying a parent complex $[Mo(C_6H_4S_2)_2(PMePh_2)_2]$ with

a molecular weight of 778 for ^{98}Mo losing its phosphine ligands (molecular weight 200) successively.

In the absence of $(Me_3Si)_2NMe$, $[MoCl_2(dttd)]$ reacts with $PMePh_2$ and gives the same product indicating the reactivity of $[MoCl_2(dttd)]$ towards phosphines. This reactivity has also been observed in the cases of $[Mo(O)_2(dttd)]$ and $[Mo(NO)_2(dttd)]$ [223, 225], which form seven coordinated intermediates, such as $[Mo(NO)_2(PR_3)(dttd)]$ (R=Me, Et, Ph), after the nucleophilic attack of phosphines on the Mo centres. This is probably due to the fact that the distortion from an octahedral geometry of a Mo(dttd) core leaves plenty of room for the incoming phosphine ligand(s). In the reaction of $[MoCl_2(dttd)]$, a seven coordinated intermediate $[MoCl_2(dttd)(PMePh_2)]$ was not obtained, but rather the elimination of the chloride ligands, and the $-CH_2CH_2-$ bridge from the dttd ligand. The cleavage of S-C bonds in thioether parts of ligating ligands has been reported in the synthesis of crown thioethers [228]. It has also been observed that WCl_5 and WCl_6 react with thioethers leading to a series of reactions which include S-dealkylation reactions. The decomposition of complex $[MoCl_2(dttd)]$ in strong polar solvents such as DMSO or DMF may be due to the similar reactions, i.e. the chloride ligands are eliminated.

CHAPTER VI

EXPERIMENTAL SECTION

6.1 Equipment for Reactions.

Reactions which are sensitive to air and moisture were carried out under a N_2 atmosphere by using either a glove-box or Schlenk/N_2-vacuum line techniques. The glove-box, supplied by Kewanee Sci. and Eng. Co., was equipped with columns to remove oxygen, moisture and gaseous substances produced from reactions and/or evaporated from volatile solvents from the atmosphere.

The N_2-vacuum line was used for air sensitive reactions which needed reflux and vacuum evaporation. The nitrogen line was connected to a supply of pre-dried ($CaCl_2$) nitrogen (regular grade) at a pressure of 32 oz./in.^{2} The vacuum line was connected to a rotary vacuum pump.

6.2 Characterization

Elemental Analysis [239]

Since the yields were very low, elemental microanalysis were only performed for carbon, hydrogen and nitrogen for three of these model complexes by the Microanalysis Service of the Institute of Chemistry of Louis Pasteur University of Strasbourg. The dimethylhydrazido molybdenum complex failed to crystallize and decomposed in the presence of Et_2O, thus the purity was in question. The calculated and observed results are shown in Table 5.1. They are in reasonable agreement with the formulations. The

Table 6.1 Results of elemental analysis and mass spectroscopy.

		$C_{15}H_{15}ClMoNS_4$ [MoCl(NMe)(dttd)] (1)	$C_{20}H_{17}ClMoS_4$ [MoCl(NPh)(dttd)] (2)	$C_{26}H_{22}ClMoNS_4$ [MoCl($NNPh_2$)(dttd)] (3)
	FW*	468.5	540.5	621.5
	MS*	470	542	623
(C%)	C*	38.42	45.24	50.20
	F*	38.46	43.13	49.13
(H%)	C	3.22	3.20	3.56
	F	3.33	2.78	3.10
(N%)	C	2.99	2.63	4.50
	F	2.69	2.41	3.93

* FW: formula molecular weight, MS: mass of molecule,
C: calculated percent, F: found percent.

formulas listed in Table 5.1 were confirmed by mass spectroscopy. The mass spectra show strong parent peaks (m/e) at 470 for complex (**1**), 542 for (**2**), 623 for (**3**) and 499 for the dimethylhydrazido complex with isotope distributions corresponding to the presence of one chloride and one molybdenum.

Mass Spectroscopy

Samples were run on a Kratos Concept 2H Spectrometer, at an accelerating voltage of 6 kV. The bombarding particles were 12 kV Cesium ions (Cs^+). Samples dissolved in a gly/3nba matrix prior to bombardment.

^{1}H NMR Spectroscopy

Proton NMR spectra were measured on a 80 MHz Bruker WP-80SY Fourier transform spectrometer. Samples were dissolved in $CDCl_3$, and TMS was used as an internal standard. The chemical shifts are expressed in ppm relative to the TMS signal (δ=0.0 ppm).

IR and FTIR

The IR spectra were recorded on a Perkin-Elmer 599 B infrared spectrophotometer. The FTIR spectra were obtained on a Bomem Michelson 102 spectrometer and plotted after base line adjustment. NaCl or CsI windows were used depending on the frequency regions being examined. Solid samples were run as mull in mineral oil (nujol) in the dry box. For FTIR work the reference (air) was scanned before each sample.

UV-VIS

UV-VIS absorptions were obtained on a Cary 219 Spectrometer. Samples were dissolved in DMF (concentration: 0.0004~0.0006 M), and a quartz cell (10 mm) was used.

Cyclic Voltammetry

Cyclic voltammetry experiments were performed by using a Bruker E1 310M potentiostat connected to an Ifelec 1f 3802 xy recorder. A Hg hanging drop electrode was used as the working electrode with a drop surface area 1.82×10^{-2} cm^2. A platinum wire was used as the auxiliary electrode. The reference electrode used is a saturated calomel electrode (SEC), it was separated from the cell by a salt bridge containing the same solvent and the supporting electrolyte, 0.1 M NBu_4ClO_4.

X-Ray Crystallography

A suitable size single crystal was chosen and sealed in a capillary tube under a Bausch & Lomb graduated microscope in a plastic N_2 filled glove-bag. The space group was determined from Weissenberg and precession photographs taken on Kodak "No Screen" film and polaroid film (type 57, high speed) on cameras made by Charles Supper Co. The X-ray (Mo k_α) source was a Mo target tube made by Marconi Avionics Ltd. It was powered at 40 kV and 20 mA by a Phillips X-ray generator.

Two reciprocal axes and their interaxial angle were found from the zero-level Weissenberg photograph. The other reciprocal axis and two remaining angles were found and identified from the zero level precession photographs. The angles and the lengths of the reciprocal cell edges were measured using a film measuring device made by Charles

Supper Co. The space group was deduced from the symmetry and the systematic absences displayed on the zero and the first level Weissenberg and precession photographs.

Data collection was performed on a Picker nuclear FACS-1 four circle diffractometer. X-rays were generated from a TX8 Mo tube, made by Marconi Avionics Ltd, driven at 40 kV and 20 mA. The power was supplied by a Picker constant potential diffraction generator (Model 6238E). The computational work was carried out by a Digital PDP8/a computer. The programs used to drive the Picker FACS-1 diffractometer, and those used in the data processing, solution and refinement of the structure are part of the NRC (Canada) crystallographic package for the PDP8 minicomputer [250]. Unit cell parameters, and details about the solution and refinement of the structure, are given in Table 3.5 and 4.1 for [MoCl($NNPh_2$)(dttd)] and [(dttd)Mo(μ-NMe)(μ-S-dttd)MoCl]·$3CH_2Cl_2$, respectively. The final non-hydrogen atom positions, the mean isotropic thermal parameters and the anisotropic thermal parameters are given in Appendix I-IV. The positions of H atoms for the dimer is presented in Appendix V.

6.3 Chemicals and Solvents

Chemicals and Solvents were purchased from Aldrich Chemical Co., Sigma Chemical Co., Alfa products, Anachemia Chemicals Ltd., J.T. Baker Inc. and ACP Chemicals Inc. All chemicals were used directly without further purification. Solvents were dried before use.

Tetrahydrofuran (THF) was dried over a sodium dispersion paraffin (50%) for three days under N_2. The dryness was tested with benzophenone, which gives a dark blue colour if excess sodium exists and the solvent is dry and oxygen free. The mixture was

fractionally distilled under N_2. The distillate was sealed in a bottle under nitrogen and stored in the glove-box.

Dry diethyl ether (Et_2O) was obtained following the same procedure described for dry THF.

Acetonitrile (MeCN) was dried over calcium hydride (CaH_2) for two days, and distilled under N_2. The dry acetonitrile was stored in glove-dry-box immediately.

Dichloromethane (CH_2Cl_2) was dried with Linde type 4A molecular sieves for 3 days and fractionally distilled under N_2. The dry CH_2Cl_2 was purged of O_2 with a stream of N_2 for half an hour before use.

Pentane and hexane were first treated with concentrated sulfuric acid to remove unsaturated hydrocarbon impurities. After separation they were washed 3 times with deionized water, and dried with calcium chloride for 48 h. The purified pentane and hexane were obtained by fractional distillation under N_2.

6.4 Description of Experiments

6.4.1 Syntheses

Potassium Methylxanthate [249]

Anhydrous potassium hydroxide (84 g, 1.5 mole) was dissolved in methanol (99%,170 ml) in a 500-ml three-neck flask with a reflux condenser and a 250-ml dropping funnel. Then carbon disulfide CS_2 (114 g, 1.5 mole) was added dropwise into the stirred KOH/MeOH solution from the dropping funnel over a period of 2 h, meanwhile the temperature of the solution in the flask was kept below 20° C. After the addition of CS_2, the mixture was stirred further for 2 h, then cooled at 0° C in a refrigerator for 8 h. The

yellow cotton-like crystalline product, potassium methyl xanthate was isolated by suction filtration and followed by washing with two 20 ml portions of cold methanol and dried in the air. The yield recovered was 121.5 g (55%). More could be obtained from the mother liquor. Higher yields (~70%) were obtained if the addition of CS_2 was followed by treatment of ethanol (99%, 300 ml) instead of cooling to 0° C.

1,2-Di(o-aminophenylthio)ethane (DAPTE) [231]

Small pieces of fresh sodium metal (9.2 g, 0.4 mole) were added to ethanol (99%, 150 ml) in a 500-ml three neck flask fitted with a 250-ml dropping funnel, a condenser and a magnetic stirrer. The Na/EtOH mixture was stirred for about 2 hours until all the sodium metal had dissolved.

To the stirred solution, 2-aminothiophenol (50 g, 0.4 mole) was added through the dropping funnel over a period of 30 minutes. Then in a one-hour period, 1,2-dibromoethane (37.6 g, 0.2 mole) was added through the dropping funnel and the mixture was stirred for a further hour. Then 300 ml deionized water was added to the flask. A yellow precipitate formed as the water was added into the flask. This precipitate was collected by suction filtration and washed thoroughly with cold water.

The crude product was redissolved in 200 ml hot ethanol (~60° C) in a 350-ml beaker. After hot filtration the filtrate was concentrated to 150-ml by evaporation at boiling point and cooled to room temperature. The pure product was isolated by suction filtration after the filtrate was kept at -5° C for 6 hours, and it was washed with two 20 ml portions of cold ethanol and dried in the air. The yield was 49.1 g, 89%.

Dttd-H_2 [231]

DAPTE (11 g, 0.04 mole) was added slowly into a 350-ml beaker charged with dilute HCl (30 ml, 0.36 mole concentrated HCl mixed with 60 ml deionized water) at ice bath temperature. The mixture was stirred, for about 0.5 h, till the solution became clear. To this solution sodium nitrite solution (6.9 g, 0.10 mole dissolved in 30 ml deionized water) was added dropwise at such a rate that the temperature of the solution in the beaker did not rise above 5° C. (about 2 h). The excess HNO_2 was destroyed by addition of urea 1.2 g, 0.02 mole) since the excess nitrous acid interferes with subsequent reactions of the diazonium salt. (Urea can react with nitrous acid to form nitrogen, carbon dioxide. and water. Any excess urea does not interfere with subsequent reactions). The diazonium salt solution was then treated with sodium carbonate (21.2 g, 0.2 mole) to reduce the acidity.

The xanthanation was catalyzed by $NiSO_4$. The diazonium salt solution was treated with 0.2 g (0.00125 mole) of $NiSO_4$ followed by slow dropwise addition of potassium methylxanthate solution (13.14 g, 0.9 mole dissolved in 30 ml deionized water) at such rate that the temperature did not excess 5° C. Xanthanation occurred immediately and the evolution of N_2 started at ~3° C. The resulting brown oil-like arylmethylxanthate was extracted by three 80 ml portions of diethyl ether. The brown coloured ether solution was collected in a 300-ml flask and dried over anhydrous sodium sulfate or magnesium sulfate for 24 h.

Lithium aluminum hydride (4.94 g, 0.13 mole) was mixed with 50 ml dry diethyl ether in a 500-ml three-neck flask fitted with a condenser, a 250-ml dropping funnel and a magnetic stirrer.The brown coloured dry arylmethylxanthate ether solution was added

dropwise through the dropping funnel into the flask at such a rate that the temperature was maintained to keep a mild reflux. On completion of this addition the mixture was heated under reflux for another 1 h. After the flask cooled to the room temperature, 40 ml water was added dropwise through the dropping funnel to destroy the excess lithium aluminum hydride. The mixture in the flask was acidified with dilute H_2SO_4 (120 ml, 10%). The brown coloured ether layer was collected in a 500-ml separatory funnel and the aqueous layer was treated with another 60 ml ether. The ether layers were collected together and dried over anhydrous sodium sulfate for 24 h. The crude yellow oil-like product, dttd·H_2 was obtained from the clear ether solution after evaporation of the ether solvent under vacuum at room temperature.

The raw product was dissolved in 15 ml THF and treated with a sodium hydroxide ethanol solution (NaOH 2 g, 0.05 mole in 35 ml ethanol). The mixture was a brown coloured solution. It was concentrated under vacuum to a viscous solution and then treated with 300 ml ether to precipitate Na_2(dttd). This white salt was separated by suction filtration and washed with ether to colourless washings. The white solid was dissolved in 100 ml deionized water in a 300 ml beaker followed by addition of 100 ml ether. Then the Na_2(dttd) solution was acidified with 30 ml 6 N HCl (0.18 mole). The ether layer was separated in a separatory funnel, and the remaining dttd·H_2 in the aqueous layer was extracted by 180 ml ether (60 ml x 3). The ether phase was collected in a 350-ml flask and dried with anhydrous Na_2SO_4/$MgSO_4$ for 24 hours. The clear dttd·H_2 ether solution was decanted into a dry flask. Normally the pure product, dttd·H_2 is a yellow oil obtained from the ether solution by evaporation of the ether solvent under vacuum at room temperature.

N,N-Bis(trimethylsilyl)aniline

n-Butyllithium in hexane, 6.75 ml of 1.6 M (10.8 mmole) measured by a syringe, were added dropwise into a 50-ml Erlenmeyer flask charged with 1.00 g of aniline (10.8 mmole) in 25 ml hexane. The mixture was stirred magnetically. A white precipitate formed and the mixture in the erlenmeyer flask was allowed to stand in the glove-dry-box for 20 m after completing the addition of butyllithium. The precipitate was separated by decantation followed by washing with hexane (10 ml x 2) and dried under vacuum.

The precipitate was dissolved in 20 ml of diethyl ether and treated by dropwise addition of trimethylsilylchloride (1.17 g, 10.8 mmole in 5 ml ether). A white precipitate formed and was removed by filtration. The brown coloured filtrate was treated with 6.50 ml (10.40 mmole) of butyllithium/hexane, and the mixture was stirred further for 30 m. Then the solvent was removed under vacuum and the residue was dissolved in 20 ml of THF. To the brown coloured THF solution, trimethylsilylchloride (1.20 g,10.48 mmole in 10 ml THF) was added dropwise and the mixture was stirred constantly for one hour. The resultant white precipitate was filtered off and the solvent was removed at room temperature under vacuum.

The product, an almost colourless oil was obtained by distillation of the liquid residue under vacuum at 75° C. Yield: 2.14 g, 84%.

N,N-Bis(trimethylsilyl)-*N',N'*-dimethylhydrazine

The procedure of the preparation is essentially the same as that given above for N,N-bis(trimethylsilyl)aniline.

In a 50-ml erlenmeyer flask, *1,1*-dimethylhydrazine (0.60 g, 10 mmole) in 10 ml

diethyl ether and 10 ml hexane was treated with 6.25 ml of 1.6 M (10 mmole) butyllithium in hexane, then followed by treatment of 1.09 g of trimethylsilylchloride (10 mmole) in 5 ml diethyl ether. The white LiCl precipitate was filtered off and the pale yellow coloured filtrate was treated by dropwise addition of 6.25 ml of butyllithium/hexane. The solvent was removed under vacuum after the addition, and the residue was dissolved in 20 ml of THF followed by treatment of 1.09 g of trimethylsilylchloride (10 mmole) in 5 ml THF. The mixture was warmed to ~ 60° C with a hair drier for 30 m. The white precipitate was filtered off and the solvent was removed under vacuum at room temperature. The liquid residue was distilled under high vacuum at 70° C to yield 2.18 g (53.4%) of product, an almost colourless oil.

_N,N_-Bis(trimethylsilyl)-_N'_,_N'_-diphenylhydrazine

_N,N_-Diphenylhydrazine hydrochloride (2.21 g, 10 mmole) in 20 ml THF was treated with 12.6 ml of 1.6 M (20.2 mmole) butyllithium in hexane. The white precipitate, LiCl was filtered off and the solvent was removed under vacuum. The residue was redissolved in 20 ml THF, and the resultant solution was treated by dropwise addition of 1.09 g (10 mmole) of trimethylsilylchloride in 5 ml THF. The clear solution was treated with 6.4 ml of 1.6 M (10.2 mmole) butyllithium in hexane and warmed to about 60° C for 30 m. Then another 1.09 g (10 mmole) of trimethylsilylchloride in 5 ml THF was introduced. The mixture was stirred at 60° C for 30 m. The white precipitate, LiCl was filtered off and the solvent was removed under vacuum. The product was obtained as yellow coloured viscous oil by distillation of the dark brown liquid residue under high vacuum at ~125° C. Yield: 1.89 g, 57%.

Precursor Complex [Mo(dttd)Cl_2]

Five grams (18.2 mmole) of molybdenum (V) chloride was mixed slowly with 25 ml acetonitrile in a 50-ml Erlenmeyer flask charged with a magnetic stirrer. The mixture was stirred for 2 h and allowed to stand for 12 h. The brown precipitate, [$MoCl_4(CH_3CN)_2$] was isolated by suction filtration then washed with three portions of 5 ml acetonitrile, and dried under vacuum. Yield: 4.74 g, 81%.

Four grams (12.5 mmole) of [$MoCl_4(CH_3CN)_2$] was mixed with 30 ml THF and stirred for 4 h. The brown slurry was converted to orange coloured [$MoCl_4(THF)_2$]/THF slurry. Then this slurry was treated by slow dropwise addition of 3.90 g (12.6 mmole) of Dttd·H_2 in 10 ml THF over a period of 2 h, and followed by stirring a further 3 h. The resultant black precipitate, [Mo(dttd)Cl_2] was isolated by suction filtration and washed with THF (10 ml x 2). The yield recovered after drying under vacuum is 4.53 g, (76.3%).

Methylimido Mo(V) Complex, [MoCl(NMe)(dttd)]

In a typical preparation 0.400 g (0.84 mmole) of [Mo(dttd)Cl_2], in the form of a suspension in 50 ml THF was treated with 0.221 g (1.26 mmole) of *N,N*-bis(trimethylsilyl)methylamine in a 100-ml two-neck flask fitted with a condenser and connected to the N_2/vacuum system. The mixture was stirred for 4 h at ~52° C under N_2. After cooling to the room temperature the THF was removed under vacuum and the solid residue was treated with ~10 ml CH_2Cl_2. Then the reddish violet CH_2Cl_2 solution was concentrated to ~5 ml in volume. The concentrated solution was transferred to a silica gel (40-140 mesh) chromatographic column (2.5 x 15 cm) and eluted with CH_2Cl_2 under N_2. Some undissolved dark brown coloured solid residue was left behind. The brownish grey

head fraction was discarded and the intensely violet fraction was collected. The following greenish fraction was also discarded. The product was purified again by passing the concentrated violet solution through another silica gel chromatographic column. Then the pure violet fraction was concentrated to about 4 ml, and treated with about 0.5 ml of diethyl ether. The product, shiny black crystals were obtained, after cooling at -25° C for 24 h, by removal of the mother liquor through a needle using the N_2/vacuum system, and washed twice with ether (~2 ml x 2) before drying under vacuum. Yield: 0.220 g, 56% based on Mo. This compound is relatively stable in the solid state.

Phenylimido Mo(V) Complex [MoCl(NPh)(dttd)]

The method of syntheses of the phenylimido Mo(V) complex and its purification follows the procedure for the methylimido Mo(V) complex given above. Thus, 0.400 g (0.84 mmole) of [Mo(dttd)Cl_2] was mixed with 0.637 g (2.69 mmole) of *N,N*-bis(trimethylsilyl)aniline in 50 ml THF. The mixture was heated under N_2 and reflux for 8 h. The product was purified twice on silica gel columns, and the blue fraction was collected. The crystalline product was obtained as described above and the yield recovered was 0.101 g, 22%.

Dimethylhydrazido Mo(V) Complex [MoCl(NNMe$_2$)(dttd)]

The preparation of the dimethylhydrazido Mo(V) complex follows the procedure given above. The precursor complex, [Mo(dttd)Cl_2] (0.40 g, 0.84 mmole) was treated with 3.5 equivalents of *N,N*-bis(trimethylsilyl)-*N',N'*-dimethylhydrazine (0.60 g, 2.94 mmole) in 50 ml THF in a 100-ml two-neck flask fitted with a condenser. The mixture was heated

to reflux at about 72° C under N_2 for 16 h. The solution became dark red. A CH_2Cl_2/THF (20:1 in volume) mixture was used as eluent in chromatographic separation, otherwise the desired product, in the red band, moved very slowly. After twice purification with silica gel columns under N_2, the red eluate was concentrated under vacuum and cooled for 24 h at -25° C. The mother liquor was removed using the N_2/vacuum system with a long needle. Instead of crystals, a red glassy solid was obtained. It was washed twice with pentane and dried under vacuum. Yield: 0.092 g, 22%.

The addition of ether, which could reduce the solubility of the other model complexes in CH_2Cl_2 in the crystallization step, caused a complete destruction of the product leading to the formation of an insoluble beige precipitate. Some other combined common solvents were also tried, but no crystals were obtained, except with the combination of CH_2Cl_2 and pentane: to the CH_2Cl_2 solution, a few drops of pentane were added. Some crystal-like grains were observed after four days cooling at -5° C.

Diphenylhydrazido Mo(V) Complex [MoCl(NNPh$_2$)(dttd)]

The synthesis of the diphenylhydrazido Mo(V) complex follows the procedure given above. Thus, 0.4 g (0.84 mmole) of [Mo(dttd)Cl_2] was mixed with 3.5 equivalents of *N,N*-bis(trimethylsilyl)-*N,N*-diphenylhydrazine (0.96 g, 2.93 mmole) in 50 ml THF. The mixture was refluxed for 16 h under N_2. After chromatographic purification with silica gel columns, the purple eluate was concentrated to about 2 ml in volume and treated with 2 drops of diethyl ether. The crystals were obtained after cooling the solution at -25° C for 24 h. Yield: 0.183 g, 35%.

6.4.2 Reduction

Zinc Amalgam

Zinc dust (5 g, 0.076 mole) was added in a small portions, to a 300-ml beaker charged with 130 g clean mercury, 250 ml of 4 N HCl and a stirrer. The zinc dust/ aqueous phase formed, the Zn dust sank and dissolved in the mercury phase. The aqueous phase was discarded by decantation. The mercury phase was washed twice with water (50 ml x 2) followed by washing three times with dry diethyl ether (20 ml x 3). The trace ether on the surface was adsorbed by filter paper, and the resultant zinc amalgam was stored in the glove-box. Zinc content: < 3.66% in weight.

Note: The zinc amalgam will solidify if the zinc content is equal or over 5% in weight.

Sodium Amalgam

In the dry-box, 0.23 g fresh metal sodium (10 mmole) was added, in small portions, into a 200-ml beaker charged with 200 g clean mercury and a stirrer. White fumes appeared as each small piece of metal sodium dissolved in the stirred mercury. The resultant sodium amalgam was stored in a clean vessel. Sodium content: 0.115% in weight.

Note: The sodium amalgam will solidify if the sodium content is over 1.5% in weight.

One-Electron Reduction of the Model Complexes

In a typical reduction reaction, 0.1~0.2 g of model complexes, such as [MoCl(NMe)(dttd)] (0.21~0.42 mmole), in 20 ml THF were added to a 100-ml flask, in which an equivalent quantity of sodium amalgam was previously stirred in 15 ml THF

for ~20 m. Then the mixture was stirred continuously for about 30~45 m. The initial purple solution became brownish black. This solution was separated by suction filtration, then concentrated to about 1 ml in volume and cooled at -25° C. No crystals were obtained.

Two-Electron Reduction of the Model Complexes Using Zn Amalgam

The 2-electron reduction was conducted following the procedure described above. 0.1~0.2 g of the model complexes were dissolved in THF first and then added to the reducing agent system which contained excess zinc amalgam. The amalgam was stirred in THF for about 30 minutes before addition of the Mo complex solution. Excess zinc amalgam was used due to the uncertainty of the precise content of zinc: the Mo(III) could not be further reduced by zinc. The mixtures of zinc amalgam and model complex was stirred for a further 2 h. The resultant dark green coloured solution was filtered, concentrated and cooled at -25° C.

Two-electron Reduction of the Model Complexes Using Na Amalgam

The reduction was carried out following the procedure given above. Thus 0.1~0.2 g of the model complexes were dissolved in THF and then added to the flask containing two equivalents of sodium amalgam (based on Mo) and 20 ml THF. The mixture was stirred for a further 20-30 m. The resulting dark green coloured solution was filtered, concentrated and cooled at -25° C.

Reduction of the Model Complexes in the Presence of H^+

The reduction procedures are as the same as that described in one- or two-electron reduction except that one or two equivalents of a proton source, such as trifluoroacetic acid, thiophenol or *1*-butanethiol were mixed with the model complex/THF solution before the reduction reactions. No crystals were obtained from any of the one-electron reduction experiments.

In 2-electron reduction, when sodium amalgam and two equivalents of a proton source were used, a blue solution was obtained after filtration. The resulting blue solution was concentrated and cooled at 0~-5° C for 3 days. Black crystals and a white precipitate were observed. Then the solvent was removed under vacuum and the solid residue was treated with THF (4 ml x 3). The blue coloured clean THF solution was collected in a Schlenk tube, then it was concentrated to about 1.5 ml in volume and cooled at 0~-5° C for 2 days. The crystals were washed twice with 3 ml degassed dry THF/nujol mixture (1:2 in volume) under N_2/vacuum system after removal of the mother solution. Then a suitable crystal was selected in a N_2-plastic bag under a microscope and sealed in a capillary tube (ϕ = 0.3 mm) for the X-ray crystallographic work.

Reduction of the Model Complexes with the Presence of Organophosphines

This kind of reduction was performed following the procedure described above. The monophosphines such as PMe_3 $PMePh_2$, PPh_3 or PBu_3 were dissolved in THF/CH_2Cl_2 and mixed with model complex/THF solution before reduction. One- and two-electron reduction gave brownish black or dark green solution respectively. No crystals were observed after concentration and cooling at -25° C for one week or longer; instead, an oil

layer was observed floating on the surface of the dark green solution.

Large Cation Exchange

The fresh reduced model complex/THF solution was treated with one or two equivalents of PPh_4Cl or NBu_4Cl in CH_2Cl_2. The mixtures were stirred for 15~24 h and allowed to stand for 24~36 h. Then the mixtures were filtered. The filtrate was concentrated and cooled at 0~-5° or -25° C. No crystals were obtained before it decomposed.

Preparation of [(dttd)Mo(μ-NMe)(μ-S-dttd)MoCl]

Zinc amalgam (15 g, ~0.4 mmole/g) was mixed with 15 ml THF and stirred for 0.5 h. Then complex [MoCl(NMe)(dttd)] (0.25 g, 0.44 mmole)/THF (20 ml) solution was added. The initially purple solution became dirty green over a atirring period of about 2.5 h. A dark green solution was obtained after suction filtration. To this filtrate, a solution of 0.328 g (0 88 mmole) Ph_4PCl in 10 ml CH_2Cl_2 was then added dropwise. The mixture was stirred for 15 h and allowed to stand for 36 h. The solvent was removed under vacuum and the residue was redissolved in 15 ml CH_2Cl_2, followed by slow addition of 10 ml diethyl ether. After standing for 36 h, the dark green solution was separated from a brown precipitate by suction filtration. The solvent of the filtrate was removed again under vacuum, and the black residue was dissolved in 20 ml CH_2Cl_2. Then 0.087 g (0.44 mmole) of $PMePh_2$ was added and the solution was stirred for 24 h. This mixture, a clear dark green solution, was concentrated to about 2 ml in volume under vacuum and kept at 0° C for 2 weeks. The black precipitate and some black crystals were separated from

the solution by decantation, washed with pentane twice (5 ml in total) and dissolved in 10 ml CH_2Cl_2. The dark green solution was concentrated to about 1.5 ml and kept at 0° C for 3 days. The crystals recovered are black cuboids. One of them was carefully selected and sealed in a capillary tube for X-ray crystallographic work.

CHAPTER VII

CONCLUSION

New types of imido and hydrazido molybdenum(V) complexes, [MoCl(NMe)(dttd)] (**1**), [MoCl(NPh)(dttd)] (**2**), [MoCl(NNMe$_2$)(dttd)] (**3**) and [MoCl(NNPh$_2$)(dttd)] (**4**) have been synthesized and characterized. Instead of a metal-phosphine core, which has been used widely in study of the intermediates and the mechanism of the N_2-fixation, all of these model complexes contain a metal-sulfur core, i.e. a molybdenum-tetradentate sulfur rigid unit, which bears a closer resemblance to the FeMo-cofactor in nitrogenases than the metal-phosphine cores.

The tetradentate sulfur ligand precursor, dttd·H_2 was synthesized following an improved method. The yield has been increased from ~24%, the literature value, to ~56%. The relatively low yield is due to the long preparation procedure and particularly the inefficient diazotization-xanthanation-reduction synthetic route.

The imido and hydrazido ligand precursors, trimethylsilylamine and trimethylsilylhydrazines have been prepared. In the synthesis of the model complexes, the quantities of the precursors needed, the reaction time and the yields are quite different due to the basicity of the nitrogen atom ligating the molybdenum centre.

The elemental analyses and the mass spectra are in agreement with the molecular formulas given above. The UV-VIS spectra of the model complexes (**1**), (**2**) and (**4**) showed the typical absorptions of the imido and hydrazido complexes in the region of 550-580 nm. These absorptions are probably due to the transition of electrons from d_{xy} orbitals to the degenerate d_{xz}, d_{yz} orbitals or from n to π^* orbitals. The UV-VIS studies

also revealed that complexes (**1**) and (**4**) have relatively stronger Mo≡N multiple bonds than complexes (**2**) and (**3**), respectively. This is in agreement with arguments about conjugation between the metal centre, the αN and the substituents on the αN atom.

Complexes (**1**), (**2**) and (**4**) showed a similar redox behaviour in electrochemistry. They underwent irreversible two-electron process at a certain potential between 0.1 V and -1.8 V. Probably no protonation occurred with the presence of $(CF_3)_2CHOH$ during the electroredox process. The irreversibility may be due to the change of the M-N bonds, since a 2e reduction of the model complexes produces a d^3 core which possesses an unfavourable electron configuration for the multiple bonds

The molecular structure of complex (**4**) clearly shows a Mo-N multiple bond with a Mo-N distance of 1.751 Å and a linear Mo-N-N unit with a Mo-N-N angle of 172.7°. The molecular structure also suggests a sp^2 hybridization of the βN atom, implying a wide delocalization of π electrons within the $MoNNPh_2$ unit. This is confirmed by the N-N double bond character.

The molecular structure and the difficulty in protonation of these model complexes before reduction suggest that the hydrazido complex (**4**) favours canonical form **B**, in which electron density drifts towards the Mo(V) centre, leaving behind a relatively positively charged βN. The imido complexes (**1**) and (**2**) adopt canonical form **D**, which is also unfavourable for protonation directly on the N atom before reduction.

The canonical form **A** hydrazido complexes with lower oxidation state metal centres, i.e. Mo(IV) centres, may be favoured for protonation on the βN atoms, leading to the formation of ammonia since the lone pairs localize principally on the βN atoms making them good nucleophiles. In order to obtain Mo(IV) imido and hydrazido

complexes, one-electron reduction was attempted to reduce the Mo(V) centres of the model complexes. However the Mo(IV) anions were not stable under the reduction conditions and further reduced to Mo(III) species, in which the Mo-N multiple bonds were cleaved. In the presence of H^+, the protonation of Mo(III) species probably occurred on the αN or the metal centres rather than the β N atoms. Consequently hydrazine may be the major product of the reduction-protonation of the hydrazido complexes. The imido Mo(IV) anions were not stable and were further reduced to Mo(III) species, also. They probably gave amines under the reduction-protonation conditions.

Removal of the chloride ligands from the Mo(V) model complexes to obtain Mo(IV) complexes with phosphines failed due to the reactivity of the Mo(dttd) core towards the phosphines.

The two-electron reduction of complex (**1**) resulted in the formation of a Mo(III)-Mo(IV) dimer, in which each metal centre is seven coordinated, and methylimido and sulfur bridge Mo atoms. The molecular structure shows the coplanarity of the two molybdenum atoms, the nitrogen atom and the carbon atom in the methyl group, suggesting some π interaction between the lone pair of the nitrogen atom and the dπ orbitals of the two molybdenum atoms. While the delocalization of the lone pair leads to Mo-N bonds having multiple bond character, it decreases the basicity of the imido nitrogen atom, thus decreasing the possibility of protonation on the nitrogen atom.

Because these model complexes eliminated the imido or hydrazido ligands under reduction-protonation conditions, it appears that the hydrazido molybdenum (V) complexes with a canonical form **B** are not favourable to the protonation on the βN to give ammonia. The major product may be hydrazine since the reduction cleaves the Mo-N

multiple bonds. In order to obtain the hydrazido Mo(dttd) complexes in a form closer to **A**, a Mo(IV) centre is required. Since the Mo(IV) hydrazido complexes are difficult to obtain from the Mo(V) model complexes through the modification of the coordination sphere, a new synthetic route must be explored. Perhaps if the $[MoCl_4(THF)_2]$ is first treated with the hydrazido ligand precursors, then followed by the coordination of the dttd ligands this may be achieved.

Appendix I Fractional Coordinates and Mean Isotropic Thermal Parameters for [Mo(dttd)Cl($NNPh_2$)].*

atom	x	y	z	B, ($Å^2$)
MO	0.08659(9)	0.01139(13)	0.22907(11)	3.09(9)
CL	0.1514 (3)	0.1361 (4)	0.1780 (4)	4.3 (3)
S1	0.1564 (3)	-0.1209 (5)	0.2002 (4)	4.3 (4)
S2	0.0528 (3)	-0.0225 (4)	0.0902 (3)	3.3 (3)
S3	0.0057 (3)	-0.1098 (4)	0.2585 (3)	3.6 (3)
S4	-0.0028 (3)	0.1161 (4)	0.2185 (3)	3.8 (3)
C1	-0.0682 (10)	0.0531 (15)	0.2548 (12)	3.2 (12)
C2	-0.0649 (10)	-0.0432 (17)	0.2735 (13)	3.6 (12)
C3	-0.1185 (11)	-0.0952 (17)	0.3014 (13)	4.1 (13)
C4	-0.1738 (12)	-0.0435 (19)	0.3134 (14)	5.2 (15)
C5	-0.1754 (12)	0.0518 (19)	0.2972 (13)	5.4 (15)
C6	-0.1231 (10)	0.1041 (16)	0.2696 (12)	3.7 (12)
C7	-0.0091 (11)	-0.1684 (16)	0.1691 (13)	3.8 (14)
C8	-0.0177 (10)	-0.0975 (16)	0.1043 (13)	3.6 (13)
C9	0.1081 (10)	-0.1063 (17)	0.0559 (13)	3.8 (13)
C10	0.1487 (11)	-0.1487 (15)	0.1026 (13)	3.8 (14)
C11	0.1958 (12)	-0.2141 (17)	0.0767 (15)	5.4 (16)
C12	0.1943 (12)	-0.2309 (17)	-0.0042 (16)	5.4 (16)
C13	0.1500 (13)	-0.1903 (18)	-0.0528 (14)	5.0 (15)
C14	0.1043 (12)	-0.1274 (19)	-0.0235 (15)	5.4 (15)
C15	0.1908 (10)	0.0032 (17)	0.4167 (12)	4.2 (13)
C16	0.2002 (10)	-0.0102 (17)	0.4944 (13)	4.0 (12)
C17	0.2584 (12)	-0.0446 (19)	0.5168 (15)	5.4 (16)
C18	0.3045 (11)	-0.0709 (17)	0.4640 (14)	4.7 (14)
C19	0.2921 (11)	-0.0607 (21)	0.3864 (14)	5.6 (16)

Appendix I Continued

C20	0.2340 (11)	-0.0211 (20)	0.3626 (14)	5.6 (16)
C21	0.0891 (12)	0.1018 (16)	0.4388 (13)	4.2 (13)
C22	0.1184 (13)	0.1694 (17)	0.4860 (13)	4.6 (14)
C23	0.0764 (13)	0.2238 (18)	0.5342 (13)	5.6 (16)
C24	0.0146 (15)	0.2059 (20)	0.5332 (14)	6.5 (17)
C25	-0.0131 (14)	0.1419 (20)	0.4824 (14)	6.5 (18)
C26	0.0228 (11)	0.0848 (18)	0.4331 (13)	4.7 (15)
N2	0.1317 (9)	0.0455 (13)	0.3922 (10)	3.9 (11)
N1	0.1120 (9)	0.0239 (15)	0.3224 (10)	4.8 (11)

---

* Numbers in parentheses represent esd's for the last digit(s) of the preceding number.

B is the arithmetic mean of the principal axes of the thermal ellipsoid.

Appendix II Thermal Ellipsoids for $[MoCl(NNPh_2)(dttd)]$.*

Atom	U_{11}	U_{22}	U_{33}	U_{12}	U_{13}	U_{23}
MO	3.86(11)	4.22(12)	3.67(11)	-0.08(12)	-0.52(11)	-0.19(12)
CL	4.8 (4)	4.8 (4)	6.7 (5)	-0.3 (4)	0.4 (4)	-0.5 (4)
S1	5.0 (5)	5.4 (4)	6.0 (5)	0.6 (4)	-0.9 (4)	0.2 (4)
S2	4.2 (4)	4.3 (4)	4.1 (4)	0.1 (3)	-0.4 (3)	-0.2 (3)
S3	4.8 (4)	4.3 (4)	4.7 (4)	0.9 (3)	-0.3 (3)	-0.3 (3)
S4	4.6 (4)	4.5 (4)	5.2 (4)	-0.0 (3)	0.2 (4)	-0.3 (4)
C1	5.2 (16)	3.3 (13)	3.8 (16)	0.9 (12)	0.2 (12)	-0.5 (12)
C2	3.0 (14)	7.6 (17)	3.1 (15)	0.8 (12)	-1.2 (12)	-0.3 (14)
C3	4.5 (17)	6.8 (18)	4.1 (16)	-1.6 (14)	0.7 (13)	-0.2 (14)
C4	6.1 (19)	9.0 (21)	4.8 (18)	-1.4 (17)	1.5 (15)	-0.1 (16)
C5	7.9 (20)	8.5 (20)	4.0 (17)	-1.4 (17)	0.1 (15)	0.3 (15)
C6	3.1 (15)	7.1 (18)	3.8 (15)	1.0 (13)	-0.4 (13)	-1.5 (15)
C7	5.4 (19)	3.4 (16)	5.5 (17)	0.3 (13)	-1.5 (15)	-0.6 (13)
C8	3.3 (17)	4.9 (17)	5.5 (17)	1.1 (13)	-1.1 (13)	-0.7 (14)
C9	2.7 (15)	5.1 (18)	6.6 (17)	-0.7 (12)	0.6 (13)	-0.1 (14)
C10	6.4 (20)	3.5 (15)	4.7 (17)	-0.7 (13)	1.5 (14)	-1.2 (14)
C11	6.7 (21)	4.2 (18)	9.4 (23)	-1.1 (15)	2.2 (17)	-0.9 (16)
C12	5.8 (19)	4.7 (21)	10.0 (23)	-0.6 (15)	1.6 (16)	0.2 (16)
C13	8.5 (22)	5.2 (18)	5.4 (18)	-0.3 (16)	1.1 (16)	-0.9 (15)
C14	7.3 (20)	6.3 (19)	6.7 (19)	-0.7 (16)	2.0 (16)	-3.5 (16)
C15	4.8 (15)	7.0 (18)	4.2 (15)	0.8 (16)	-1.2 (12)	-0.8 (15)
C16	5.0 (15)	5.0 (16)	5.3 (15)	-0.6 (15)	-2.0 (13)	-0.0 (14)
C17	7.3 (21)	5.9 (20)	7.5 (20)	-0.4 (16)	-1.1 (17)	-1.0 (16)
C18	4.6 (17)	6.3 (19)	6.8 (19)	-1.8 (15)	-0.4 (15)	0.9 (15)
C19	4.2 (19)	11.9 (23)	5.3 (18)	-2.5 (17)	0.0 (15)	2.7 (17)
C20	4.6 (18)	11.0 (24)	5.7 (18)	-0.9 (17)	1.9 (14)	1.5 (18)

Appendex II Continued

C21	7.3 (19)	4.8 (16)	3.8 (16)	0.1 (15)	-1.0 (15)	1.5 (13)
C22	9.2 (22)	4.0 (17)	4.3 (16)	1.2 (15)	-2.1 (16)	1.2 (14)
C23	10.3 (23)	6.6 (21)	4.1 (17)	0.6 (17)	-1.0 (16)	0.7 (15)
C24	13.7 (29)	6.9 (20)	3.9 (18)	2.0 (19)	-0.9 (19)	0.6 (16)
C25	12.2 (29)	6.7 (21)	5.8 (20)	3.4 (20)	0.8 (20)	2.1 (17)
C26	5.4 (19)	7.0 (19)	5.4 (17)	1.4 (15)	1.6 (14)	1.8 (15)
N2	4.7 (14)	6.0 (14)	4.4 (13)	0.3 (11)	-1.5 (11)	0.4 (11)
N1	5.6 (13)	8.3 (17)	4.4 (13)	-2.8 (13)	-1.7 (11)	-0.1 (12)

* Numbers in parentheses represent esd's for the last digit(s) of the preceding number.

B is the arithmetic mean of the principal axes of the thermal ellipsoid.

Appendix III Fractional Coordinates and Mean Isotropic Thermal Parameters for [(dttd)Mo(μ-NMe)(μ-S-dttd)MoCl]·3CH_2Cl_2.

atom	x	y	z	$B_{,}(Å^2)$
MO1	0.88792(6)	0.11994(9)	0.32857(4)	3.28 (4)
MO2	0.76063(7)	0.15117(10)	0.36798(4)	3.49 (4)
S1	1.01946(20)	0.2301 (3)	0.34598(15)	4.00 (13)
S4	0.77943(20)	-0.0289 (3)	0.31650(13)	3.75 (12)
S5	0.81218(21)	0.0796 (3)	0.46952(14)	4.21 (13)
S2	0.95995(20)	-0.0213 (3)	0.27361(13)	3.64 (12)
S3	0.96303(20)	-0.0073 (3)	0.41249(13)	3.68 (12)
S7	0.70609(22)	0.3208 (3)	0.41547(14)	4.57 (14)
CL	0.83565(22)	0.1936 (3)	0.23195(14)	4.85 (15)
S6	0.62955(22)	0.0419 (3)	0.37875(15)	4.80 (15)
S8	0.66075(21)	0.2258 (3)	0.28184(14)	4.62 (14)
C1	1.0723 (8)	0.1625 (11)	0.3016 (5)	3.8 (5)
C2	1.1494 (8)	0.2188 (11)	0.2974 (5)	4.3 (5)
C3	1.1942 (9)	0.1718 (12)	0.2621 (6)	5.0 (6)
C4	1.1689 (10)	0.0652 (14)	0.2327 (6)	5.5 (7)
C5	1.0979 (8)	0.0066 (12)	0.2363 (6)	4.4 (6)
C6	1.0510 (7)	0.0549 (10)	0.2708 (5)	3.4 (5)
C7	1.0077 (8)	-0.1360 (10)	0.3271 (6)	4.1 (5)
C8	1.0421 (7)	-0.0852 (11)	0.3875 (5)	4.1 (5)
C9	0.8995 (8)	-0.1309 (11)	0.4128 (5)	4.1 (5)
C10	0.9266 (9)	-0.2170 (12)	0.4585 (5)	4.5 (6)
C11	0.8788 (11)	-0.3166 (12)	0.4597 (7)	5.8 (7)
C12	0.8008 (11)	-0.3288 (12)	0.4156 (7)	5.8 (7)
C13	0.7711 (8)	-0.2405 (11)	0.3733 (6)	4.5 (6)
C14	0.8203 (8)	-0.1415 (10)	0.3707 (5)	3.9 (5)

Appendix III Continued

C15	0.7439 (9)	-0.0340 (12)	0.4782 (5)	4.6	(6)
C16	0.7683 (11)	-0.1166 (14)	0.5275 (6)	6.0	(7)
C17	0.7188 (11)	-0.1996 (13)	0.5360 (6)	5.9	(7)
C18	0.6378 (12)	-0.2143 (15)	0.5005 (8)	7.3	(9)
C19	0.6116 (10)	-0.1400 (14)	0.4497 (7)	6.2	(8)
C20	0.6660 (9)	-0.0516 (12)	0.4427 (5)	4.6	(6)
C21	0.5735 (9)	0.1634 (15)	0.4042 (7)	6.0	(7)
C22	0.6277 (10)	0.2539 (15)	0.4461 (7)	6.2	(8)
C23	0.6409 (8)	0.4045 (11)	0.3573 (5)	4.2	(5)
C24	0.6095 (9)	0.5143 (13)	0.3682 (7)	5.9	(7)
C25	0.5620 (10)	0.5865 (16)	0.3249 (7)	6.8	(8)
C26	0.5450 (12)	0.5489 (18)	0.2677 (9)	8.5	(10)
C27	0.5740 (10)	0.4353 (16)	0.2564 (7)	6.6	(8)
C28	0.6246 (8)	0.3634 (12)	0.2992 (6)	4.7	(6)
ME	0.8936 (10)	0.3548 (11)	0.4050 (6)	5.1	(6)
N	0.8573 (6)	0.2464 (8)	0.3752 (4)	3.4	(4)
ME1	0.8764 (14)	0.0318 (18)	0.1131 (7)	8.4	(10)
CL1A	0.9488 (4)	0.0911 (4)	0.0812 (3)	8.3	(3)
CL1B	0.7806 (4)	0.0135 (7)	0.0599 (3)	11.7	(4)
ME2	0.6274 (16)	0.024 (3)	0.1447 (13)	14.4	(18)
CL2A	0.6221 (6)	-0.1342 (9)	0.1526 (5)	18.6	(7)
CL2B	0.5697 (7)	0.0585 (15)	0.0766 (5)	24.4	(10)
ME3	0.6943 (14)	0.402 (3)	0.1429 (10)	12.1	(16)
CL3A	0.7501 (6)	0.3367 (8)	0.1008 (3)	13.8	(5)
CL3B	0.6193 (6)	0.4888 (12)	0.1148 (5)	21.3	(8)

* Numbers in parentheses represent esd's for the last digit(s) of the preceding number.

B is the arithmetic mean of the principal axes of the thermal ellipsoid.

Appendix IV Thermal Ellipsoids for [(dttd)Mo(μ-NMe)(μ-S-dttd)MoCl]·3CH_2Cl_2.

Atom	U_{11}	U_{22}	U_{33}	U_{12}	U_{13}	U_{23}
MO1	4.58(6)	3.43(5)	4.73(6)	-0.10(5)	0.51(5)	-0.22(5)
MO2	4.73(6)	4.55(6)	4.30(6)	0.13(5)	0.52(5)	-0.27(5)
S1	5.55(20)	3.61(17)	6.85(22)	-0.64(15)	1.41(17)	-0.37(15)
S4	5.30(19)	4.34(18)	5.06(18)	-0.53(15)	0.78(15)	-0.65(14)
S5	6.09(21)	5.74(21)	4.42(18)	-0.21(17)	0.46(15)	-0.03(16)
S2	5.45(19)	3.84(17)	5.00(19)	-0.11(14)	0.82(15)	-0.27(14)
S3	5.65(19)	3.96(17)	4.46(17)	-0.50(15)	0.18(15)	-0.05(14)
S7	6.07(21)	6.46(22)	5.23(20)	1.09(18)	0.66(17)	-0.82(17)
CL	6.91(22)	6.41(22)	5.87(21)	0.32(18)	1.31(17)	0.82(17)
S6	5.49(21)	7.26(24)	6.00(22)	-0.55(18)	0.88(17)	0.02(18)
S8	6.03(22)	6.64(22)	4.81(19)	0.81(18)	-0.10(16)	0.02(17)
C1	6.1 (8)	4.3 (7)	4.4 (7)	0.2 (6)	0.7 (6)	0.9 (6)
C2	6.4 (8)	4.7 (7)	5.5 (8)	-1.3 (7)	0.7 (7)	0.9 (6)
C3	7.1 (10)	5.2 (8)	8.0 (10)	-1.2 (7)	2.1 (8)	0.4 (7)
C4	8.6 (11)	8.7 (11)	5.9 (9)	-0.8 (9)	4.0 (8)	-0.1 (8)
C5	5.6 (8)	5.8 (8)	6.8 (9)	-0.8 (7)	2.6 (7)	-2.3 (7)
C6	5.7 (8)	3.7 (6)	3.8 (6)	-1.1 (6)	0.1 (5)	0.3 (5)
C7	5.2 (8)	3.8 (7)	7.0 (9)	0.8 (6)	1.0 (7)	0.5 (6)
C8	4.2 (7)	4.9 (8)	6.5 (9)	-0.7 (6)	0.1 (6)	2.0 (7)
C9	7.0 (9)	4.4 (7)	5.3 (8)	-1.2 (6)	2.0 (7)	-1.3 (6)
C10	8.2 (10)	4.9 (8)	5.5 (8)	1.6 (7)	2.3 (7)	1.0 (7)
C11	11.0 (13)	4.7 (8)	8.6 (11)	1.1 (8)	4.2 (10)	0.8 (8)
C12	11.6 (13)	3.4 (7)	10.0 (12)	-1.9 (8)	5.2 (10)	0.2 (8)
C13	6.2 (8)	4.5 (8)	7.9 (9)	-2.1 (7)	2.6 (7)	-1.5 (7)
C14	6.6 (9)	3.6 (7)	6.0 (8)	-0.2 (6)	2.4 (7)	-0.1 (6)
C15	8.7 (10)	5.4 (8)	4.6 (7)	0.1 (7)	2.0 (7)	-0.4 (6)

Appendix IV Continued

C16	10.0 (12)	8.1 (11)	4.8 (8)	1.7 (9)	0.3 (8)	1.3 (8)
C17	10.9 (13)	6.2 (10)	7.2 (10)	-0.8 (9)	3.0 (9)	1.3 (8)
C18	12.5 (15)	6.3 (10)	12.2 (15)	-1.8 (10)	5.6 (12)	2.3 (10)
C19	8.9 (12)	6.8 (10)	10.0 (12)	-1.9 (9)	3.5 (10)	0.6 (9)
C20	8.1 (10)	6.1 (9)	4.2 (7)	-0.1 (8)	1.2 (7)	-0.0 (6)
C21	4.9 (9)	8.6 (11)	10.3 (12)	0.5 (8)	1.6 (8)	0.5 (10)
C22	9.1 (12)	8.4 (12)	8.1 (10)	1.7 (9)	3.5 (9)	0.8 (9)
C23	5.1 (8)	5.2 (8)	6.0 (8)	0.7 (6)	0.8 (6)	0.2 (6)
C24	6.6 (9)	6.1 (9)	11.2 (13)	0.0 (8)	2.9 (9)	-1.3 (9)
C25	7.4 (11)	8.9 (12)	9.9 (12)	4.0 (9)	0.9 (9)	-0.4 (10)
C26	10.4 (14)	10.7 (15)	12.4 (15)	5.6 (12)	2.2 (12)	2.4 (12)
C27	7.3 (11)	10.1 (13)	8.4 (11)	2.1 (10)	1.0 (9)	1.2 (10)
C28	6.0 (9)	6.3 (9)	5.7 (8)	0.4 (7)	0.4 (7)	0.8 (7)
ME	8.1 (10)	3.9 (8)	8.6 (10)	-0.7 (7)	1.8 (8)	-2.1 (7)
N	5.5 (6)	4.2 (6)	3.9 (5)	0.1 (5)	1.0 (5)	0.9 (4)
ME1	16.0 (19)	10.9 (15)	6.4 (11)	3.6 (14)	2.7 (11)	1.7 (10)
CL1A	13.4 (4)	6.8 (3)	16.5 (5)	-0.8 (3)	5.7 (4)	0.7 (3)
CL1B	12.0 (5)	16.6 (6)	17.1 (6)	-1.3 (4)	2.4 (4)	-4.1 (5)
ME2	11.6 (20)	19.4 (29)	23.4 (29)	5.2 (19)	-0.6 (19)	-8.8 (24)
CL2A	16.6 (9)	17.8 (9)	36.7 (14)	1.9 (7)	0.4 (9)	-5.3 (9)
CL2B	17.9 (9)	53.6 (24)	28.2 (12)	13.4 (12)	12.4 (9)	19.1 (14)
ME3	10.8 (17)	25.2 (33)	12.5 (18)	7.8 (19)	4.3 (14)	6.2 (20)
CL3A	21.3 (8)	20.2 (8)	13.6 (5)	3.4 (7)	4.5 (6)	2.9 (5)
CL3B	16.3 (7)	37.6 (17)	34.2 (13)	11.6 (9)	12.1 (8)	21.1 (12)

* Numbers in parentheses represent esd's for the last digit(s) of the preceding number.

B is the arithmetic mean of the principal axes of the thermal ellipsoid.

Appendix V Hydrogen atom positions for [(dttd)Mo(μ-NMe)(μ-S-dttd)MoCl]·3CH_2Cl_2.

atom	x	y	z
H2	1.17163	0.29806	0.32241
H3	1.24787	0.21773	0.25751
H4	1.20518	0.02783	0.20672
H5	1.07888	-0.07526	0.21289
H10	0.98406	-0.20417	0.49183
H11	0.89949	-0.38375	0.49293
H12	0.76406	-0.40761	0.41535
H13	0.71054	-0.24904	0.34275
H16	0.82932	-0.10800	0.55750
H17	0.74159	-0.25909	0.57239
H18	0.59780	-0.27810	0.51042
H19	0.55201	-0.15222	0.41803
H24	0.62291	0.54376	0.41287
H25	0.53892	0.67066	0.33540
H26	0.51014	0.60449	0.23237
H27	0.55574	0.40264	0.21215
H7A	1.05723	-0.17785	0.31399
H7B	0.96160	-0.20230	0.32792
H8A	1.06731	-0.15701	0.41729
H8B	1.09127	-0.02363	0.38727
H21A	0.53236	0.12284	0.42608
H21B	0.53719	0.21105	0.36652
H22A	0.58861	0.32378	0.45487
H22B	0.65858	0.21000	0.48667

REFERENCES

1. J.E. Huheey, *Inorganic Chemistry: Principles of Structure and Reactivity*, Harper & Row, New York, **1983**, 891.

2. R.A. Henderson, G.J. Leigh, C.J. Pickett, *Adv. Inorg. Chem. and Radiochem.*, **1983**, 27, 197.

3. J. Chatt, *Transition Metal Chemistry*, Ed. by A. Müller, E. Diemann, **1981**, 207.

4. R.H. Holm, E.D. Simhon, *Molybdenum Enzymes*, Ed. by T.G. Spiro, Princeton University, **1985**, 1.

5. F.A. Cotton, G. Wilkinson, *Inorganic Chemistry*, **1988**, 1373.

6. P.J. Stephens, *Molybdenum Enzymes*, Ed. by T.G. Spiro, Princeton University, **1985**, 117.

7. M. Jidai, K. Tominari, Y. Uchida, A. Misono, *J.C.S., Chem. Commun.* **1969**, 1392.

8. M. Hidai, K. Tominari, Y. Uchida, *J. Am. Chem. Soc.*, **1972**, 94, 110.

9. J. Chatt, G.A. Heath, R.L. Richares, *J.C.S., Dalton Trans.*, **1974**, 2074.

10. J.M. Manriquez, J.E. Bercaw, *J. Am. Chem. Soc.*, **1974**, 96, 6229.

11. M.W. Anker, J. Chatt, G.J. Leigh, A.G. Wedd, *J. Chem. Soc., Dalton Trans.*, **1975**, 2639.

12. G.L. Geoffroy, M.G. Bradley, R.Pierantozzi, *Transition Metal Hydrides*, Ed. by R. Bau, **1978**, 181.

13. T. Tatsumi, H. Tominaga, M. Hidai, Y, Uchida, *J. Organomet. Chem.*, **1980**, 199, 63.

14. M. Sato, T. Tatsumi, T. Kodama, M. Hidai, T. Uchida, Y. Uchida, *J. Am. Chem. Soc.*, **1978**, 100, 4447.

15. D.F. Harrison, H. Taube, *J. Am. Chem. Soc.*, **1967**, 89, 5760.

16. S.M. Rocklage, R.R. Schrock, *J. Am. Chem. Soc.*, **1982**, 104, 3077.

17. T. Uchida, Y. Ucyhida, M. Hidai, T. Kodama, *Acta Cryst.*, **1975**, B31, 1197.

18. B.R. Davis, N.C. Payne, J.A. Ibers, *J. Am. Chem. Soc.*, **1969,** 91, 1240.

19. J.E. Fergusson, J.L. Love, W.T. Robinson, *Inorg. Chem.*, **1972,** 11, 1662.

20. G.S. Girolami, J.E. Salt, G. Wilkinson, M. Thornton-Pett, M.B. Hursthouse, *J. Am. Chem. Soc.*, **1983,** 105, 5954.

21. T. Yoshida, T. Adachi, M. Kaminaka, T. Ueda, *J. Am. Chem. Soc.*, **1988,** 110, 4872.

22. J.M. Manriquez, R.D. Sanner, R.E. Marsh, J.E. Bercaw, *J. Am. Chem. Soc.*, **1976,** 98, 8351.

23. F.A. Forder, K. Prout, *Acta Cryst.*, **1974,** B30, 2778.

24. P.D. Cradwick, J. Chatt, R.H. Ctabtree, R.L. Richards, *J.C.S., Chem. Commun.*, **1975,** 351.

25. M.R. Churchill, H.J. Wasserman, *Inorg. Chem.*, **1981,** 20, 2899.

26. T. Takahashi, T. Kodama, A. Watakbe, Y. Uchida, M. Hidai, *J. Am. Chem. Soc.*, **1983,** 105, 1680.

27. H.F. Klein, K. Ellrich, K. Ackermann, *J.C.S., Chem, Commun.*, **1983,** 888.

28. C. Krüger, Y.H. Tsay, *Angew, Chem. Int. Ed. Engl.*, **1973,** 12, 998.

29. G.P. Pez, P. Apgar, P.K. Crissey, *J. Am. Chem. Soc.*, **1982,** 104, 482.

30. K.P. Huber, G. Herzberg, *Molecular Spectra and Molecular Structure, (IV), Constant of Diatomic Molecules*, **1979,** 420.

31. P.G. Wilkinson, *Can. J. Phys.*, **1956,** 34, 250.

32. A.K. Rappé, *Inorg. Chem.*, **1984,** 23, 995.

33. M. Jidai, *Molybdenum Enzymes*, Ed. by T.G. Spiro, Princeton University, **1985,** 287.

34. C.M. Che, H.W. Lam, T.C. Lau, *J.C.S., Chem. Commun.*, **1989,** 1883.

35. R.R. Schrock, M. Wesolek, A.H. Liu, K.C. Wallace, J.C. Dewan, *Inorg. Chem.*, **1988,** 27, 2050.

36. J. Chatt, R.C. Fay, R.L. Richards, *J. Chem. Soc., (A)*, **1971,** 702.

37. J.M. Manriquez, R.D. Sanrier, R.E. Marsh, J.E. Bercaw, *J. Am. Chem. Soc.*, **1976,** 98, 8351.

38. C.B. Powell, M.B. Hall, *Inorg. Chem.*, **1984,** 23, 4619.

39. K. Jonas, D.J. Brauer, C. Krüger, P.J. Roberts, Y.H. Tsay, *J. Am. Chem., Soc.*, **1976,** 98, 74.

40. M.A. Andrews, C.B. Knobler, H.D. Kaesz, *J. Am. Chem. Soc.*, **1979,** 101, 7260.

41. T. Takahashi, Y. Mizobe, M. Sato, Y. Uchida, M. Hidai, *J. Am. Chem. Soc* , **1980,** 102, 7461.

42. J. Jeffery, M.F. Lappert, R.I. Riley, *J. Organomet. Chem.*, **1979,** 181, 25.

43. J.W. Lauher, R. Hoffmann, *J. Am. Chem. Soc.*, **1976,** 98, 1729.

44. R. Hoffmann, M.M.L. Chen, D.L. Thorn, *Inorg. Chem,*. **1977,** 16, 503.

45. T. Yamabe, K. Hori, T. Minato, K. Fukui, *Inorg. Chem.*, **1980,** 19, 2154.

46. J. Chatt, J.R. Dilworth, RlL. Richard, *Chem, Rev.*, **1978,** 78, 589.

47. J. Chatt, C.M. Elaon. N.E. Hooper, G.J. Leigh, *J.C.S., Dalton Trans.*, **1975,** 2392.

48. H. Binder, D. Sellmann, *Angew. Chem. Int. Ed. Engl.*, **1973,** 12, 1017.

49. M. Hidai, Y. Mizobe, *Reactions of Coordinated Ligands,* Ed. by P.S. Braterman, **1989,** vol. 2, 53.

50. J.N. Murrell, A.Al-Derzi, G.J.Leigh, M.F. Guest, *J.C.S., Dalton Trans.*, **1980,** 1452.

51. J. Chatt, M.E. Fakley, R.L. Richards, J. Mason, I.A. Stenhouse, *J. Chem. Res. (S),* **1979,** 44.

52. J.M. Manriquez, D.R. McAlister, J.E. Bercaw, *J. Am. Chem. Soc.*, **1978,** 100, 3078.

53. N.J. Lazarowych, R.H. Morris, J.M. Ressner, *Inorg. Chem,* **1986,** 25, 3926.

54. J. Chatt, A.J. Pearman, R.L. Richards, *Nature,* **1975,** 253, 39.

55. J. Chatt, A.J. Pearman, R.L. Richards, *J.C.S. Dalton, Trans.*, **1977,** 1852.

56. G.L. Geoffroy, M.G. Brandley, R. Pierantozzi, *Transition Metal Hydrides,* Ed. by R. Bau, Am. Chem. Soc., Washington **1978,** 181.

57. T. George, B.B. Kaul, *Inorg. Chem.*, **1990,** 29, 4969.

58. J.A. Baumann, T.A. George, *J. Am. Chem. Soc.*, **1980, 102, 6153.**

59. G.E. Bossard, T.A. George, R.K. Lester, *Inorg. Chim, Acta,* **1982,** 64, L227.

60 C.R. Brulet, E.E. van Tamelen, *J. Am. Chem. Soc.*, **1975,** 97, 911.

61. M. Hidai. *Current Perspectives in Nitrogen Fixation,* Ed. by A.H. Gibson, W.E. Newton, Proceedings of the Fourth International Symposium on Nitrogen Fixation, New York, **1981,** 26.

62. A. Watakabe, T. Takahashi, D. Jin, K. Yokotake, Y. Uchida Ho Hidai, *J. Organomet. Chem.*, **1983,** 254, 75.

63. M. Hidai, T. Takahashi, I. Yokotake, Y, Uchida, *Chem. Lett.*, **1980,** 645.

64. H. Nishihara, T. Mori, Y. Tsuruta, K. Nakano, T. Saito, Y. Sasaki., *J. Am. Chem. Soc.*, **1982,** 104,4367.

65. T. Tatsumi, H. Tominaga, M. Hidai, Y. Uchida, *J. Organomet. Chem.*, **1980,** 102, 7461.

66. C.J. Pickett, J. Talarmin, *Nature,* **1985,** 317, 462.

67. S.N. Anderson, M.E. Fakley, R.L. Richards, J. Chatt, *J.C.S., Dalton Trans.*, **1981,** 1973.

68. J. Chatt, M.E. Fakley, P.B. Hitchcock, R.L. Richards, N.T. Luong-Thi, D.L. Hughes, *J. Organomet. Chem.*, **1979,** 172, C55.

69. J. Chatt, G.J. Leigh, H. Neukonn, C.J. Pickett, D.R. Stanley, *J.C.S., Dalton Trans.*, **1980,** 121.

7\ T.A. George, R.C. Tisdale, *Inorg Chem.* **1988,** 27, 2909.

71 J.A. Baumann, G.E. Bossard, T.A. George, D.B. Howell, L.M. Koczon, R.K. Laster, C.M. Nldding, *Inorg, Chem.*, **1985,** 24, 3568.

72. T.A. George, L.M. Koczon, R.C. Tisdale, K. Gebreyes, J. Zubieta, *Polyhedron,* **1990,** 9, 545.

73. K. Gebreyes, T.A. George, J. Zubieta, R.C. Tisdale, *J. Inorg. Chem.*, **1986,** 25, 405.

74. F. Armstrong, *Nature,* **1985,** 317, 576.

75. W.A. Nugent, J.M. Mayer, *Metal-Ligand Multiple Bonds,* John Wiley & Sons, **1988,** 288.

76. T.A. George, L. Ma, S.N. Shailk, R.C. Tisdale, J. Zubieta, *Inorg. Chem.*, **1990,** 29, 4789.

77. T.A George, R.C. Tisdale, *J. Am. Chem. Soc.*, **1985,** 107, 5157.

78. T.A. George, R.C. Tisdale, *Polyhedron,* **1986,** 5, 297.

79. T.A. George, R.C. Tisdale, *Polyhedron,* **1989,** 8, 1756.

80. R.N.F. Thorneley, R.R. Eady, D.J. Lowe, *Nature,* **1978,** 272, 557.

81. J. Chatt, G.A. Heath, G.J. Leigh, *J.C.S., Chem. Comm.*, **1972,** 444.

82. J. Chatt, G.A. Heath, R.L. Richards, *J.C.S., Chem. Comm.*, **1972,** 1010.

83. M.N. Chisholm, K. Folting, J.C. Huffman, A.L. Ratermann, *J.C.S., Chem. Comm.*, **1981,** 1229.

84. G.A. Heath, R. Mason, K.M. Thomas, *J. Am. Chem. Soc.*, **1974,** 96, 259.

85. R.A. Henderson, *J.C.S., Dalton Trans.*, **1982,** 917.

86. C.J. Pickett, K.S. Ryder, J. Talarmin, *J.C.S., Dalton Trans.*, **1986,** 1453.

87. J. Chatt, J.R. Dilworth, *J.C.S., Chem. Comm.*, **1975,** 983.

88. J.R. Dilworth, P.L. Dahlstrom, K.R. Hyde, J. Zubieta, *Inorg. Chim. Acta,* **1983,** 71, 21.

89. J. Chatt, R. Choukroun, J.R. Dilworth, J. Hyde, P. Vella, J. Zubieta, *J. Trans. Met. Chem.*, **1979,** 4, 59.

90. W.A. Nugent, R.L. Harlow, *J. Am. Chem. Soc.*, **1980,** 102, 1759.

91. M.E. Noble, J.C. Huffman, R.A.D. Wentworth, *Inorg, Chem.*, **1982,** 21, 2101.

92. C.Y. Chou, J.C. Huffman, E.A. Maatta, *Inorg. Chem.*, **1986,** 25, 822.

93. C.Y. Chou, D.D. Derore, S.C. Huchktt, E.A. Maatta, J.C. Huffman, F. Takusagawa, *Polyhedron,* **1986,** 5, 301.

94. D.L. Thorn, W.A. Nugent, R.L. Harlow, *J. Am. Chem. Soc.,* **1981,** 103, 357.

95. K. Stahl, F. Weller, K. Dehnicke, P.Z. Paetzold, *Anorg. Allg. Chem.,* **1986,** 534, 93.

96. D.M. Berg, P.R. Sharp, *Inorg. Chem.,* **1987,** 26, 2959.

97. A.J. Nielson, J.M. Waters, *Aust. J. Chem.,* **1983,** 36, 243.

98. S. Gambarotta, A. Chiesi-Villa, C. Guastini, *J. Organomet. Chem.,* **1984,** 270, C49.

99. J.H. Osborne, A.L. Rheigold, W-C. Trogler, *J. Am. Chem. Soc.,* **1985,** 107, 7945.

100. N. Wiberg, H.W. Häring, U.Z. Schubert, *Naturforsch,* **1980,** 35B, 599.

101. R.J. Burt, J.R. Dilworth, G.J. Leigh, J A. Zubieta, *J.C.S., Dalton Trans.,* **1982,** 2295.

102. P.L. Dahlstrom, J.R. Dilworth, P. Shulman, J. Zubieta, *J. Inorg. Chem.,* **1982,** 21, 933.

103. M.W. Bishop, J. Chatt, J.R. Kilworth, M.B. Hursthouse, M Motevalli, *J.C.S., Dalton, Trans.,* **1979,** 1600.

104. V.W. Day, T.A. George, S.T.A. Iske, S.D. Wagner, *J. Inorg. Chem.,* **1982,** 21, 933.

105. D.L. Hughes, *Acta Cryst.,* **1981,** B37, 557.

106. R.A. Henderson, *J.C.S., Dalton Trans.,* **1982,** 917.

107. M. Hidai, K. Komori, T. Kodama, D.M. Jin, Y. Mizobe, *J. Organomet. Chem.,* **1984,** 272, 155.

108. J.A. Mayer, C.J. Curtis, J.E. Bercaw. *J. Am. Chem. Soc.,* **1983,** 105, 2651.

109. R. C. Murray, R.R. Schrock, *J. Am. Chem. Soc.,* **1985,** 107, 4557.

110. W.A. Nugent, R.L. Harlow, *Inorg. Chem.,* **1980,** 19, 777.

111. P.A. Bates, A.J. Nielson, J.M. Waters, *Polyhedron,* **1985,** 4, 1391.

112. T.C. Jones, A.J. Nielson, C.E.F. Rickard, *J.C.S., Chem. Comm.*, **1984,** 205.

113. B.R. Ashcroft, D.C. Bradley, A.J. Nielson, E.F.F. Richard, *J.C.S., Chem. Comm.*, **1987,** 170.

114. J. Chatt, B.A.L. Crichton, J.R. Dilwouth, P. Dalhstrom, R. Gutkowska, J. Zubieta, *J. Inorg. Chem.*, **1982,** 21, 2383.

115. Y. Takahashi, N. Onoyama, K. Sugiyama, *Chem. Lett.*, **1978,** 525.

116. L.R. Chamberlain, I.P. Rothwell, J.C. Huffman, *J.C.S., Chem. Comm.*, **1986,** 1203.

117. K.W. Chiu, R.A. Jones, A.M.R. Galas, M.B. Hursthouse, *J.C.S., Dalton Trans.*, **1981,** 2088.

118. W. Liese, K. Dehnicke, J.Z. Strahle, *Naturforsch.* **1979,** 34B, 693.

119. G. LaMonica, S. Cenini, *J.C.S., Dalton Trans.*, **1980,** 1145.

120. S. Gambarotta, C.J. Guastini, *J. Organomet. Chem.*, **1984,** 270, C49.

121. C.Y. Chou, J.C. Huffman, E.A. Maatta, *J.C.S., Chem. Comm.*, **1984,** 1184.

122. C.Y. Chou, E.A. Maatta, *Inorg. Chem.*, **1984,** 23, 2912.

123. W.A. Herrmann, R. Dammel, H. Bock, H. Pfisterer, *J. Organomet. Chem.*, **1983,** 254, 219.

124. W. Hussain, G.J. Leigh, C.J. Pickett, *J.C.S., Chem. Comm.*, **1982,** 747.

125. P. Jernakoff, G.L. Geoffroy, A.L. Rheingold, S.J. Geib, *J.C.S., Chem. Comm.*, **1987,** 1610.

126. J. Chatt, J.R. Dilworth, *J.C.S., Chem. Comm.*, **1972,** 549.

127. E.A. Maatta, B.L. Haymore, R.A.D. Wentworth, *Inorg. Chem.*, **1980,** 19, 1055.

128. B.L. Haymore, E.A. Maatta, R.A.D. Wentworth, *J. Am. Chem. Soc.*, **1979,** 101, 2063.

129. E.A. Maatta, R.A.D. Wentworth, *Inorg. Chem.*, **1979,** 18, 2409.

130. I.S. Kolomnikov, Y.D. Koreshkov, T.S. Lobeeva, M.E. Volpin, *J.C.S., Chem. Comm.*, **1970,** 1432.

131. S.F. Pedersen, R.R. Schrock, *J. Am. Chem. Soc.*, **1982,** 104, 7483.

132. A.D. Horton, R.R. Schrock, J.H. Freudenberger, *Organometallics,* 1987, 6893.

133. D.C. Bradley, M.B. Hursthouse, K.M.A. Malik, A.J. Nielson, R.L. Short, *J.C.S., Dalton Trans.*, **1983,** 2651.

134. A.J. Nielson, *Inorg. Synth.*, **1986,** 24, 194.

135. E.A. Maatta, *Inorg. Chem.*, **1984,** 23, 2560.

136. G. LaMonica, S. Cenini, *Inorg. Chim. Acta,* **1973,** 29, 183.

137. R. Rossi, A. Marchi, A. Duatti, L. Wagon P. DiBernardo, *Trans Met. Chem.*, **1985,** 10, 151.

138. S.M. Rocklage, R.R. Schrock, *J. Am. Chem. Soc.*, **1980,** 102, 7808.

139. S.M. Rocklage, R.R. Schrock, *J. Am. Chem. Soc.*, **1982,** 104, 3077.

140. H.W. Turner, J.D. Fellmann, S.M. Rocklage, R.R. Schrock, M.R. Churchill, H.J. Wasserman, *J. Am. Chem. Soc.*, **1980,** 102, 7809.

141. R.A. Henderson, G. Daries, J.R. Dilworth, R.N.F. Thornely, *J.C.S., Dalton. Trans.*, **1981,** 40.

142. P.C. Bevan, H. Chatt, J.R. Dilworth, R.A. Henderson, G.J. Leigh, *J.C.S., Dalton. Trans.*, **1982,** 821.

143. M.W. Bishop, J. Chatt, J.R. Dilworth, B.D. Neaves, P. Dahlstrom, J. Hyde, J. Zubieta, *J. Organomet. Chem.*, **1981,** 213, 109.

144. J.T. Groves, T. Takahashi, *J. Am. Chem. Soc.*, **1983,** 105, 2073.

145. P.A.B. Shapley, Z.Y. Own, J.C. Huffman, *Organometallics,* **1986,** 5, 1269.

146. P.A.B. Shapley, Z.Y. Own, *J. Organomet. Chem.*, **1987,** 335, 269.

147. M. Hidai, T. Kodama, M. sato, M. Harakawa, Y. Uchida, *Inorg, Chem.*, **1976,** 15, 2694.

148. C.J. Pichett, K.S. Ryder, J. Talarmin, *J.C.S., Dalton Trans.*, **1986,** 1453.

149. J. Chatt, A J. Pearman, R.L. Richard, *J.C.S., Dalton Trans.*, **1976,** 1520.

150. J.A. Baumann, G.E. Bossard, T.A. George, D.B. Howell, L.M. Koczon, R.K. Lester, C.M. Noddings, *Inorg. Chem.*, **1985,** 24, 3568.

151. W. Hussain, G.J. Leigh, H.M. Ali, C.J. Pickett, *J.C.S., Dalton Trans.*, **1988,** 553.

152. G.E. Bossard, D.C. Busby, M. Chang, T.A. George, S.D.A. Iske, Jr., *J. Am. Chem. Soc.*, **1980,** 102, 100.

153. D.C. Busby, T.A. George, *Inorg. Chem.*, **1979,** 18, 3164.

154. J.R. Dilworth, S.A. Harrison, D.R.M. Wallon, E. Schweda, *Inorg. Chem.*, **1985,** 24, 1594.

155. J. Chatt, A.A. Diamantis, G.A. Heath, N.E. Hooper, G.J. Leigh *J.C.S., Dalton Trans.*, **1977,** 688.

156. D.C. Busby, T.A. George, S.D.A. Iske, Jr., S.D. Wagner, *Inorg. Chem.*, **1981,** 20, 22.

157. J. Chatt, R.A. Head, G.J. Leigh, *J.C.S., Dalton Trans.*, **1980,** 1129.

158. K. Komori, T. Kodama, D-M. Jin, T. Takahashi, Y. Uchida, M. Hidai, *Chem. Lett.*, **1983,** 465.

159. J. Chatt, G.J. Leigh, H, Neukonn, D.J. Pickett, D.R. Stanley, *J.C.S., Dalton Trans.*, **1980,** 121.

160. J.A. Carroll, D. Sutton, *Inorg. Chem.*, **1980,** 19, 3137.

161. C.F. Barrientos-Penna, F.W.B. Einstein, T. Jones, D. Sutton, *Inorg. Chem.*, **1982,** 21, 2578.

162. Nugent, J.M. Mayer, *Metal-Ligand Multiple Bonds,* John Wiley & Sons, **1988,** 21.

163. W.A. Nugent, B.L. Haymor, *Coord. Chem. Rev.*, **1980,** 31, 123.

164. R.T. Baker, J.F. Whitney, S.S. Wreford, *Organometallics,* **1983,** 2, 1049.

166. A.K. Rappé, *Inorg. Chem.*, **1986,** 25, 4686.

167. K. Tatsumi, R. Hoffmann, *Inorg. Chem.*, **1981,** 20, 3771.

168. J. Weber, C.D. Garner, *Inorg. Chem.*, **1980,** 19, 2206.

169. D. Collison, C.D. Garner, F.E. Mabbs, J.A. Salthouse, T.J. King, *J.C.S., Dalton*

Trans., **1981,** 1820.

170. A.K. Rappé, W.A.III. Goddard, *J. AM. Chem. Soc.*, **1982,** 104, 448.

171. A.K. Rappé, W.A.III. Goddard, *J. Am. Chem. Soc.*, **1982,** 104, 3287.

172. R.A. Wheeler, M.H. Whangbo, T. Hughbanks, R. Hoffmann, J.K. Burdett, T.A. Albright, *J. Am. Chem. Soc.*, **1986,** 108, 222.

173. A. Mayr, M.F. Asaro, M.A. Kgelsberg, S.L. Lee, D. van Engon, *Organometallics,* **1987,** 6, 432.

174. A. Mayr, G.A. McDermott, A.M. Dorries, *Organometallics,* **1985,** 4, 608.

175. A.B. Bocarsly, R.E. Cameron, H.D. Rubin, G.A. McDermott, C.R. Wolff, A. Mayr, *Inorg. Chem.*, **1985,** 24, 3976.

176. R.J. Goddard, R. Hoffmann, E.D. Jemmis, *J. Am. Chem. Soc.*, **1980,** 102, 7667.

177. W.A. Nugent, R.J. McKinney, R.V. Kasowski, F.A. van Catledge, *Inorg. Chim. Acta,* **1982,** 65, L91.

178. N.M. Kostic, R.F. Fenske, *J. Am. Chem. Soc.*, **1981,** 103, 4677.

179. J.A. Jorgensen, R. Hoffmann, *J. Am. Chem. Soc.*, **1986,** 108, 1867.

180. H. Nakatsuji, J. Ushio, S. Han, T. Yonezawa, *J. Am. Chem. Aoc.*, **1983,** 105, 426.

181. W.A. Nugent, J.M. Mayer, *Metal-Ligand Multiple Bonds,* John Wiley & Sons, **1988,** 220.

182. R.A. Henderson. *J.C.S., Dalton Trans.*, **1983,** 51.

183. E.A. Carter, W.A.III. Goddard, *J. Am. Chem. Soc.*, **1986,** 108, 2180 and 4746.

184. K.W. Chou, W.K. Wong, G. Wilkinson, A.M.R. Galas, M.B. Hursthouse, *Polyhedron,* **1982,** 1, 31.

185. D.M.T. Chan, W.A. Nugent, *Inorg. Chem.*, **1985,** 24, 1422.

186. G.W. Parshall, W.A. Nugent, D.M.T. Chan, W. Tam, *Pure Appl. Chem.*, **1985,** 57, 1809.

187. P.C. Bevan, J. Chatt, M. Hidai, G.J. Leigh, *Organomet, Chem.*, **1978,** 160, 165.

188. Y. Mizobe, Y. Uchida, M. Hidai, *Bull. Chem. Soc. Jpn.*, **1980,** 53, 1781.

189. S.M. Rocklage, R.R. Schrock, *J. Am. Chem. Soc.*, **1982,** 104, 3077.

190. J. Chatt, R.J. Rosser, F. King, G.J. Leigh, *J.C.S., Dalton Trans.*, **1976,** 2453.

191. P.A. Adcock, F.R. Keene, R.S. Smythe, M.R. Snow, *Inorg. Chem.*, **1984,** 23, 2336.

192. J.D. Land, R.A. Henderson, *J.C.S., Dalton Trans.*, **1987,** 197.

193. J.D. Land, R.A. Henderson, *J.C.S., Dalton Trans.*, **1986,** 2155.

194. J. Chatt, B.A.L. Crichton, J.R. Dilworth, P. Dahlstrom, J.A. Zubieta, *J.C.S., Dalton Trans.*, **1982,** 1041.

195. P.C. Bevan, J. Chatt, G.J. Leigh, E.G. Leelamani, *J. Organomet. Chem.*, **1977,** 139, C59.

196. M. Hidai, Y. Mizobe, *Reactions of Coordinated Ligands*, Ed. By P.S. Braterman, **1989,** Vol. 2, 53.

197. J. Chatt, C.T. Can, G.J. Leigh, C.J. Pickett, D.R. Stanley, *J.C.S., Dalton Trans.*, **1980,** 2032.

198. J.R. Dilworth, C. Kan, R.L. Richards, J. Mason, I.A. Stenhouse, *J. Organometal. Chem.*, **1980,** 201, C24.

199. G.L. Hillhouse, B.L. Haymore, S.A. Bistram, W.G. Herrmann, *Inorg. Chem.*, **1983,** 22, 314.

200. D. Sellmann, E. Böhlen, M. Waeber, G. Huttner, L. Zsolnai, *Angew, Chem. Int. Ed. Engl.*, **1985,** 24, 981.

201. L. Blum, I.E. Williams, R.R. Schrock, *J. Am. Chem. Soc.*, **1984,** 106, 8316.

202. T. Takahashi, Y, Mizobe, M. Sato, Y. Uchida, H. Hidai, *J. Am. Chem. Soc.*, **1979,** 101, 3405.

203. T. Yamabe, K. Kori, K. Fukui, *Inorg. Chem.*, **1982,** 21, 2816.

204. J. Chatt, J.R. Dilworth, P.L. Dahlstrom, J. Zubieta, *J.C.S., Chem. Comm.*, **1980,** 786.

205. J. Chatt, M.E. Fakley, P.B. Hitchcock, R.L. Richards, N.T. Luong-Thi, *J.C.S., Dalton Trans.*, **1982,** 345.

206. J.A. McCleverty, A.E. Rae, I. Wolchowicz, N.A. Bailey, J.M.A. Smith, *J.C.S., Dalton Trans.*, **1983,** 71.

207. K. Tanaka, M. Noriya, T. Tanaka, *Inorg. Chem.*, **1986,** 25, 835.

208. M.Y. Aatipin, L.P. Didenko, L.M. Kachapina, A.E. Shilov, A.K. Hilova, Y.T. Struchkov., *J.C.S., Chem. Comm.*, **1989,** 1467.

209. S. Kuwabata, S. Uezumu, K. Tanaka, T. Tanaka, *J.C.S., Chem. Comm.*, **1986,** 135.

210. D. Coucouvanis, A. Salifoglou, M.G. Kanatzidis, W.R. Dunham, A. Simopoulos, *Inorg. Chem.*, **1988,** 27, 4066.

211. K. Tanaka, M. Moriya, S. Uezumi, T. Tanaka, *Inorg. Chem.*, **1988,** 27, 137.

212. C.P. Gibson, L.F. Dahl, *Organomt tallics,* **1988,** 7, 535.

213. P.T. Bishop, J.R. Dilworth, S. Morton, *J. Organomet. Chem.*, **1988,** 33, 373.

214. J. Jordanov, H.M.J. Hendriks, N. Duypre, A. Viari, P. Vigny, G. Diakun, *Inorg, Chem.*, **1988,** 27, 2997.

215. D. Coucouvanis, P.R. Challen, S.M. Koo, W.M. Davis, W. Butler, W.R. Dunham, *Inorg. Chem.*, **1989,** 28, 4181.

216. S. Ciurli, R.H. Holm, *Inorg. Chem.*, **1989,** 28, 1685.

217. N.Y. Zhu, Y.F. Zhen, X.T. Wu, *J.C.S., Chem. Comm.*, **1990,**

218. Q.T. Liu, L.R. Huang, H.Q. Liu, X.J. Lei, D.X. Wu, B.S. Kang, J.X. Lu, *Inorg. Chem.*, **1990,** 29, 4131.

219. P. Li, M.D. Curtis, *Inorg. Chem.*, **1990,** 29, 1242.

220. S. Ciurli, J.J. Carney, R.H. Holm, G.C. Papaefthymiou, *Inorg. Chem.*, **1989,** 28, 2696.

221. A. Müller, E. Diemann, *Transition Metal Chemistry,* Ed. by A. Müller, E. Diemann, **1981,** 221.

222. C.J. Pickett, G.J. Leigh, *J.C.S., Chem. Comm.*, **1981,** 1033.

223. B.B. Kaul, J.H. Enemark, S.L. Merbs, J.T. Spence, *J. Am. Chem. Soc.*, **1985,** 107, 2885.

224. P. Subtamanian, S. Burgmayer, S. Richards, V. Szalai, T.G. Spiro, *Inorg. Chim.*, **1990,** 29, 3849.

225. D. Sellmann, J. Keller, M. Moll, D.F. Campana, M Haase, *Inorg. Chim. Acta,* **1988,** 141, 243.

226. B.B.Kaul, D. Selimann, *Z. Naturforsch,* **1983,** 38b, 562.

227. C.D. Garner, S. Bristow, *Molybdenum Enzymes,* Ed. by T.G. Spiro, Princeton University, **1985,** 384.

228. A.J. Blake, M. Schröder, *Advances in Inorganic Chemistry,* Ed. by A.G. Sykes, **1990,** 35, 2.

229. F.A. Cotton, G. Wilkinson, *Advanced Inorganic Chimistry,* John Wiley & Sons, **1988,** 531

230. S.G. Murray, F.R. Hartley, *Chem. Rev.*, **1981,** 81, 365.

231. D. Sellmann, E. Bohlen, *Z. Natruforsch,* **1982,** 37b, 1026.

232. K. Peter, C. Vollhardt, *Organic Chemistry,* W.H. Freeman and Company, **1987,** 1121.

233. H.E. Baumgarten, *Organic Syntheses,* **1973,** 5, 1050.

234. J.F. Klebe, *J. Am. Chem. Soc.*, **1964,** 86, 4400.

235. U. Warmagal, H. Niederprüm, *Z. Anorg. u. Allgem. Chem.*, **1961,** 310, 38.

236. C.T. Pouchert, *The Aldrich Library of Infrared Spectra,* **1981,** 1544c.

237. D.J. Pasto, C.R. Johnson, *Organic Structure Determination,* Prentice-Hall, **1969,** 136.

238. K, Nakamoto, *Infrared and Raman Spectra of Inorganic and Coordination Compounds,* John Wiley & Sons, **1978,** 161.

249. P.H. Bird, Unpublished results.

240. W.A. Nugent, J.M. Mayer, *Metal-Ligand Multiple Bonds,* John Wiley & Sons, **1988,** 123.

241. J.H. Osborne, W.C. Trogler, *Inorg. Chem.*, **1985,** 24, 3098.

242. J.T. Dilworth, J.A. Zubieta, *J.C.S., Chem. Comm.* **1981,** 132.

243. K. Gebreyes, J. Zubieta, T.A. George, L.M. Koczon, T.C. Tisdale, *Inorg. Chem.* **1986,** 25, 405.

244. W.A. Nugent, J.M. Mayer, *Metal-Ligand Multiple Bonds,* John Wiley & Sons, **1988,** 180.

245. R. Mattes, H. Scholand, U. Mikloweit, V. Schrenk, *Zeitschrift fur Naturforschung, B Chem. Sci.,* **1987,** 42, 589.

246. A.C. Kizano, J.F. Richardson, M.E. Noble, *Inorg. Chem.,* **1989,** 28, 1453.

247. J.A.M. Canich, F.A. Cotton, K.R. Dunbar, L.R. Felvello, *Inorg. Chem.,* **1988,** 27, 804.

248. M.H. Chisholm, C.E. Hammond, J.C. Huffman, *J.C.S., Chem. Comm.,* **1987,** 1423.

249. B.S. Furniss, A.J. Hannaford, V. Rogers, P.W.G. Smith, A.R. Tatchell, *Vogel's Textbook of Practical Organic Chemistry,* Longman, **1978,** 4th Ed., 588.

250. A.C. Larsen, E.J. Gabe, *Computing in Crystallography* Ed.by H. Schlenk, R. Olthof-Hazekamp, H. Van Koningsveld, J.C. Bassi, Delft, Holland, **1978,** 81.